ศิลาเคมีและการแปรสภาพของชุดหินแปรลานสาง จังหวัดตาก

นางสาวสมพร วงษ์ลักษณ์

จุฬาลงกรณ์มหาวิทยาลัย
Chulalongkorn University

บทคัดย่อและแฟ้มข้อมูลฉบับเต็มของวิทยานิพนธ์ตั้งแต่ปีการศึกษา 2554 ที่ให้บริการในคลังปัญญาจุฬาฯ (CUIR)
เป็นแฟ้มข้อมูลของนิสิตเจ้าของวิทยานิพนธ์ ที่ส่งผ่านทางบัณฑิตวิทยาลัย
The abstract and full text of theses from the academic year 2011 in Chulalongkorn University Intellectual Repository (CUIR)
are the thesis authors' files submitted through the University Graduate School.

วิทยานิพนธ์นี้เป็นส่วนหนึ่งของการศึกษาตามหลักสูตรปริญญาวิทยาศาสตรมหาบัณฑิต
สาขาวิชาธรณีวิทยา ภาควิชาธรณีวิทยา
คณะวิทยาศาสตร์ จุฬาลงกรณ์มหาวิทยาลัย
ปีการศึกษา 2558
ลิขสิทธิ์ของจุฬาลงกรณ์มหาวิทยาลัย

PETROCHEMISTRY AND METAMORPHISM OF LANSANG METAMORPHIC SUITES, CHANGWAT TAK

Miss Somporn Wonglak

A Thesis Submitted in Partial Fulfillment of the Requirements

for the Degree of Master of Science Program in Geology

Department of Geology

Faculty of Science

Chulalongkorn University

Academic Year 2015

Copyright of Chulalongkorn University

Thesis Title	PETROCHEMISTRY AND METAMORPHISM OF LANSANG METAMORPHIC SUITES, CHANGWAT TAK
By	Miss Somporn Wonglak
Field of Study	Geology
Thesis Advisor	Associate Professor Chakkaphan Sutthirat, Ph.D.
Thesis Co-Advisor	Associate Professor Christoph A. Hauzenberger, Dr.rer.nat.

Accepted by the Faculty of Science, Chulalongkorn University in Partial Fulfillment of the Requirements for the Master's Degree

.....Dean of the Faculty of Science

(Associate Professor Polkit Sangvanich, Ph.D.)

THESIS COMMITTEE

.....Chairman

(Professor Montri Choowong, Ph.D.)

.....Thesis Advisor

(Associate Professor Chakkaphan Sutthirat, Ph.D.)

.....Thesis Co-Advisor

(Associate Professor Christoph A. Hauzenberger, Dr.rer.nat.)

.....Examiner

(Assistant Professor Pitsanupong Kanjanapayont, Dr.rer.nat.)

.....External Examiner

(Prayath Nantasin, Dr.rer.nat.)

จุฬาลงกรณ์มหาวิทยาลัย
Chulalongkorn University

สมพร วงษ์ลักษณ์ : ศิลาเคมีและการแปรสภาพของชุดหินแปรลานสาง จังหวัดตาก (PETROCHEMISTRY AND METAMORPHISM OF LANSANG METAMORPHIC SUITES, CHANGWAT TAK) อ.ที่ปรึกษาวิทยานิพนธ์หลัก: รศ. ดร.จักรพันธ์ สุทธิรัตน์, อ.ที่ปรึกษาวิทยานิพนธ์ร่วม: รศ. ดร.คริสทอบท์ ฮัวเซนเบอร์เจอร์, 111 หน้า.

เทือกเขาหินแปรทางตะวันตกของไทยวางตัวในแนวเหนือ-ใต้ ถือเป็นส่วนหนึ่งของแนวเทือกเขาเชียงใหม่-ลินซาง ส่วนหนึ่งประกอบด้วยพื้นที่อุทยานแห่งชาติลานสางที่ตั้งอยู่ทางตะวันตกของจังหวัดตาก เป็นพื้นที่ได้รับแรงกระทำจากแนวรอยเลื่อนแม่ปิงซึ่งวางตัวในแนวตะวันตกเฉียงเหนือ-ตะวันออกเฉียงใต้ หินบริเวณรอยเลื่อนแสดงการเปลี่ยนรูปมีลักษณะการเรียงตัวแบบริ้วขนานและโครงสร้างแนวเส้นให้เห็นอย่างชัดเจน การศึกษาศิลาวรรณาของหินไนส์พบว่าเนื้อหินส่วนใหญ่ละเอียดมากถึงหยาบ โดยทั่วไปประกอบด้วยแร่ควอรตซ์ แพลจิโอเคลสโพแทสเซียมเฟลด์สปาร์ ไบโอไทต์ คลอไรต์ และ แอมฟิโบล์ ส่วนหินแคลก์ซิลิเกตและหินอ่อนแสดงลักษณะเป็นชั้นแทรกอยู่ในหินไนส์ ประกอบด้วยแร่ แคลไซต์ ควอรตซ์ เฟลด์สปาร์ แอมฟลิโบล ไบโอไทต์และการ์เนต นอกจากนี้ยังพบหินแกรนิติกไนส์ที่มีองค์ประกอบค้ลายคลึงกับหินไนส์แทรกตัดเข้ามาในหินไนส์และแคลก์ซิลิเกตที่เป็นหินท้องที่ ผลการศึกษาอุณหภูมิและความดันทางธรณีบ่งชี้ว่า หินแปรในพื้นที่เกิดจากการแปรสภาพระดับสูงในกรีนชิสต์ขั้นสูง ถึงแอมฟิโบไลต์ขั้นต่ำ อุณหภูมิและความดันของการแปรสภาพ ของหินไนส์เนื้อหยาบประมาณ 545-560 องศาเซลเซียส และ 0.5-0.7 กิโลบาร์ หินไนส์เนื้อละเอียด 565-590 องศาเซลเซียสและ 5.7-7.8 กิโลบาร์ หินไนส์เนื้อละเอียดมาก 440-480 องศาเซลเซียสและ 1.1-5.7 กิโลบาร์ และหินอ่อนประมาณ 460-480 องศาเซลเซียสและ 5.9-6.8 กิโลบาร์ โดยลักษณะธรณีเคมีบ่งชี้ว่าชุดหินแปรสานสางมีองค์ประกอบของหินเริ่มต้นเป็นหินแกรนิตและหินตะกอน ก่อนเกิดการแปรสภาพอย่างไพศาล แล้วจึงเกิดพนังหินและสายแร่ตัดเข้ามาในหินท้องที่เหล่านี้ ภายหลังการแปรสภาพ เนื้อหินแสดงการเปลี่ยนลักษณะแบบอ่อนนิ่มและแบบเปราะก่อนยกตัวขึ้นสู่พื้นผิวโลก

ภาควิชา	ธรณีวิทยา	ลายมือชื่อนิสิต	.....
สาขาวิชา	ธรณีวิทยา	ลายมือชื่อ อ.ที่ปรึกษาหลัก	.....
ปีการศึกษา	2558	ลายมือชื่อ อ.ที่ปรึกษาร่วม	.....

5472249623 : MAJOR GEOLOGY

KEYWORDS: LANSANG , METAMORPHIC ROCK, WESTERN THAILAND

SOMPORN WONGLAK: PETROCHEMISTRY AND METAMORPHISM OF LANSANG METAMORPHIC SUITES, CHANGWAT TAK. ADVISOR: ASSOC. PROF. CHAKKAPHAN SUTTHIRAT, Ph.D., CO-ADVISOR: ASSOC. PROF. CHRISTOPH A. HAUZENBERGER, Dr.rer.nat., 111 pp.

Western metamorphic belt in Thailand elongated within north-south direction has been grouped into the Chiang Mai-Lincang belt. As part of this metamorphic belt, the Lansang National Park located in the west of Changwat Tak is an affected area from northwest-southeast striking Mae Ping fault. Along the fault zone, rocks have been strongly deformed yielding steep foliation and lineation. Based on petrographic study, these rocks are mainly characterized by gneisses showing very fine- to coarse-grained textures which consist of quartz, plagioclase, K-feldspar, biotite and minor amounts of chlorite and amphibole. Calc-silicate and impure marble are partly interlayered in these gneisses; they are composed of calcite, quartz, feldspar, amphibole and garnet. Moreover, granitic gneiss, intruded into the host gneisses and calc-silicate, appears to have similar composition of gneiss. Based on geothermobarometry, these rocks should have undertaken high-grade metamorphism belonging to upper greenschist to lower amphibolite facies with P-T estimates of 560-580°C and 5.7-7.5 Kbar for coarse-gained gneiss, 545-560°C and 0.5-0.8 Kbar for fine-grained gneiss, 440-500°C and 3.0-5.0 Kbar for very fine-grained gneiss and 480-510°C and 6.0-6.8 Kbar for impure marble. According to geochemistry, these rocks appear to have several evolution stages. Granitic and sedimentary protoliths, initial rocks of gneisses and calc-silicate, may have been situated in the area prior to regional metamorphism. Subsequently, dykes and veins crossed cut into these gneissic and calc-silicate rocks before later metamorphism appears to have continued and reached the ductile-brittle stage along with uplifting onto the surface.

Department:	Geology	Student's Signature	.....
Field of Study:	Geology	Advisor's Signature	.....
Academic Year:	2015	Co-Advisor's Signature	.....

ACKNOWLEDGEMENTS

This research program has been carried out at the Department of Geology, Faculty of Science, Chulalongkorn University.

First of all, I would like to express my sincere gratitude to my advisor, Associate Professor Chakkaphan Sutthirat, Department of Geology, Faculty of Science, Chulalongkorn University, for his valuable suggestion, encouragement and guidance throughout the research.

I take this opportunity to express my special thanks to Dr. Takeyuki Ogata and the short stay program from ICREMER, Akita University which provided sample preparation and SEM laboratory analysis. Sample preparation and laboratory at Chulalongkorn University were supported by Ms. Sopit poompuang, Ms. Jiraprapa Neampan and Mr. Prajin Thongchum.

I am gratefully acknowledging financial support from the 90th Anniversary of Chulalongkorn University Fund (Ratchadaphiseksomphot Endowment Fund), Graduate School, Chulalongkorn University.

Finally, I wish to extend my thanks to Ms. Jensarin Vivatpinyo, Mr. Alonkot Funka and all of geology students at Chulalongkorn University for their support and advice during this research. I must thank all members of my family and friends for their support all the time.

จุฬาลงกรณ์มหาวิทยาลัย
Chulalongkorn University

CONTENTS

Page

จุฬาลงกรณ์มหาวิทยาลัย
Chulalongkorn University

Page

จุฬาลงกรณ์มหาวิทยาลัย
Chulalongkorn University

LIST OF TABLES

LIST OF FIGURES

จุฬาลงกรณ์มหาวิทยาลัย
Chulalongkorn University

จุฬาลงกรณ์มหาวิทยาลัย
Chulalongkorn University

จุฬาลงกรณ์มหาวิทยาลัย
Chulalongkorn University

CHAPTER I
INTRODUCTION

1.1 General statement

Based on geologic setting, Thailand consists of two main tectonic micro-continents, Shan-Thai to the west and Indochina to the east. Complex tectonic setting was reported by (Bunopas and Vella, 1992) who also reported that metamorphic rocks have widely exposed in all regions of the country. However, ages of these metamorphic rocks are still ambiguous due to lacking of evidence. Most of information is described only rock types with a few data of radioactive ages. In Shan-Thai terrane, its basement infers to be occupied by Precambrian high-grade metamorphic rocks and Middle or Upper Paleozoic rocks that are characterized by continuous sedimentary sequences with overprinting of various grades of metamorphism. Metamorphic rocks are significantly elongate within north-south direction and usually show dome-shaped structure extending towards the Mae Ping Fault. They gradually change orientation to northwest-southeast onto the north (Baum et al., 1970; Department of Mineral Resources, 2007; MacDonald et al., 1993; Macdonald et al., 2010). Sinistral strike-slip fault nearby the study area is located around the Lansang National Park in Changwat Tak (see Figure 1)

Western metamorphic belt, significantly influenced by the regional high-grade metamorphism, is the oldest rocks in Thailand (Dheeradilok and Lumjuan, 1983). Most rocks usually show steep foliation and stretched lineations (Lacassin et al., 1993; Lacassin et al., 1997) which are indicator of sinistral shear movement. Two main metamorphic facies can be separated by different ranges of temperature and pressure. Amphibolite facies has been suggested for Precambrian rocks whereas greenschist

facies under lower pressure has been assigned for Lower Paleozoic rocks (Campbell, 1975).

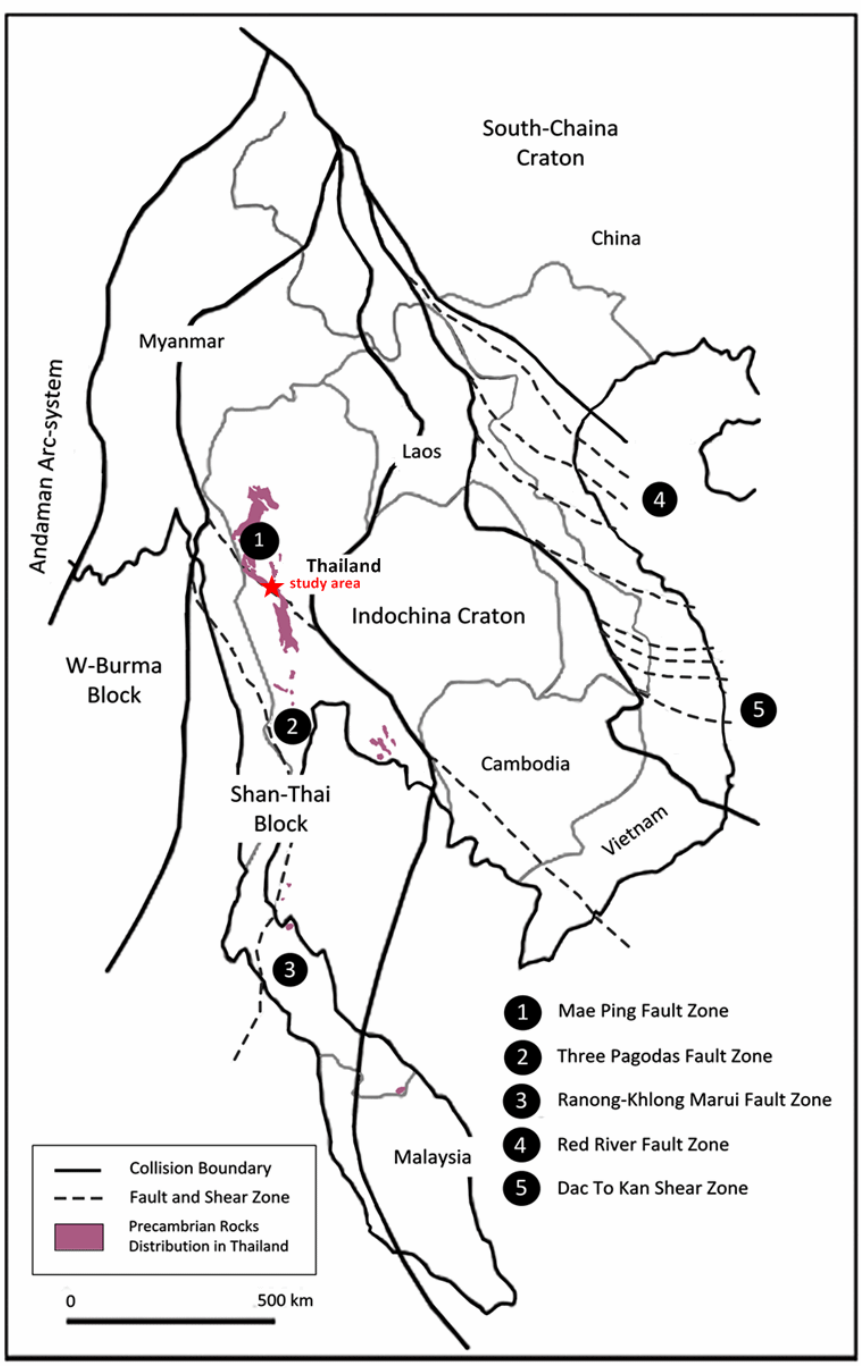

Figure 1. Map of Thailand and adjacency showing distribution of Precambrian rocks and main fault zones. North-South elongation is clearly observed in the Shan-Thai terrane (Osanai et al., 2008; Salayapongse, 2002).

Northwestern Thailand is an important area in which many researchers have studied characteristics of metamorphic core complex (Dunning et al., 1995; Kanjanapayont et al., 2011; Lacassin et al., 1993; Lacassin et al., 1997; MacDonald et al., 1993; Macdonald et al., 2010; Morley, 2004; Morley et al., 2007; Palin et al., 2013; Rhodes et al., 1997; Rhodes et al., 2000; Singharajwarapan and Saengsrichan, 1999). Their expansion was determined based on lithology and geological structure which usually form mountainous terrain with moderate to high elevations along the north-south elongate dome-shaped structures (Baum et al., 1970). The mountain range extends stretchy towards Mae Ping fault or Wang Chao fault; then it gradually changes orientation to northwest-southeast along the fault direction which is a sinistral strike-slip fault. That is located nearby the Lansang National Park in western Tak. McDonald et al. (1993; 2010) studied part of the Doi Intanon metamorphic core complex which presents a dome-shape feature of a Cordilleran-type. Its axial core complex is composed of high-grade gneissic rocks under the condition of amphibolite facies series at low pressure. It is expected to be Precambrian basement that is covered by low-grade to unmetamorphosed sedimentary rocks of Upper Paleozoic age. These rock groups can be separated by fault contact. In addition, granites have intruded into both western and eastern parts of the core complex.

Previous researchers suggested that northwest of Thailand is located between the southern part of Himalayan syntaxis and the east of dextral Sagaing fault. Metamorphic belt of the strike-slip fault zone is associated with the Mae Ping fault that had developed in Lower Cretaceous to Upper Cenozoic during transpression by plate convergence (Morley, 2004). Main rocks of Precambrian consist of high-grade paragneisses, orthogneisses and micaschists that show typically steep foliation of mineral almost flat and stretched lineations (Lacassin et al., 1993; Lacassin et al., 1997).

จุฬาลงกรณ์มหาวิทยาลัย
Chulalongkorn University

These evidences indicate shear movement. The Precambrian rocks are covered by low-grade metamorphic rocks of Lower Paleozoic age (Baum et al., 1970; Bunopas, 1981; Department of Mineral Resources, 2007; Hahn et al., 1986) In general, both rock formations are bounded by a detachment fault; there is no direct evidence to indicate continuously stratigraphic sequences of both formations (Bunopas, 1981; Hahn et al., 1986).

MacDonald et al. (1993) reported that these rocks have locally undertaken upper amphibolite facies metamorphism under low pressure prior to ductile shearing (mylonization) which can be used to separate basement and the covered rocks. Occurrences of sillimanite and cordierite indicated lower pressure metamorphism condition. Temperature-Pressure ranges during the prograde metamorphism were determined at 1-3 Kb and 600-650°C inferred from breakdown of muscovite to sillimanite and orthoclase for the gneissic rocks. Thermobarometric estimation calculated for peak progade metamorphism of gneissic rocks in Doi Inthanon metamorphic core complex were using by TWQ v1.02 and V 2.02, that results indicated temperature from ca. 725°C down to 535°C and pressure from ca. 7 kbar down to ca. 3 kbar from muscovite-biotite geothermometer and phengite geobarometer (Macdonald et al., 2010). In addition, estimated equilibrium of mineral assemblages from wollastonite-andesine-garnet-calcite-quartz was using TWQ v1.02 indicated prograde metamorphism range of temperature and pressure about 693±59°C and 5.2±0.9 kbar of calc-silicate rocks (Macdonald et al., 2010). Singharajwarapan and Saengsrichan (1999) worked on geothermobarometry calculated by THERMOCAL program of Powell and Holland (1988) which indicates peak metamorphism of 650±70°C and 3.5±1 kb at the core of orthogneiss and mantling paragneiss located around Doi Inthanon and Mae Wang areas.

According to $^{40}Ar/^{39}Ar$ dating of K-feldspar, it may present the end of ductile left-lateral shear along Mae Ping Fault Zone at about 30.5 Ma yielded 400 °C to 185 °C before rapid cooling at about 23 Ma (about 75 °C); these events were clearly taken place in Tertiary period (Lacassin et al., 1997). Fission-track dating of apatite and zircon indicates cooling period between 22 Ma and 18 Ma from 320-200 °C to 110-60 °C. Meanwhile, the Lansang gneiss had uplifted during a period of Lower Oligocene to Early Miocene. Moreover, strike-slip movement led to north-south elongated deformation overprinting in this region (Morley et al., 2007).

In addition, Kanjanapayont et al. (2011) studied U-Pb analyses of zircon with clear zone found in gneissic rocks from Lansang areas. Ending shear behavior may be between 191 ± 10 and 206 ± 4 Ma under high temperature, based on U-Pb zircon dating by LA-MC-ICP-MS technique. During this period, the high-grade metamorphism was caused by sinistral shear movement of the Mae Ping fault. This event appears to have been associated with the collision of Shan-Thai and Indochina in Permo-Triassic (Charusiri et al., 2002). Monazite of the Lansang orthogneiss yielded Th-Pb ages of about 123-114 Ma which indicates magmatic protholith emplacement in Early Cretaceous prior to metamorphism in Eocene (about 45-37 Ma) and subsequent ductile shearing (Palin et al., 2013).

Three Pagodas fault is located in the southern part of Mae Ping fault zone; these strike-slip fault zone as a result of India and Eurasia collision prior developed ductile stage in the Early Cenozoic (Morley et al., 2007). During Paleocene-Eocene period, Three Pagodas metamorphism in western Thailand had overprinted before sinistral strike-slip shearing during Eocene-Oligocene (Nantasin et al., 2012). High-grade metamorphic rocks in eastern Thailand along the NW-SE Klaeng fault consist of

amphibolite to granulite gneissic rocks. U-Pb zircon dating, yielded from LA-MC-ICP-MS, indicated age of magmatism and leucogranite intrusion at about 78.6±07 Ma and 67±1 to 72.1±0.6 Ma during Late cretaceous (Kanjanapayont et al., 2013). In the southern part of Thailand, NE-trending Ranong and Khlong Marui strike-slip zones had been dextrally transpersed during Late Cretaceous and Eocene (Kanjanapayont et al., 2012).

Moreover, Ailo Shan or Red River metamorphic belt elongated NW-SE strike-slip fault, parallel to the Mae Ping fault, is composed of high-grade gneiss covered by lower-grade pelitic metamorphic rocks (Tapponnier et al., 1990). These high-grade gneisses representing peak metamorphism stage of collision zone metamorphism in Vietnam took place at ca. 250 Ma; this indicates that Permo-Triassic metamorphism in Vietnam should have occurred during Indochina and South China collision. Subsequently, metamorphic rocks were exhumed by folding and thrusting forming orogenic belt during collision of India and Eurasia in Tertiary (Osanai et al., 2008).

จุฬาลงกรณ์มหาวิทยาลัย
Chulalongkorn University

However, chronological information of Mae Ping strike-slip fault zone domain is still in conflict, particularly in metamorphic evolution. Therefore, this study is focused on petrographical, mineralogical and geochemical characteristics of these rocks. Mineral assemblages and their chemical compositions may indicate specific P-T condition of metamorphic processes. Petrographic study of the metamorphic rocks in the study area as well as their geochemical analyses should provide significant information related to metamorphism including the protolith that can indicate evolution and tectonic process in this region.

1.2 Scope of Work

The study area is located within the Lansang National Park in Changwat Tak (See Figure 2). Geologically, it is a part of the western metamorphic belt which has multiple rock complexes related to several tectonic events caused by plate collision. Many exposures have widely distributed in the area which is mainly occupied by gneiss, calc-silicate rocks and plutonic rocks. Representatives of these rocks were systematically collected prior to petrographic study. Mineral assemblages and crucial textures of rock samples were described. Mineral chemistry of the main composition was analyzed as well as whole-rock chemical analyses of representative samples were carried out. All analytical data obtained from this study are then interpreted for original protolith and P-T ranges of metamorphism.

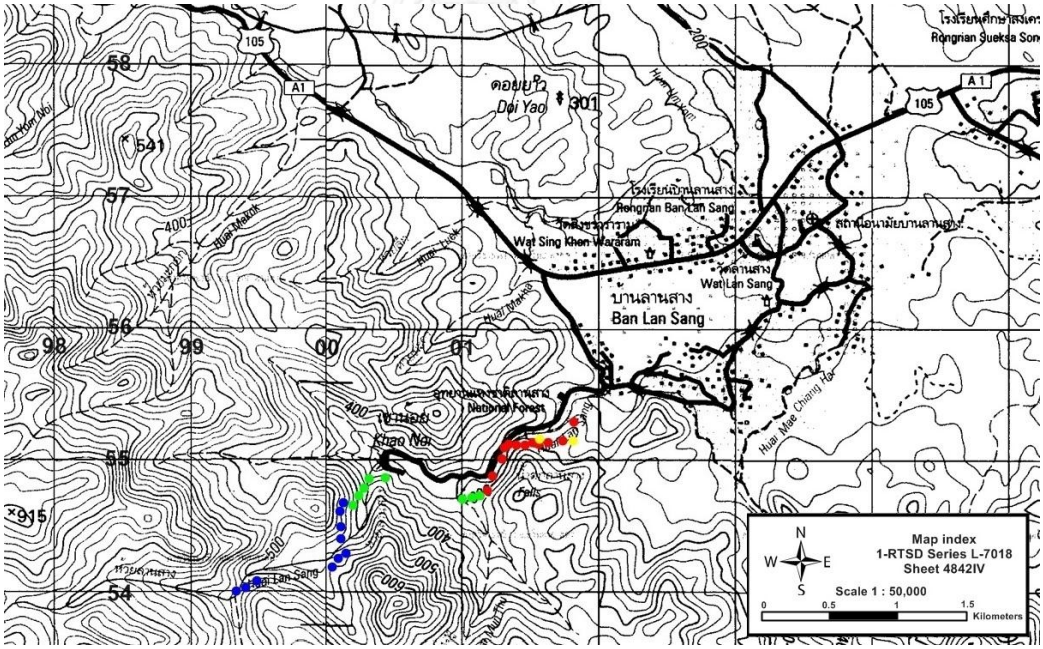

Figure 2. Topographic map (sheet 4842IV) of the study area showing locations of samples around the Lansang National Park in Changwat Tak.

1.3 Objective

The main objective is to study petrochemistry and mineral chemistry of the Lansang metamorphic suites exposed in Changwat Tak. All analytical data are interpreted for the origin of rocks and related P-T conditions of metamorphism.

1.4 Methodology

Literature reviews on geologic setting and structural geology related to metamorphism in the Lansang National Park, Changwat Tak were carried out, initially. Field study and sample collection were taken place prior to samples preparation such as thin sectioning and polished-thin sectioning for petrographic description and mineral chemical analysis. Polarizing microscope was engaged for petrographic work whereas Electron Probe Micro-Analyzer (EPMA) was used for analysis of mineral chemistry. Selected rock powders were used for whole-rock geochemistry using X-Ray Fluorescence (XRF) Spectrometer for major and minor compositions. Moreover, these rock powders were digested totally as solutions for determination of trace elements and rare earth elements (REE) using Inductively Coupled Plasma-Mass Spectrometer (ICP-MS). Finally, all results were interpreted and discussed particularly on geologic and tectonic setting. Conclusions in various aspects were then made for report writing and publication. All working steps are summarized in Figure 3 and described in detail below.

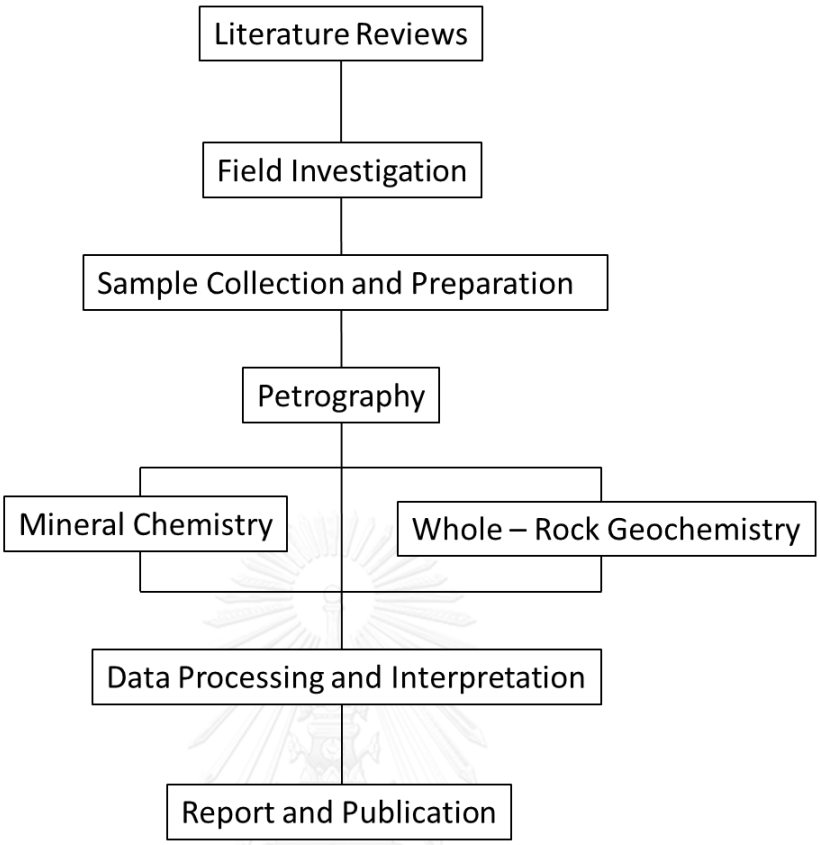

Figure 3 Schematic diagram showing steps of work in this research project.

Literature Reviews: were carried out initially to obtain general data at the beginning of research work. Geologic setting including metamorphism and structural geology along the shear zone of the Lansang National Park, Changwat Tak reported by previous researchers were reviewed in details which can also be used for further interpretation and discussion.

Sample Collection and Preparation: All samples were collected directly from the study area, Lansang National Park, during the preliminary fieldwork. More than 20 samples of metamorphic rocks were then selected and prepared for 3 main investigations including petrographic description, mineral chemistry and whole-rock geochemistry. Thin sections and polished-thin sections were prepared for petrography

and mineral chemistry, respectively; whereas, rock powders and solutions were also prepared for whole-rock analyses.

Petrography: Petrographic description was carried out initially using a polarizing microscope, based at the Department of Geology, Faculty of Science, Chulalongkorn University. Texture, mineral composition and crucial microstructure of rock samples were described and identified prior to further investigations.

Mineral Chemistry: After petrographic investigation in the previous step, crucial mineral grains were selected for chemical analysis by an Electron Probe Micro-Analyzer (EPMA; Model JEOL JXA-8100) based at the Department of Geology, Faculty of Science, Chulalongkorn University. Polished-thin sections were prepared at thickness of about 50 μm before polishing with 12, 6, 3, 1 μm diamond pastes, respectively. Mineral and oxide standards were used for calibration using a focus beam (<1 μm in diameter) under operating condition of acceleration voltage 15kV and current about 2.50×10^{-8} A. The same analytical conditions were also set for all analyses before automatic ZAF correction and report as wt% oxides. Standards comprise barite for Ba, periclase for Mg, corundum for Al, quartz for Si, eskolaite for Cr, manganosite for Mn, jadeite for Na, fayalite for Fe, wollastonite for Ca, potassium titanium phosonate for K, P and Ti. However, Cl and F were calibrated using internal standard. Chemical composition of minerals in rock samples were recalculated based on proper oxygen atoms in the mineral structure prior to determination of end-members and specific observation in some particular minerals.

จุฬาลงกรณ์มหาวิทยาลัย
Chulalongkorn University

Whole–Rocks Geochemistry: can be separated into 2 steps as described below:

1) Major and minor elements were obtained using an X-ray Fluorescence (XRF) Spectrometer (model Bruker AXS S4 PIONEER) based at the Geology Department, Faculty of Science, Chulalongkorn University. This quantitative analysis was operated at 220/380 V, 50 Hz, 8 kVA. Rock standards including DTS-2B, BHVO-2, GSP-2 and SDC-1 provided by USGS and JA-2, JB-1B, JG-1A, JG-2, JR-1 and STM-1 provided by Geological Society of Japan were selected for calibration before reporting in wt% oxides. Moreover, loss on ignition (LOI) was measured by weighting rock powders compared before and after 3 hours ignition at 1000°C in RHF 14-3 220V electric furnace based at Department of Geology, Faculty of Science, Chulalongkorn University.

2) Trace elements and rare earth elements (REE) were also analyzed by Inductively Coupled Plasma-Mass Spectrometer (ICP-MS) based at the Mineral and Geological Services, SGS (Thailand) Limited. These samples were digested totally to solution using sodium peroxide, leach with water and add the nitric acid. Detection limits were estimated at 1 ppm-0.1 %Ag, 0.01-25 %Al, 5 ppm-10 %As, 0.5 ppm-1 %Ba, 5 ppm-0.25 %Be, 0.1 ppm-0.1 %Bi, 0.1-35 %Ca, 0.2 ppm-1 %Cd, 0.1 ppm-1 %Ce, 5 ppm-1 %Co, 10 ppm-10 %Cr, 0.1 ppm-1 %Cs, 5 ppm -1 %Cu, 0.05 ppm-0.1 %Dy, 0.05 ppm-0.1 %Er, 0.05 ppm-0.1 %Eu, 0.01-30 %Fe, 1 ppm-0.1 %Ga, 0.05 ppm-0.1 %Gd, 1 ppm-0.1 %Ge, 1 ppm-1 %Hf, 0.05 ppm-0.1 %Ho, 0.2 ppm-0.1 %In, 0.1-25%K, 0.1 ppm-1 %La, 10 ppm-5 %Li, 0.05 ppm-0.1 %Lu, 0.01-30%Mg, 10 ppm-10 %Mn, 2 ppm-1 %Mo, 1 ppm-1 %Nb, 0.1 ppm-1 %Nd, 5 ppm-1 %Ni, 0.01-25 %P, 5 ppm-1 %Pb, 0.05 ppm-0.1 %Pr, 0.2 ppm-1 %Rb, 5 ppm-5 %Sc, 0.5 ppm-1 %Sb, 0.1 ppm-0.1 %Sm, 1 ppm-1 %Sn, 0.1 ppm-1 %Sr, 0.5 ppm-1 %Ta, 0.05 ppm-0.1 %Tb, 0.1 ppm-0.1 %Th,

0.01-25 %Ti, 0.05 ppm-0.1 %Tl, 0.05 ppm-0.1 %Tm, 0.05 ppm-0.1 %U, 5 ppm-1 %V, 1 ppm-1 %W, 0.5 ppm-0.1 %Y, 0.1 ppm-0.1 %Yb, 5 ppm-1 %Zn, 0.5 ppm-1 %Zr.

Data Processing and Interpretation: After all analytical techniques were carried out, all data were verified before interpretation. Subsequently, petrogenesis including initial rocks and metamorphism were discussed based on the collected data and previous works including regional geology and structural setting. Finally, conclusions in some crucial aspects were pointed out.

Report and Publication: Finally, report writing and manuscript preparation were carried out. This thesis report consists of 5 chapters. Introduction, reviewing overall researches and background in the study area and adjacency are reported along with scope of work, objective and methodology in chapter 1. Chapter 2 covers geologic setting and tectonic setting in the regional and study areas based on literature reviews. Chapter 3 describes field investigation and petrography. Chapter 4 includes whole-rock geochemistry and mineral chemistry. Finally, discussion in Chapter 5 is focused on petrogenesis, metamorphism of Lansang Metamorphic Suites. Appendices are summarized more data which are not reported in main chapters.

จุฬาลงกรณ์มหาวิทยาลัย
Chulalongkorn University

CHAPTER II
GENERAL GEOLOGY

2.1 Geologic Setting

Thailand consists of two major micro tectonic plates, Shan Thai to the west and Indo China to the east. Complex tectonic setting in Thailand was reported by Bunopas and Vella (1992) and Charusiri et al. (2002). Tectonic evolutions in this region can be subdivided into four stages. In the Archeotectonic stage, Shan-Thai and Indochina were cratonic parts of Gondwana and Pan-Cathaysia, respectively, prior to drifting away. Protolith of the high grade metamorphic basement appears to have deposited during Precambrian period. During Paleotectonic stage, Middle Paleozoic to Early Triassic, both micro-continents had separated and rotated from the parent cratons. Consequently, they began to develop sedimentary basins in both continents. The new blocks including Nakhon-Thai Ocean floor and Lampang- Chiang Rai volcanic arc occurred in this stage. Continent-continent collision during the Middle Triassic was caused by movement of Shan-Thai toward Indochina and South China. That was a part of Indosinian Orogeny. After collision in the Mesotectonic stage, granitic magmas intruded into sedimentary rocks as well as volcanic erupted onto the surface. In the Neuvotectonic stage, rapid rifting and opening of the gulf of Thailand during Late Cretaceous to Tertiary were then triggered after collision of Indian plate and Eurasia plate. Faulting after such collision was significantly constrained within three main directions including north-south, northwest-southeast and northeast-southwest.

Changwat Tak is located in northwestern Thailand between Mae Hong Son, Chiang Mai, Lamphun and Lampang to north, Uthai Thani and Kanchanaburi to the south, Sukhothai, Kamphaeng Phet, Nakhon Sawan and Uthai Thani to the east, and

Kayin State of Burma to the west. Regional geology is composed of metamorphic rocks, sedimentary rocks and unconsolidated sediments through geological times of Precambrian (> 570 Ma), Cambrian (505-570 Ma), Ordovician (438-505 Ma), Silurian - Devonian (360-438 Ma) Carboniferous (286-360 Ma), Permian (245-286 Ma), Triassic (210-245 Ma) Jurassic - Cretaceous (from 66.4 to 210 Ma), Tertiary (1.6 to 66.4 Ma) and Quaternary (0.01 to 1.6 Ma); during such periods, the sedimentary rocks had deposited in marine and continent environments. Their details are described below (see also Figure 4).

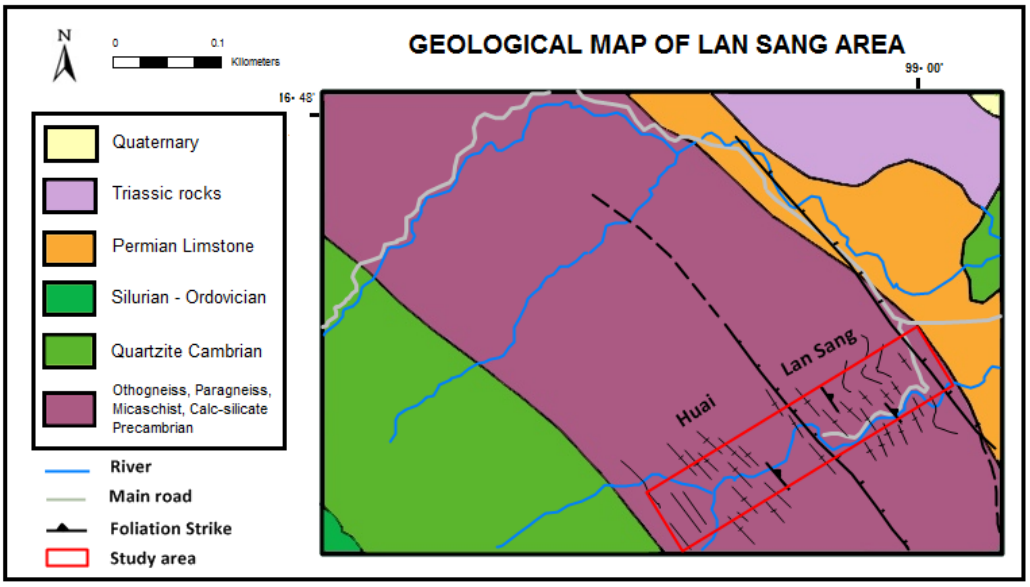

Figure 4. Geologic map of the Lansang Area (revised from Lacassin et al. (1997);Department of Mineral Resources (1999)) showing the location of study area (in the red rectangular) and geologic setting of the Mae Ping shear zone.

Precambrian rocks: Basement complex is composed of regional high-grade metamorphic rocks. Lower to Upper units are dominated by orthogneiss, paragneiss, schist, calc-silicate rock and marble. These high grade metamorphic rocks have

exposed beneath the Cambrian rock. Metamorphic grades range from greenschist facies to amphibolite facies.

Lower Paleozoic rocks:

Cambrian-Ordovician rocks consist of cross-bedding sandstone, conglomerate and siltstone interbedded with thin limestone containing Cronodon fossil. Some parts of this rock group appear to have been metamorphosed to schist, marble and quartzite.

Silurian-Devonian rocks are composed of brown to black chert interbedded with sandstone, grey shale and interbedded sub greywacke and limestone. According to Baum et al. (1970), cronodon and graptolite were found in black shale.

Upper Paleozoic rocks:

Carboniferous rocks mainly consist of sandstone and mudstone. Late Carboniferous rocks mostly display fossils, e.g., foraminifera, bryozoa, brachiopod, corals and fusulinid in the upper part (Department of Mineral Resources, 2007).

จุฬาลงกรณ์มหาวิทยาลัย
Chulalongkorn University

Permian rocks along the western part include conglomeratic limestone, sandstone interbedded with chert and thick limestone.

Mesozoic rocks: Mesozoic rocks in the western part overlie unconformable to the older rocks. These rocks can be subdivided into two groups including non-marine deposits (e.g., sandstone, siltstone and shale) and marine deposits (e.g., conglomerate, sandstone, shale, mudstone and limestone). Ages of fossil (e.g., corals) range from Middle Triassic and Middle Jurassic (Department of Mineral Resources, 2007).

Cenozoic rocks: are important sources of fossil fuel resources. Generally, Tertiary rocks appear to have deposited along intermountain basins as similar to the other parts of Northern Thailand.

Quaternary sediments: are mainly characterized by alluvial deposits.

Igneous Rocks: Granitic batholiths in this area belong to the central granite belt of Thailand. They consist of granite and gneissic granite. Ages of these igneous rocks range between 219 ± 13, 212 ± 4 and 208 ± 16 Ma (Beckinsale et al., 1979; Mickein, 1996; Teggin, 1975).

Mitchell (1977) mentioned that Southeast Asian contains three main granite belts as results of subduction and collision events in the region. Eastern belt occurred largely in Late Carboniferous to Early Triassic; Central belt took place in Late Triassic whereas western belt exposed later in Cretaceous to Early Eocene. Based on $^{40}Ar/^{39}Ar$ dating of granitiods of all belts in Thailand, their suggested that these granite belts appear to have formed in different geologic setting and tectonic event. Ages of eastern granite belt exposed within a range of 245-210 Ma during Early to Late Triassic. Central belt occurred about 220-180 Ma during in Late Triassic to Middle Jurassic. The western belt had been widely spreading in Late Cretaceous to Middle Tertiary about 80-50 Ma. S-type granites are mainly recognized in the western belt as a result of collision between Shan Thai and Indochina whereas S-type granites in the central belt were caused by collision between Shan Thai and Western Burma. On the other hand I-type granites significantly recognized in the eastern belt may have formed by subduction of oceanic plates into Shan Thai and Indo China (Charusiri et al., 1993).

It should be notified that the eastern belt granite and central belt granite have been found in the study area which can be described below.

จุฬาลงกรณ์มหาวิทยาลัย
CHULALONGKORN UNIVERSITY

Eastern Belt Granite usually exposes as small plutons or some batholiths which consist of slightly different types of granite forming complex plutons. Granites in this group are mostly cross cutting into host rocks of Upper Palaeozoic sedimentary rocks and pyroclastic rocks which are covered by the Korat sandstone. Texture of granite is characterized by equigranular grains within both coarse- and fine-grained textures. The mineral assemblages were proportionally plotted in the classification diagram of Streckeisen (1976) showing compositional range of syenogranite to gabbro (Department of Mineral Resources, 2007).

Central Belt Granite is characterized by large batholiths showing foliation in some areas which are similar to gneissic rocks. Consequently, they may be called as gneissic granite. General characteristics show coarse-grained texture with large feldspar crystals. Crystals are sometimes foliated and separated into white and black bands which are in segments of true granite that contains muscovite, tourmaline, feldspar and quartz. Moreover, fluorite, tin, tungsten and other opaque minerals occur sometimes in the central belt granite. Triangle plots designed by Streckeisen (1976) were carried out for these granite and showed compositional range of syenogranite, monzogranite, quartz syenite and quartz monzonite (Department of Mineral Resources, 2007).

Tak batolith is located between both major belts, eastern belt and central belt. It comprises calc-alkali granodioritic pluton and sub-alkali potassic pluton (Mahawat, 1990; Atherton et al., 1992). Chronological data, particularly Rb/Sr Whole-Rock Isochron, suggested that age of Tak batolith are between 208±16 Ma (Mickein, 1996).

Metamorphic rocks have exposed in all regions of SE Asia in which their structural evolution appears to have involved by India-Eurasia collision before

continental volcanic extrusion have occurred widely in the region referring the newly thermal history. The Chiang Mai-Lincang Belt (CM-LB) also has wide distribution of high grade metamorphic core complex and granitic rocks which have prominently exposed in western Thailand. Western metamorphic belt elongated within the north-south direction has been considered as part of Chiang Mai-Lincang belt. Based on tectonic setting, the Western Thailand is located in the Shan-Thai microcontinent (see Figure 5). It situates about 200 km east of the dextral Sagaing fault of Burma and 1500 km south of the eastern Himalayan syntaxis (Lacassin et al., 1993; Palin et al., 2013).

Mickein (1996) suggested that metamorphism in this area contain two main stages. The first stage, regional metamorphism, had occurred since ~200 Ma between Triassic-Jurassic periods indicated by gneiss formation in this event. The second stage had occurred between 117 and 72 Ma (inferred from U-Pb monazite) in Cretaceous before thrusting and uplifting in Oligocene – Miocene period.

จุฬาลงกรณ์มหาวิทยาลัย
Chulalongkorn University

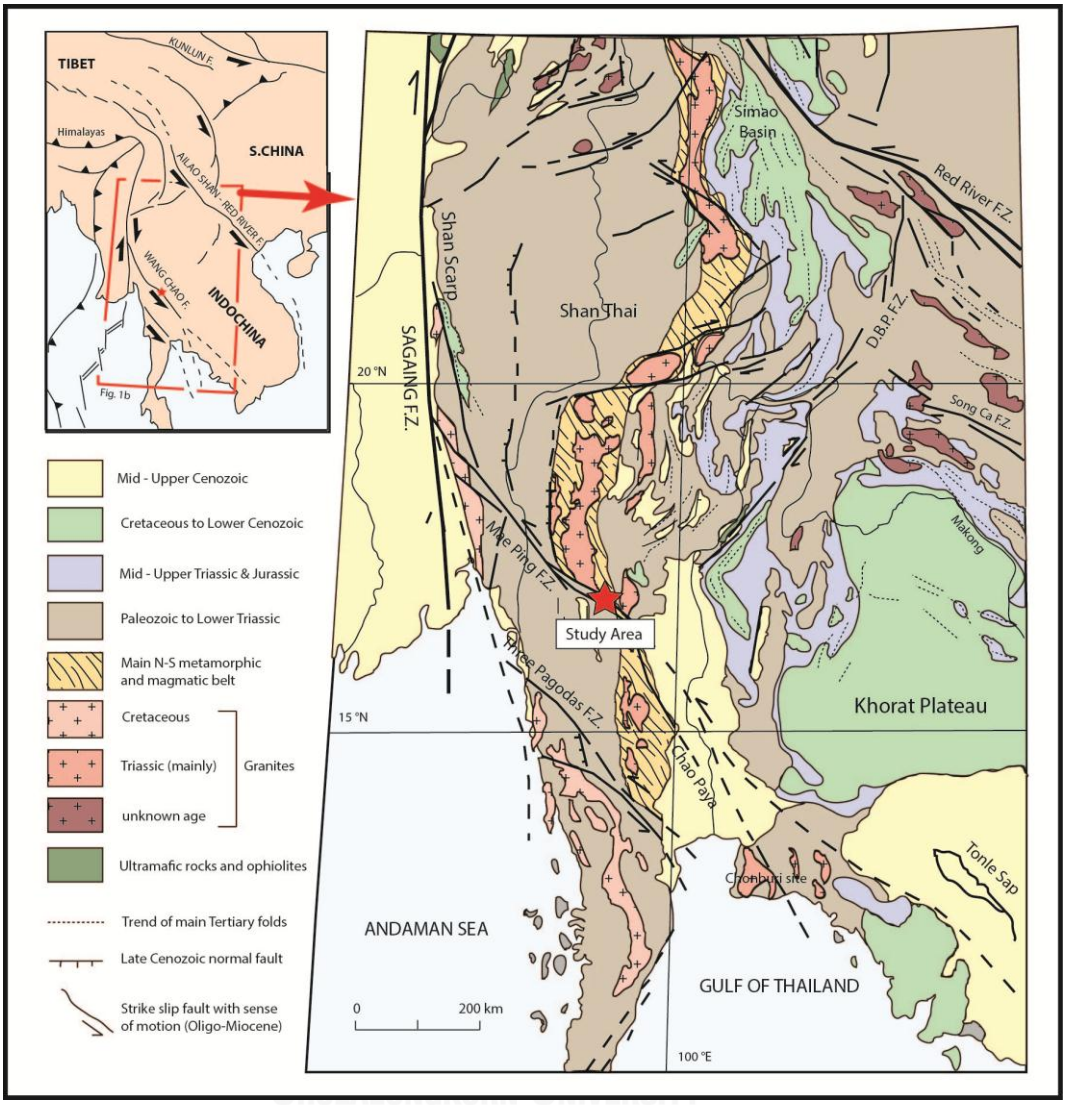

Figure 5. Map showing tectonic setting of Thailand. Mae Ping northwest-southeast striking fault are clearly observed in the Shan-Thai terrane (revised from Lacassin et al. (1997)). Red star showing the study area around the Lansang National Park, Changwat Tak. Local rocks have been considered as part of Chiang Mai-Lincang belt, which are composed of main N-S metamorphic and magmatic rocks.

Department of Mineral Resources (2007) reported that metamorphic rocks elongated within the north-south direction are related to tectonic settings. Salayapongse (2002) subdivided, based on ages and grades of metamorphism, these rocks into four belts from west to east. Western metamorphic belt is occupied by Precambrian to probably Middle or Upper Paleozoic rocks which appear to have continuously stratigraphic sequences and metamorphic grades. In general, the western metamorphic belt mainly consists of paragneiss, micaschist, quartzschist, calc-silicate and marble. Many authors have suggested that regionally high-grade metamorphic rocks or basement complex are characteristics of the Precambrian rocks.

Previous researchers (MacDonald et al., 1993; Macdonald et al., 2010) mentioned that the western metamorphic belt is an interesting and important area to be investigated particularly on regional stratigraphic correlation. In the other hand, numerous studies have been described for tectonic evolution of CM-LB core complexes which appear to have commenced in Late Eocene before uplift had taken place during Early Miocene (Macdonald et al., 2010; Morley et al., 2007; Rhodes et al., 1997; Rhodes et al., 2000).

จุฬาลงกรณ์มหาวิทยาลัย
Chulalongkorn University

The western metamorphic belts in Thailand can be divided into Doi Inthanon Metamorphic Core Complex Domain (DIMCCD) and strike-slip fault zone domain (SSFZD) (Macdonald et al. (2010), see Figure 6). These metamorphic rocks significantly elongate within the north-south direction and extend towards the Mae Ping fault. They gradually change orientation to northwest - southeast direction onto the north (Baum et al., 1970; Department of Mineral Resources, 2007; MacDonald et al., 1993; Macdonald et al., 2010).

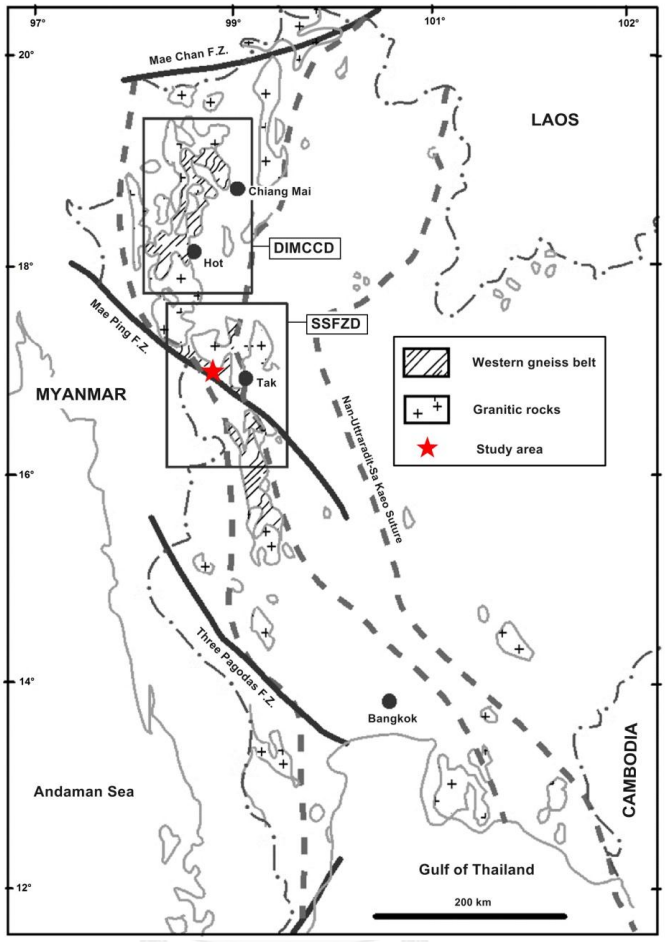

Figure 6. Map of the upper western Thailand showing distribution of gneissic rocks in the western metamorphic belt associated with igneous intrusions and the main Cretaceous strike-slip faults (Mae Ping and Mae Chan Faults). Doi Inthanon Metamorphic Core Complex Domain (DIMCCD) and The Strike-Slip Fault Zone Domain (SSFZD) are located in rectangles (revised from Macdonald et al. (2010)).

Macdonald et al. (1993; 2010) reported that Doi Inthanon Metamorphic Core Complex is N-S trending high-grade metamorphic belt extending to about 400 kilometers. Its features are similar to Cordilleran-type metamorphic core complex. This metamorphic belt comprises orthogneiss core complex with paragneiss, calc-silicate gneiss and marble in association with aplite and pegmatite. P-T ranges of peak metamorphism were estimated using TWQ v1.02 and v2.02 to generate equilibrium

reactions among mineral assemblage presents as in P-T-X diagrams. In addition, thermobarometers of orthogneiss and paragneiss using muscovite-biotite thermometer and phengite geobarometer were carried out by TWQ v1.02. Consequently, these results suggested that temperature range of about 725°C down to 535°C and pressure range of 7 kbar down to 3 kbar were taken place. In addition, P-T ranges estimated by TWQ v2.02 indicated that P-T ranges from core rim of paragneiss and granitic mylonite vary from about 650°C at 5-4 kbar to about 550°C at 3 kbar, respectively. Moreover, thermobarometric model of calc-silicate rocks representing two stages of mineral assemblages wuith in Wo+An+Grs+Cal+Qtz equilibria were also estimated P-T average between 693±59°C and 5.2±0.9 kbar using TWQ v1.02. Retrograde mineral, including zoisite at an arbitrary, suggested temperature should be about 470-530°C (at an arbitrary pressue of 3 kbar).

Stages of metamorphism along the Doi Inthanon metamorphic core complex, (reported by Macdonald et al. (2010)), appear to have been started by paragneiss metamorphism undertaking high-grade to medium pressure metamorphism between Triassic-Early Jurassic (ca. 210 Ma determined by U-Pb zircon from core of orthogneiss). Monazite age of 84 and 72 Ma (U-Pb monazite after MacDonald et al. (1993)) during Late Cretaceous may have attributed to thermal overprint up to upper amphibolite facies. The next metamorphism occurred in Late Eocene (40 Ma determined by U-Pb ages of zircon and monazite), which are compatible to the age of granitic mylonite from Doi Suthep for the early stage development leading to actual core complex. Late stage, based on $^{40}Ar/^{39}Ar$ dating of muscovite from Doi Inthanon and Doi Suthep granites, represented cooling age of about 26-15 Ma during Miocene with temperature yielded 350°C before detachment faulting and uplifting of the sheared core zone.

Geochronology studies using U-Pb zircon dating of Dunning et al. (1995) determined that the Doi Inthanon massif contains orthogneisse with initial parentage of I-type granite emplacement age of ca. 211-203 Ma which had metamorphed at about 84-72 Ma. Addition from MacDonald et al. (1993), granitic emplacement occurred at the same time, 203 ± 4 Ma before metamorphism taking place in 72 ± 1 Ma. A younger age obtained from leucogranite cross cut into Mae Klang Pluton at 26.8 ± 0.5 Ma were reported by Dunning et al. (1995).

Moreover, Fission track ages of zircon at 47±3 Ma and apatite at 40±2 Ma from Umphang gneiss for suggest that deep metamorphic rocks were uplift onto the surface during Early Eocene (Morley, 2012; Upton, 1999). These younger ages are overlapping with the Mogok metamorphic belt that was interpreted to represent age of high-grade metamorphism between 47-29 Ma using U-Pb zircon and monazite dating (Barley et al., 2003; Searle et al., 2007). Age of granitic rocks cross cutting host rock in Mogok belt were dated by U-Pb zircon at about 72, 48 and 44 Ma (Mitchell et al., 2012). Therefore, geochronological data suggest that tectonic process may start from crustal melting, metamorphism and deformation on a regional scale at the same time before developing of metamorphic core complex and sedimentary basin during Late Oligocene-Miocene (Macdonald et al., 2010; Morley and Racey, 2011; Morley et al., 2007).

In addition, large scale strike-slip faults in SE-Asia occurred after collision between India and Eurasia, such as Ailao Shan–Red River fault zone. Strike-slip fault zone domain in Thailand contains two parallel NW–SE trending shear zones, so-called Mae Ping shear zone to the north and Three Pagodas shear zone to the south.

Osanai et al. (2008) studied metamorphism in Vietnam related to adjacent areas in SE Asia. These metamorphic rocks distribute along NW-SE trending Red River zone. These rocks can be subdivided into high-grade metamorphic rocks and low-grade pelitic metamorphic rocks. A large scale of Red River fault zone extends over 1,000 km long cutting into Yunnan Province. Basement of high-grade metamorphic rocks has been considered to be Precambrian rocks covered by lower-grade Paleozoic rocks. Metamorphic core along the fault zone is made of steeply dipping with strongly foliated thin beds (Tapponnier et al., 1990).

Metamorphic evolution along the Red River shear can be subdivided in to five stages of deformation (Searle et al., 2010). It may start from early metamorphic rocks of amphibolite facies were intruded by K-feldspar orthogneisses and biotite granodiorites of mantle origin. Later stage of biotite leucogranites intruded into host rocks such as orthogneisses and migmatite before folding. Ductile stage from left-lateral strike-slip shear fabrics was occurred after crystallization with high-temperature event (about 500-550°C). Subsequently, leucogranite veins and dykes cross cut into the ductile strike-slip shear fabrics. Finally, normal faulting, prior to exhuming and uplifting of basement, may lead to thermal overprint time of Indosinian age during Late Eocene–Oligocene. U-Th-Pb ages of granites were obtained at between the earlier deformed leucogranites (31.9-24.2 Ma) and the late cross cutting dykes (about 21.7 Ma).

Three Pagodas shear zone (TPSZ) is approximately 25 km wide and 250 km long. Many researchers have interpreted this fault zone cutting through the lower central plain continue to the Gulf of Thailand (Bunopas, 1981; Lacassin et al., 1997; Morley, 2002; Polachan et al., 1991; Tapponnier et al., 1986). Along the NW–SE trending Three Pagodas shear zone, Thabsila metamorphic complex was exposed. Generally, rocks

comprised 4 main units: unit A is composed of marble, mica schist and quartzite; unit B comprises mylonites; unit C is composed of calcsilicate; unit D comprises gneissic rocks. P–T estimations of four units calculated by geothermobarometry and pseudosection were taken place using Perplex, Mathematica package PET. Unit A undertaken medium amphibolite facies conditions of 550-650°C and 5-6.5 kbar based on Grt-Bt thermometer and Grt-Pl-Bt barometer. While units B based on Grt-Bt thermometer and GASP and GRAIL barometer, unit c based on anorthite and meionite, unit D used Grt–Bt thermometer and GRAIL barometer, for model calculation for temperature and pressure estimation yielded about 640-710°C and 5.5-8 kbar for these units (Nantasin et al., 2012). Chronological data of metamorphic zircon rims from LA-ICP-MS yielded metamorphism age between 51–57 Ma related to India and Eurasia collision. Subsequently, cooling age from Rb–Sr isochron ages of biotite is about 32–36 Ma with cooling temperature of 350-300°C.

In eastern Thailand, Nong Yai Gneiss along Klaeng fault zone includes high-grade metamorphic rocks which elongate in N-S direction extend about 30 km. Most rocks are composed of amphibolite to granulite high-grade gneissic rocks. Deformation history and geochronology of Nong Yai gneiss indicate tectonic evolution. LA-MC-ICP-MS U-Pb zircon dating suggested the leucogranite intrusion took place at 78.6±0.7 Ma and magmatic crystallization; these were followed by a second crystallization at 67±1 to 72.1±0.6 Ma in the Late Cretaceous during Western Burma and Shan Thai collision (Kanjanapayont et al., 2013).

In the study area, the Lansang National Park located in the west of Changwat Tak, is a part of affected area from northwest-southeast striking faulting. This can be indicated by cross cutting and sinistral displacement into the metamorphic belt of the

area. Kanjanapayont et al. (2011) summarized the regional geology of this area and reported that mylonitized greenschist-facies gneiss covers about 5 km wide. Rocks consist only of high-grade paragneisses and orthogneisses that show steep foliation and stretched lineations (Lacassin et al., 1993; Lacassin et al., 1997). They are covered by the Lower Paleozoic low grade metamorphic rocks and sedimentary rocks. Morley (2004) suggested that the shear zones within this area are associated with the Mae Ping fault in which it was developed in Lower Cretaceous to Upper Cenozoic during tectonic extension.

Palin et al. (2013) mentioned that the Mae Ping strike-slip motion extends over 600 km, exposures of high-grade orthogneiss in the Lansang National Park contain of strong mylonitic textures and ductile-brittle shear rocks. Two crystallization stages inferred from geochronological analysis of monazite in orthogneiss, with core regions Th–Pb ages between about 123 and 114 Ma. These evidences indicate magmatic protolith emplacement for the Lansang orthogneiss during Early Cretaceous. Rim region ages range between about 45–37 Ma which can indicate metamorphism occurring during the. In addition, monazite from granite dyke at Bhumipol Lake produced Th–Pb age of 66.2±1.6 Ma. This age was interpreted as timing of dyke emplacement, shear movement, magmatism and high-grade metamorphism, respectively. All geochronological data are reported in Appendix A.

CHAPTER III
PETROGRAPHY

More than 20 samples of metamorphic rocks from the study area around the the Lansang Nation Park, Changwat Tak were collected and prepared as thin sections for initial petrographic investigation (see Figure 7). Classification of rock types were obtained from petrographic description under polarizing microscope.

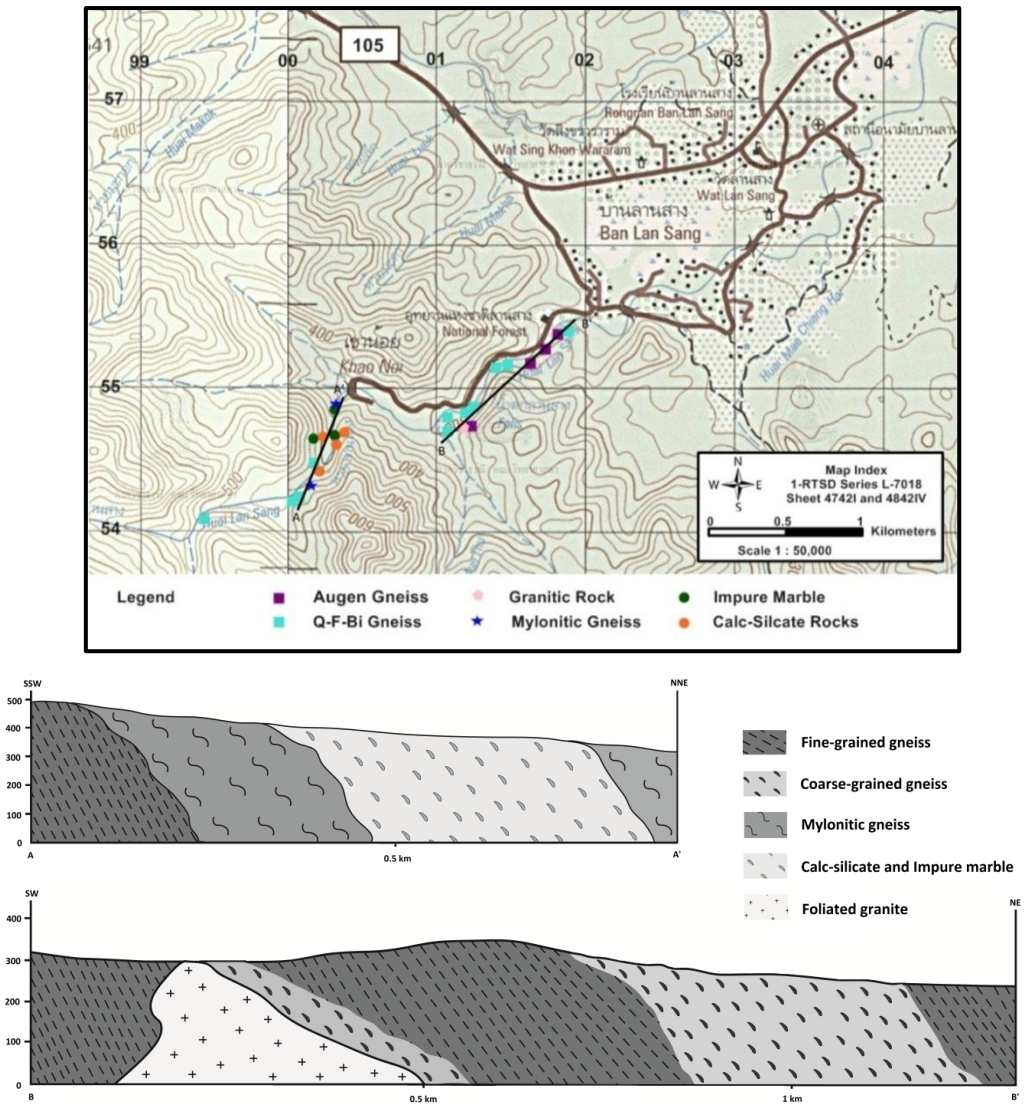

Figure 7. Topographic map (4842IV) showing sample locations around the Lansang National Park, Changwat Tak and geologic cross sections of the area.

3.1 Field Observation

Lansang National Park is located 19 kilometers south of Tak City. The Lansang National Park covers an area of 104 square kilometers. Generally, the general altitude ranges from 250 to 1,065 meters at Doi Oomyod. Metamorphic rocks along the Mae Ping strike-slip fault zone are composed of gneissic rocks, calc-silicate rocks and plutonic rocks.

Field investigation was carried out to collect background information and rock formation of Lansang metamorphic suites in the study area. Observation and field data are summarized in Appendix B.

Local rocks in the Lansang area are usually dipping towards northwest direction. They mostly reveal mylonitic texture with shear ductile-brittle deformation. Intrusions are found widely distributing as both concordant to discordant dykes. These dykes are described as foliated biotite microgranite which seems likely gneiss, deformed leucogranite and pegmatite veins. Their foliations are parallel to the host rocks in this area. In addition, evidences of ductile shear and brittle stages are also observed as subsequent process of these rocks (see Figure 8).

For instant, Lansang metamorphic suites may be involved by the initial proportion of host rocks including gneissic rocks and calc-silicate rocks. Subsequently, granitic dyke, pegmatite and luecocratic vein appear to have cross cut into these host rocks. Regional metamorphism has occurred before ductile-brittle stage from strike-slip movement along the Mae Ping Fault zone.

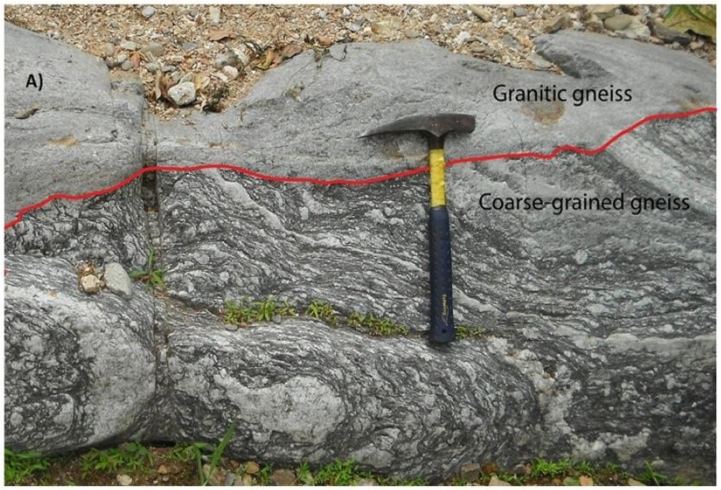

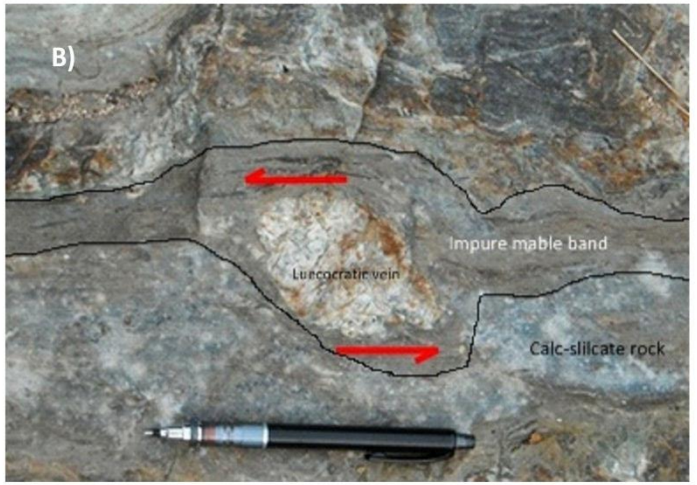

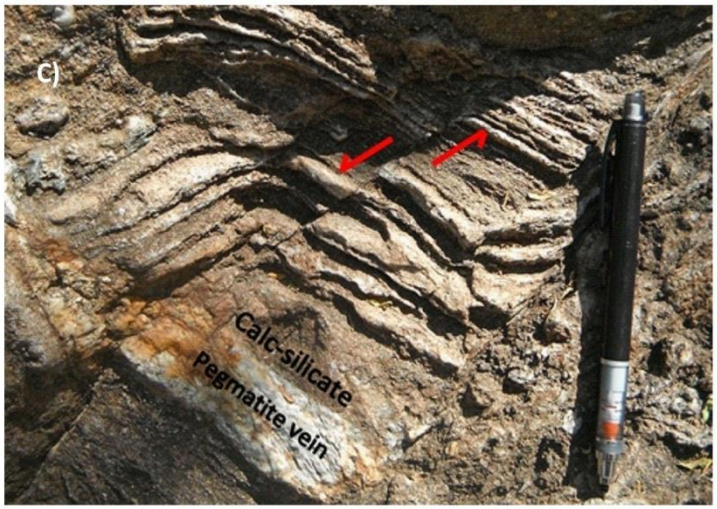

Figure 8. Outcrops showing evolution of ancient tectonic in this area: A) Granitic gneiss intruded into coarse-grained gneiss; B) Sheared leucocratic vein with impure marble band of calc- silicate rock show intense movement; C) Fault cross cut the strongly-deformed calc-silicate with garnet-bearing pegmatite vein.

3.2 Petrographic Investigation

The Lansang metamorphic suites show distributions of the main rock units including gneissic rocks, calc-silicate rocks and foliated granite. These rocks locally show mylonitic texture and ductile shear stretch of mineral. Detailed descriptions of each group are reported below.

3.2.1 Gneissic Rocks

The gneissic rocks are the most often found in the Lansang National Park. Large outcrops are naturally exposed along Huai Lansang. These samples clearly consist of quartz, feldspar and biotite in hand specimen. Gneissic rocks can be separated into two main groups which are characterized clearly by grain sizes in field observation including very fine-grained to coarse-grained gneissic rocks associated with pegmatite vein, luecrocratic vein and dyke. Fine-grained rock layers show foliated and interbeded coarse-grained crystals, porphyroblastic to augen gneissic texture of quartz, plagioclase and K-feldspar. Stretched porphyroblasts are evidences of the ductile shear stage including boudinage, rotating of clast, and σ-type of leucocratic vein. Moreover, some areas show brittle stage including minor faults, cracks and joints overprinting ductile shear texture.

Petrographic study can subdivide gneissic rocks, based on average grain size and mineral composition, into three groups including coarse-grained gneiss, fine-grained gneiss and very fine-grained gneiss.

Coarse-grained gneiss

These samples are coarse-grained gneissic rocks (ranging between 0.3 to 2.5 cm in diameter); they have greyish to dark grey color. Porphyritic to augen gneissic texture are generally observed as shown in Figure 9. Coarse-grained gneisses were

collected from 4 locations in the Lansang National Park. These samples usually contain porphyroblastic feldspar that shows ductile shear stage. Mineral assemblages are mostly composed of 35% quartz, 25% plagioclase, 20% K-feldspar and 20% biotite with accessories of chlorite, zircon, monazite and opaque mineral. Coarse-grained gneiss contains two layers similar to fine-grained gneiss. Leucosomes consist of quartz, K-feldspar and plagioclase which are ranging from medium- to coarse-grained granoblastic groundmass. They are usually subhedral to anhedral grains. Medium- to coarse-grained porphyroblasts of K-feldspar show ductile subhedral grain and grain rotation which appears to associate with lateral shear in the area. Melanosomes, interbanded with white bands, contain lepidoblastic biotite. Chlorite may occur along boundaries of biotite; they indicate greenschist facies (see in Figure 9D).

In general, petrographic features of rock are recognized as granoblastic groundmass and porphyroblastic K-feldspar within the white band. Lepidoblastic biotites are usually found in dark bands (Figure 9C). The other textures are augen mylonitic texture (Figure 9B) and poikilitic texture.

จุฬาลงกรณ์มหาวิทยาลัย
Chulalongkorn University

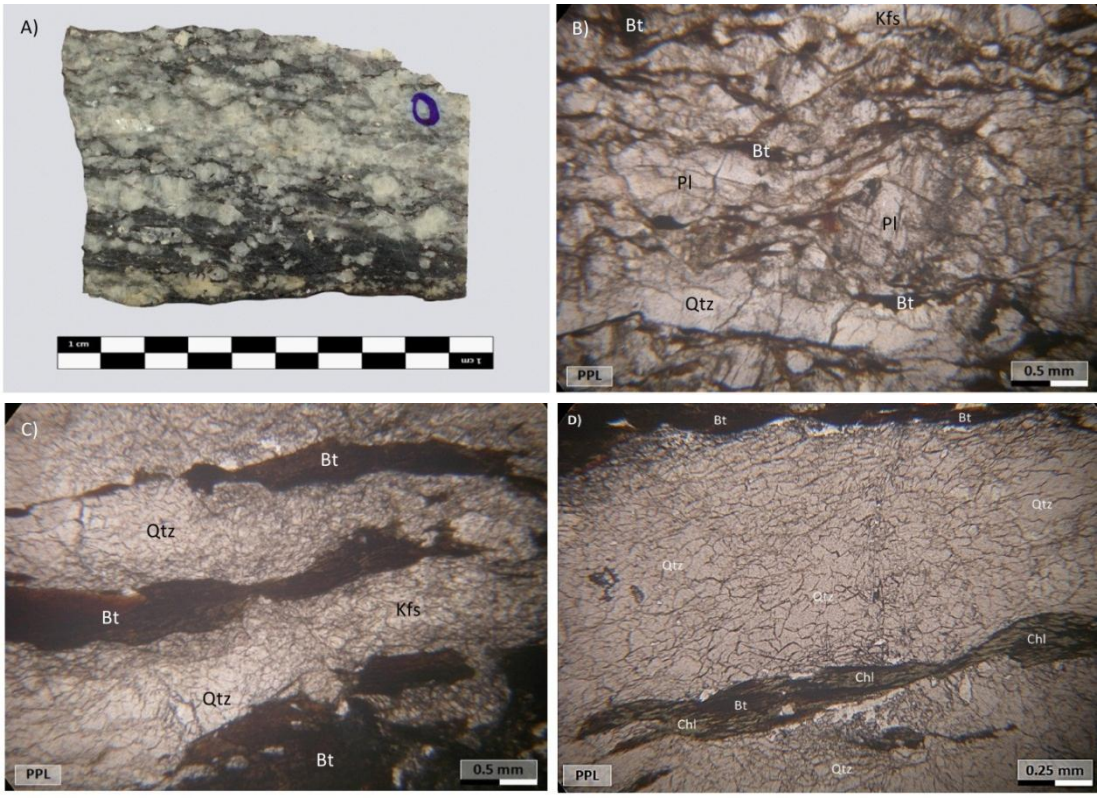

Figure 9. Coarse-grained gneiss: A) a coarse-grained slab sample showing K-feldspar (Kfs) porphyroblast; B) photomicrograph showing augen mylonitic texture (PPL); C) isogranular texture of groundmass and biotite (Bt) lepidoblast (PPL); D) medium to coarse-grained groundmass which chlorite (Chl) occurred along boundaries of lepidoblastic biotite.

จุฬาลงกรณ์มหาวิทยาลัย
Chulalongkorn University

Fine-grained gneiss

These specimens are fine-grained gneissic rocks. They usually have pale grey to dark grey colors that are mostly observed in this area (see Figure 10). Rock collection of fine-grained gneiss includes 11 samples. Mineral assemblages contain essentially of 35% quartz, 25% plagioclase, 25% K-feldspar, 15% biotite and minor contents of chlorite, amphibole, monazite, apatite, zircon and opaque mineral. Some samples show rare amount of amphibole. These rocks show two distinctive layers including leucosome and melanosome. Leucosomes are mostly composed of 35% quartz, 25% plagioclase,

20% K-feldspar. Fine to medium-grained granoblastic quartz and feldspar usually form subhedral to anhedral. The common texture including granoblastic texture is observed in these bands. Melanosomes mostly consist of 15% biotite with minor contents of amphibole and chlorite in some areas. Anhedral lepidoblatic biotite crystals range in size from fine to medium grain, which chlorite occurs along boundaries of biotite indicates greenschist facies (Figure 10B). Medium- to fine-grained nematoblastic amphiboles are subhedral to anhedral rhombohedral crystal showing strong pleochroism. Fine-grained chlorites are mostly anhedral crystals formed around boundaries of biotite which seem to be indication of retrograde process (see Figure 10C).

Petrographic features of these rocks are mainly granoblastic texture which isogranular texture of white bands. Biotite and small amount of amphibole show lepidoblastic and nematoblastic textures, respectively. The other textures are augenmylonitic texture, blastomylonitic texture (Figure 10D), nematoblastic texture, mosaic texture and poikilitic texture. Moreover, porphyroblastic texture may also be observed in some areas.

จุฬาลงกรณ์มหาวิทยาลัย
Chulalongkorn University

Petrographic characteristics of fine-grained gneiss in this area show two stages of metamorphism; amphibolite facies are composed of quartz, plagioclase, K-feldspar, biotite and amphibole with absence of muscovite. The later stage is greenschist facies which consist of quartz, plagioclase, chlorite, biotite and K-feldspar.

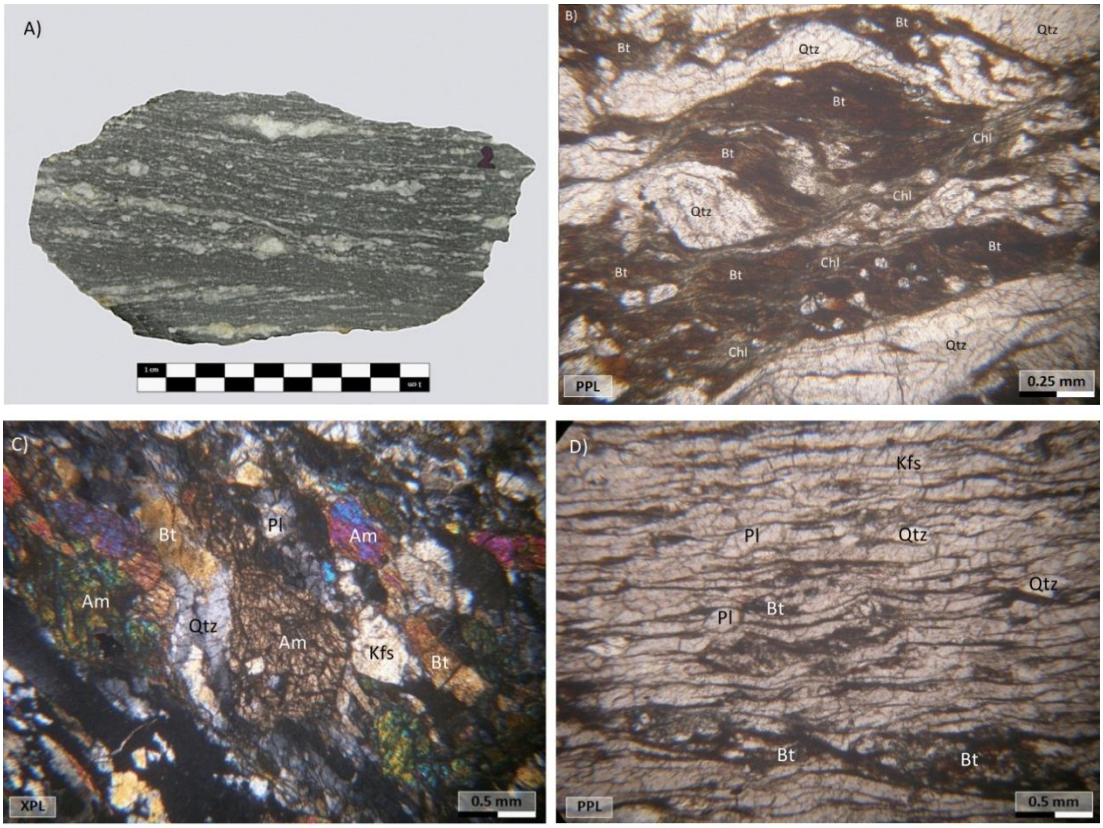

Figure 10. Fine-grained gneiss: A) a fine-grained greyish slab sample; B) photomicrograph showing granoblasts of quartz (Qtz) interbanded with biotite (Bt) and chlorite (Chl) lepidoblastic textures (PPL); C) photomicrograph showing subhedral to anhedral amphiboles (Am) showing perfect cleavages (XPL); D) fine-grained gneiss with blastomylonitic texture (PPL).

Very fine-grained gneiss

Very fine-grained gneisses are similar to feature of gneissic rocks undertaken mylonitic ductile stage. Two samples were collected from two outcrops nearby Lansang waterfall and Pa Pueng waterfall in which they occur beside thick band of calc-silicate and impure marble. Mineral compositions of fine-grained groundmass are mainly composed of 45% quartz, 20% biotite and 35% feldspar. Porphyroblasts of plagioclase and K-feldspar range from medium to fine grains which show augenmylonitic texture (Figure 11D). Chlorites occur around the boundaries of fine-grained biotite and other

groundmasses which indicate greenschist facies. Monazite and zircon are rarely observed in these samples (see Figure 11).

In addition, rock features are hetrogranular texture with various grain sizes. The coarse-grained feldspars clearly show porphyroblastic texture (Figure 11B). Most porphyroblasts have rounded grain and show rotated and stretched crystals (Figure 11C). The other textures are augenmylonitic texture and poikilitic texture.

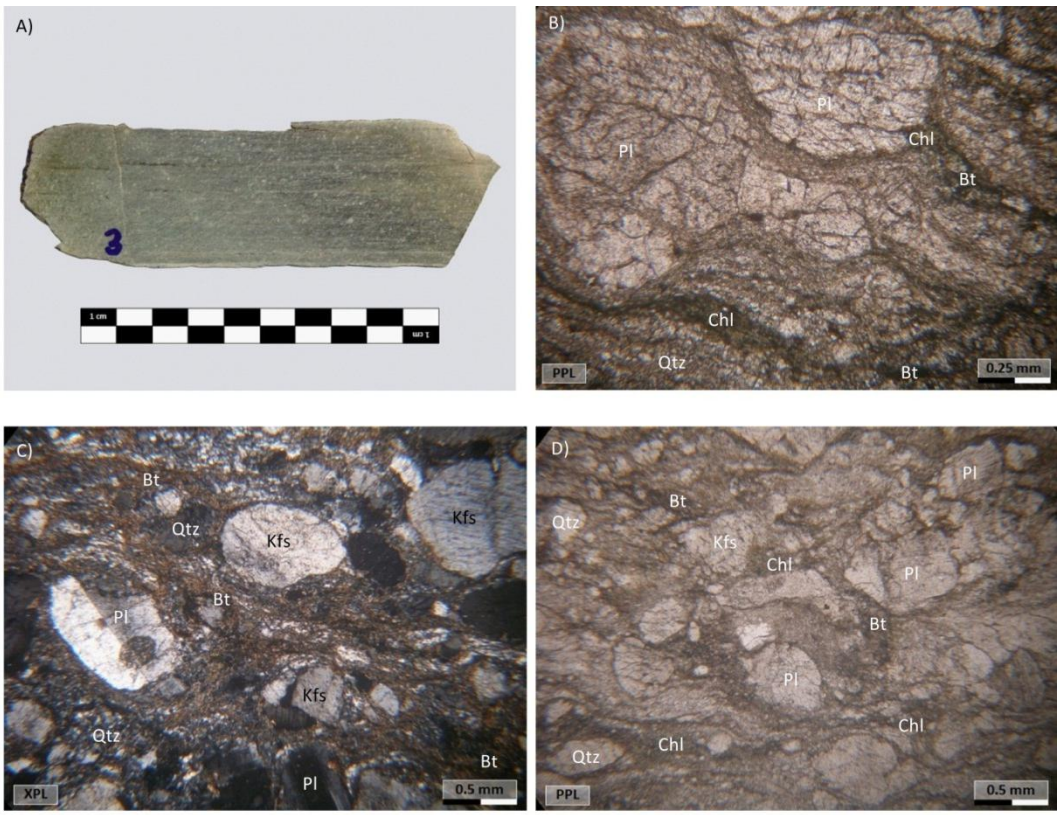

Figure 11. Very fine-grained gneiss: A) a greenish grey to dark grey slab sample; B) photomicrograph showing coarse-grained porphyroblastic plagioclase (Pl) and fine-grained layer of biotite (Bt) and chlorite (Chl) (PPL); C) heterogranular texture with rotated clasts of plagioclase (Pl) and K-feldspar (Kfs); D) augenmylonitic texture with rounded and stretched class of quartz (Qtz), plagioclase (Pl) and K-feldspar (Kfs) (PPL).

3.2.2 Calc-Sillicate Rocks

In general, calc-silicate rock and impure marble are found interbanded with gneissic rock with strong deformation that show foliation parallel to the other rocks in this area. These rock exposures are natural outcrop occurred as thin layer to thick band (> 1m), especially at the Lansang waterfall. Calc-silicate rock contains several layers of green, purple, brown, white bands with dark grey of impure marble which show stretched ductile clasts of leucocratic vein which cross cut into these rocks before shear-lateral stretching (see Figure 8B). Sample collection of 7 samples and their petrographic details are reported below.

Calc-silicate rock usually contains calcium-bearing silicate minerals probably formed by impure limestone and other sedimentary rocks. These rocks consist of several layers made by alternating mylonitization of green, brown and white bands which are composed of 35 quartz, 45% feldspar, 17% calcite, 2% garnet and minor amounts of amphibole, biotite, diopside and chlorite (see Figures 12). The dark grey band consists of fine-grained calcite matrix and minor clasts of feldspar, quartz, amphibole and biotite. These rocks show granoblastic and porphyroblastic textures with hetrogranular texture of several grain sizes. The darker bands show sutured or saccharoidal texture of recrytalized calcite. The other textures are poikilitic texture and blastomylonitic texture (Figure 12C).

In addition, pale to dark grey impure marble bands contain majority of fine- to medium-grained calcite matrix (over 80-90%) and minor clasts of quartz, feldspar, garnet, diopside, fine-grained amphibole and biotite. Granoblastic textures of groundmass with hetrogranular grains are commonly observed (Figure 12F). Coarse-

grained rocks clearly show porphyroblastic texture and poikilitic texture. Minerals' reaction rims indicate alteration of these rocks can be often observed (Figures 12E).

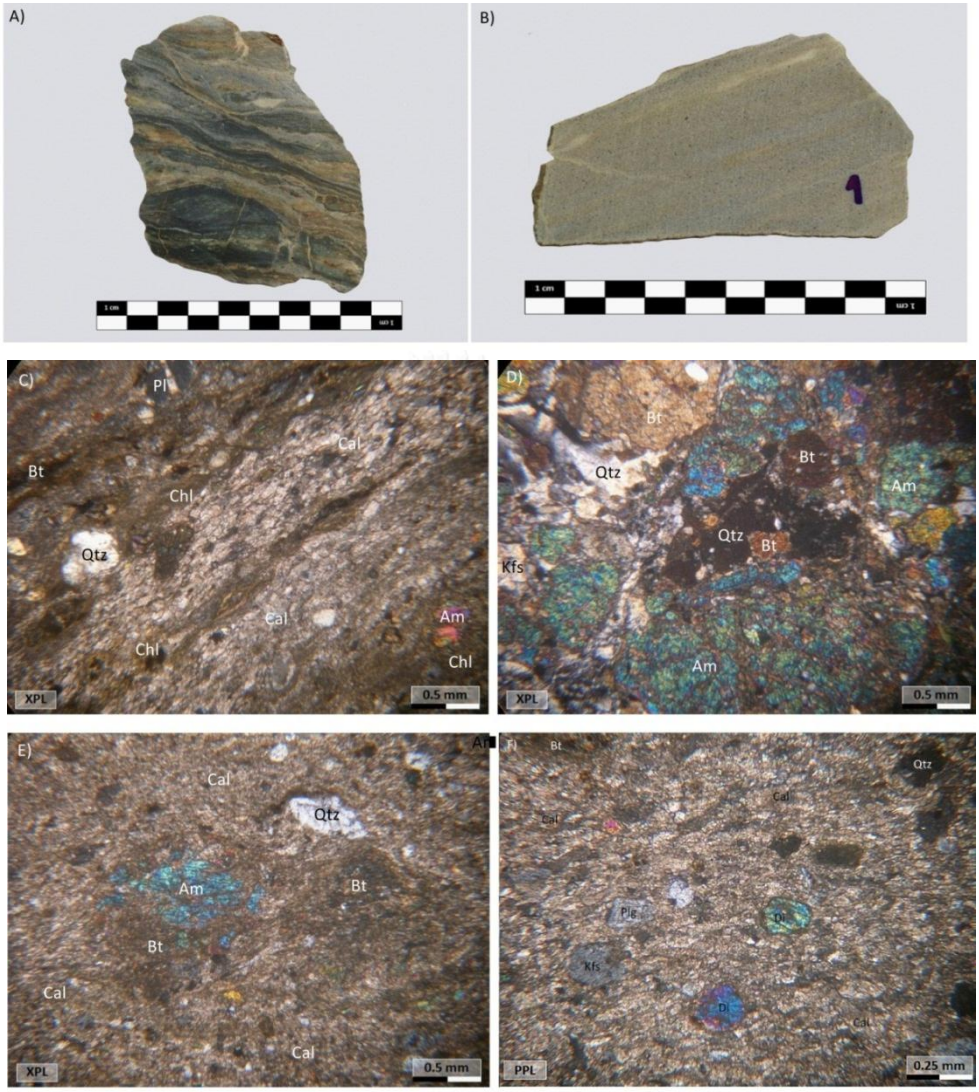

Figure 12. Calc-silicate rocks: A) a slab presenting alternating of several layers in calc-silicate rocks; B) a slab showing pale grey fine-grained impure mable; C) photomicrograph showing gneissic blastomylonitic band associated with fine-grained calcite (Cal) band show suture or saccharoidal texture (XPL); D) mineral composition of amphibole (Am), biotite (Bt), calcite (Cal), plagioclase (Pl) and quartz (Qtz) (XPL); E) fine-grained calcite (Cal) matrix with porphyroblasts of amphibole (Am) showing reaction rim besides fine-grained biotite (Bt) (XPL); F) pophyroblasts of diopside (Di) and feldspar (Fel) and amphibole (Am) embedded within fine-grained calcite matrix.

3.2.3 Granitic Gneiss

Granitic gneiss in this area is found in association with host rocks including gneissic rock and calc-silicate rock. These granite gneisses subsequently intruded into coarse-grained gneiss and calc-silicate rocks. However, these intrusions show foliation parallel to those observed in the host rocks. In addition, they are characterized by various types including pegmatite, leucocratic and microgranites which also show ductile deformation similar to the host rocks (see Figure 8A).

These rocks contain 40% quartz, 35% feldspar, 10-15% biotite and small amount of chlorite with rare accessories of zircon, monazite and opaque minerals (see Figure 13). Rock samples are medium-grained texture with average grain sizes ranging between 0.05-1.0 cm in diameter. Granoblastic quatz and feldspar with lepidoblastic biotite (Figure 13B) usually form as anhedral crystals. Petrogrphic features are hetrogranular texture with poikilitic texture and triple junction.

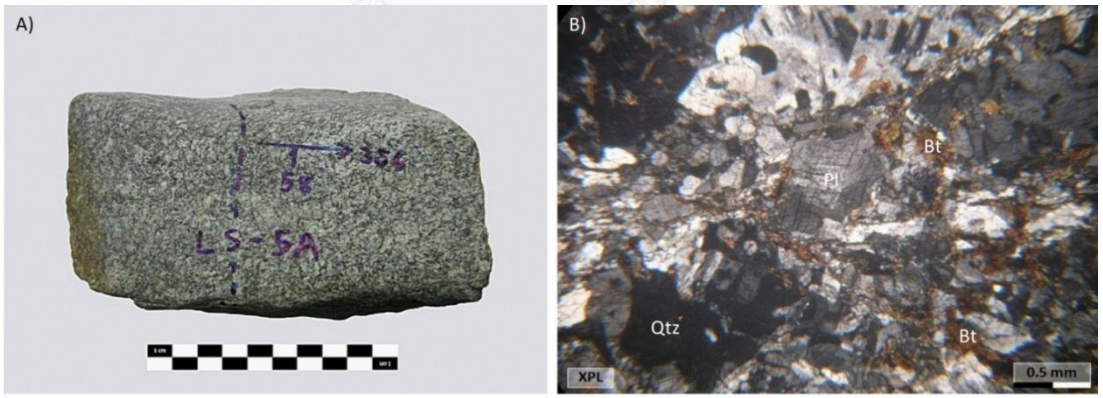

Figure 13. Granitic gneiss: A) a hand specimen showing foliation; B) poikilitic texture and triple junction in some areas (XPL) with mineral composition of granoblastic quartz (qtz) and plagioclase (Pl) and lepidoblastic biotite (Bt) (XPL).

CHAPTER IV
WHOLE-ROCK GEOCHEMISTRY AND MINERAL CHEMISTRY

4.1 Whole-Rock Geochemistry

Gneissic rocks, calc-sillicate rocks and foliated-granite were analyzed for whole-rock geochemical compositions. These samples were analyzed for major and minor oxides by X-ray Fluorescence (XRF) Spectrometer based at Department of Geology, Faculty of Science, Chulalongkorn University. Trace elements and rare earth elements (REE) of gneissic rocks and foliated-granite were determinate by Inductively Coupled Plasma-Mass Spectrometer (ICP-MS) based at the mineral and geological services by SGS (Thailand) Limited. The results are compared to the other published data, for consideration of initial rock and tectonic setting.

In addition, mineral chemistry of each rock type is also analyzed by Electron Probe Micro-Analyzer (EPMA) at Department of Geology, Faculty of Science, Chulalongkorn University. After petrographic study, representative samples of each type were selected, based on petrographic features including crucial textures and mineral assemblages, for mineral chemistry analysis. The investigation of metamorphic equilibriums was carried out based on these data which will be reported in the next chapter. Therefore, peak metamorphism can be constructed from P-T condition estimated by chemical compositions of metamorphic minerals in these samples.

4.1.1 Major Oxides

Major and minor compositions of each rock type using XRF are reported in weight% oxides including SiO_2, Al_2O_3, Fe_2O_3, FeO, MgO, CaO, MnO, K_2O, Na_2O, TiO_2 and P_2O_5. Representative analyses were selected and summarized in Table 1 and Table 2.

For gneissic rocks, coarse-grained gneisses are composed of 64.2-72.0 wt% SiO_2 (av. 67.4%), 12.3-15.8 wt% Al_2O_3 (av. 14.4%), 0.3-0.5 wt% Fe_2O_3 (av. 0.4%), 3.0-4.4 wt% FeO (av. 3.5%), 1.2-2.6 wt% MgO (av. 1.8%), 0.5-3.4 wt% CaO (av. 2.3%), 4.6-8.4 wt% K_2O (av. 6.5%), 1.3-3.8 wt% Na_2O (av. 2.5%), 0.7-0.9 wt% TiO_2 (av. 0.7%) and about 0.2 wt% P_2O_5.

Fine-grained gneisses are composed of 61.8-79.2 wt% SiO_2 (av. 66.6%), 6.3-15.8 wt% Al_2O_3 (av. 13.2%), 0.2-0.7 wt% Fe_2O_3 (av. 0.5%), 1.4-6.0 wt% FeO (av. 4.4%), 2.1-3.4 wt% MgO (av. 2.8%), 2.3-6.8 wt% CaO (av. 4.0%), 1.5-6.5 wt% K_2O (av. 4.9%), 0.6-2.7 wt% Na_2O (av. 2.1%), 0.3-1.0 wt% TiO_2 (av. 0.8%) and 0.3-0.4 wt% P_2O_5 (av. 0.3%).

Very fine-grained gneisses are composed of 64.4-69.4 wt% SiO_2 (av. 66.9%), 15.1-17.5 wt% Al_2O_3 (av. 16.3%), about 0.3 wt% Fe_2O_3, 2.4-2.8 wt% FeO (av. 2.6%), 1.2-1.5 wt% MgO (av. 1.3%), 4.0-4.7 wt% CaO (av. 4.4%), 3.1-3.4 wt% K_2O (av. 3.2%), 3.8-4.4 wt% Na_2O (av. 4.1%) and 0.4-0.5 wt% TiO_2 (av. 0.4%).

จุฬาลงกรณ์มหาวิทยาลัย
Chulalongkorn University

For calc-sillicate rocks, they can be separated into two distinctive bands, calc-silicate and impure marble. The calc-silicate bands consist of 50.2-62.6 wt% SiO_2 (av. 57.9%), 8.6-10.0 wt% Al_2O_3 (av. 9.3%), about 0.3 wt% Fe_2O_3, 2.6-3.0 wt% FeO (av. 2.8%), 3.3-6.3 wt% MgO (av. 4.4%), 9.6-20.4 wt% CaO (av. 14.0%), 3.0-4.5 wt% K_2O (av. 3.8%), 0.8-1.3 wt% Na_2O (av. 1.0%) and 0.3-0.4 wt% TiO_2 (av. 0.3%). On the other hand, impure marble bands yield 27.3-35.6 wt% SiO_2 (av. 30.1%), 2.0-4.6 wt% Al_2O_3 (av. 3.1%), about 0.1 wt% Fe_2O_3, 0.9-1.2 wt% FeO (av. 1.1%), 1.6-2.2 wt% MgO (av. 2.0%), 39.8-55.2 wt% CaO (av. 50.0%), about 0.2 wt% MnO, 1.0-1.9 wt% K_2O (av. 1.3%), 0.1-0.5 wt% Na_2O (av. 0.3%) and about 0.1 wt% TiO_2.

Granitic gneiss (only one analysis available for this study) consists of 68.4 wt% SiO_2, 15.3 wt% Al_2O_3, 0.2 wt% Fe_2O_3, 2.2 wt% FeO, 0.8 wt% MgO, 3.0 wt% CaO, 5.8 wt% K_2O, 3.3 wt% Na_2O and 0.4 wt% TiO_2.

Table 1. Whole-rock analyses of gneissic rocks and granitic gneiss from the Lansang National Park, Changwat Tak. Major and Minor oxides (%wt) obtained from XRF analysis and trace elements (ppm) obtained from ICP-MS analysis.

Name	Gneissic Rocks												Granitic gneiss
	Coarse-grained Gneiss			Fine-grained Gneiss							Very fine-grained Gneiss		
	LS-5B	LS-23A	LS-23B	LS-1A	LS-1B	LS-4A	LS-4B	LS-10A	LS-10B	LS-12B	LS-12A	LS-16A	LS-5A
SiO_2	64.19	71.93	66.10	79.20	64.97	62.37	67.64	62.28	61.77	67.88	69.36	64.40	68.38
Al_2O_3	15.19	12.31	15.77	6.26	13.73	15.75	13.14	14.59	14.69	14.14	15.07	17.48	15.34
Fe_2O_3	0.49	0.33	0.34	0.15	0.64	0.56	0.51	0.60	0.67	0.31	0.27	0.31	0.24
FeO	4.42	3.00	3.08	1.37	5.74	5.01	4.58	5.38	6.02	2.76	2.44	2.76	2.19
MgO	2.60	1.20	1.60	2.85	2.74	2.84	2.61	3.11	3.38	2.12	1.17	1.47	0.84
CaO	2.93	0.53	3.36	6.80	2.37	3.59	2.81	5.33	5.06	2.33	4.01	4.69	2.95
MnO	bdl	bdl	bdl	bdl	0.17	bdl	bdl	bdl	bdl	bdl	bdl	bdl	bdl
K_2O	6.33	8.43	4.58	1.52	6.21	5.81	5.03	4.83	4.30	6.54	3.06	3.38	5.79
Na_2O	2.38	1.32	3.78	0.54	1.93	2.59	2.24	2.46	2.43	2.66	3.78	4.38	3.33
TiO_2	0.85	0.66	0.70	0.29	0.97	0.78	0.96	0.81	0.96	0.51	0.37	0.50	0.41
P_2O_5	bdl	bdl	0.24	bdl	bdl	0.29	bdl	bdl	0.25	0.39	bdl	bdl	bdl
LOI	0.71	0.71	0.86	0.54	1.28	0.94	0.85	0.86	1.41	0.96	0.94	0.69	1.21
Total	100.09	100.42	100.42	99.52	100.74	100.54	100.36	100.25	100.94	100.60	100.47	100.05	100.68
Elements (ppm)													
Ba	1150.00	700.00	1110.00	510.00	930.00	1030.00	810.00	930.00	1260.00	930.00	740.00	610.00	1040.00
Ce	88.20	67.80	109.00	56.60	58.30	86.90	112.00	55.20	62.60	112.00	36.80	29.90	54.80
Co	39.90	43.20	35.10	151.00	34.40	33.00	59.10	36.00	37.00	41.80	26.30	49.40	51.60
Cr	70.00	<10	40.00	90.00	80.00	70.00	90.00	50.00	60.00	80.00	<10	20.00	20.00
Cs	4.50	2.70	3.20	1.30	2.70	7.70	5.50	5.40	2.30	14.50	3.60	16.50	3.00
Cu	<10	<10	<10	80.00	20.00	<10	<10	<10	10.00	<10	<10	<10	<10
Dy	2.37	0.75	4.51	3.78	10.70	3.91	2.11	5.46	4.41	3.93	1.14	1.40	1.72
Er	1.19	0.19	2.30	2.22	12.30	1.82	0.98	3.15	2.52	1.95	0.61	0.90	0.91
Eu	1.48	0.69	1.05	0.90	1.18	1.14	0.84	1.22	1.48	1.23	0.60	0.72	0.69
Ga	18.00	14.00	20.00	7.00	15.00	19.00	17.00	18.00	17.00	19.00	20.00	24.00	18.00
Gd	3.62	2.32	5.45	3.95	4.34	5.65	3.67	5.75	4.87	5.55	1.60	1.68	2.28
Hf	6.00	<1	6.00	6.00	8.00	8.00	11.00	4.00	5.00	7.00	3.00	4.00	5.00
Ho	0.44	0.10	0.89	0.80	3.29	0.74	0.39	1.13	0.93	0.74	0.21	0.30	0.34
La	46.70	33.40	57.00	26.60	30.50	44.90	59.20	27.20	32.40	54.20	21.40	16.20	29.60
Lu	0.14	<0.05	0.21	0.32	1.85	0.21	0.12	0.42	0.34	0.24	0.08	0.16	0.12
Nb	11.00	9.00	8.00	8.00	14.00	11.00	13.00	10.00	10.00	22.00	4.00	6.00	6.00
Nd	33.60	25.30	42.40	22.90	23.20	38.20	41.50	26.30	27.70	47.10	13.50	12.00	21.10
Ni	28.00	13.00	17.00	14.00	34.00	31.00	30.00	23.00	25.00	28.00	12.00	13.00	12.00
Pb	38.00	48.00	28.00	12.00	24.00	30.00	26.00	30.00	28.00	51.00	27.00	27.00	33.00
Pr	9.52	7.51	12.10	6.35	6.54	10.20	12.10	6.75	7.24	13.10	3.93	3.36	6.01
Rb	204.00	196.00	132.00	55.10	208.00	221.00	215.00	163.00	114.00	292.00	110.00	173.00	153.00
Sc	9.00	<5	6.00	<5	20.00	10.00	10.00	13.00	14.00	7.00	<5	<5	<5
Sm	5.10	4.10	7.20	4.40	4.30	6.80	5.90	6.10	5.30	8.00	2.10	2.10	3.60
Sr	170.00	160.00	730.00	90.00	100.00	180.00	140.00	150.00	180.00	210.00	590.00	810.00	420.00
Ta	1.00	0.80	0.90	2.40	1.10	0.90	1.20	1.20	1.00	3.90	0.60	2.10	1.00
Tb	0.46	0.22	0.80	0.64	1.10	0.75	0.45	0.94	0.74	0.76	0.20	0.24	0.35
Th	25.00	27.40	21.40	12.60	15.30	20.80	28.50	12.10	8.40	39.90	8.60	7.10	16.60
Ti	bdl	bdl	bdl	bdl	bdl	bdl	bdl	bdl	bdl	bdl	bdl	bdl	bdl
Tm	0.17	<0.05	0.30	0.35	2.02	0.25	0.14	0.46	0.37	0.27	0.08	0.15	0.13
U	1.43	0.62	3.61	2.73	1.55	1.51	1.10	1.30	0.95	10.50	3.88	5.64	2.14
V	65.00	12.00	48.00	17.00	66.00	48.00	73.00	79.00	89.00	36.00	33.00	44.00	33.00
W	bdl	bdl	bdl	bdl	bdl	bdl	bdl	bdl	bdl	bdl	bdl	bdl	bdl
Y	12.50	2.60	24.30	21.80	94.30	19.90	10.40	30.50	24.50	20.70	6.20	8.90	9.50
Yb	1.00	0.10	1.70	2.20	13.40	1.50	0.90	2.80	2.40	1.70	0.60	1.10	0.90
Zn	48.00	22.00	45.00	10.00	30.00	63.00	57.00	39.00	60.00	41.00	46.00	48.00	34.00
Zr	210.00	5.40	227.00	203.00	266.00	264.00	368.00	142.00	177.00	222.00	127.00	138.00	152.00

*bdl = below detection limit

Table 2. Whole-rock analyses of calc-sillicate rocks from the Lansang National Park, Changwat Tak. Major and Minor oxides (%wt) obtained from XRF analysis.

Name	Calc-sillicate Rocks					
	Calc-Silicate Rock			Impure Mable		
	LS-13B	LS-13D	LS-14B	LS-12C	LS-13A	LS-14A
SiO_2	62.60	60.97	50.18	27.52	35.63	27.27
Al_2O_3	9.95	9.38	8.57	1.96	4.58	2.87
Fe_2O_3	0.29	0.34	0.29	0.10	0.14	0.13
FeO	2.64	3.04	2.63	0.90	1.24	1.15
MgO	3.49	6.31	3.31	2.19	1.56	2.04
CaO	12.09	9.64	20.37	55.07	39.80	55.23
MnO	bdl	bdl	bdl	bdl	0.17	0.21
K_2O	3.96	4.46	3.02	0.96	1.88	0.96
Na_2O	0.84	0.88	1.32	0.05	0.53	0.37
TiO_2	0.30	0.39	0.28	0.05	0.11	0.08
P_2O_5	bdl	bdl	bdl	bdl	bdl	bdl
LOI	4.02	2.07	9.90	28.89	21.37	29.17
Total	100.17	97.48	99.88	117.69	107.01	119.48

*bdl = below detection limit

Harker-type variation diagrams were applied from major and minor oxides (see Figure 14). Major and minor oxides of coarse-grained gneiss, fine-grained gneiss, very fine-grained gneiss and granitic gneiss are fallen within the same ranges which indicate high contents of SiO_2, Al_2O_3, CaO, K_2O and Na_2O. Coarse-grained gneiss shows decreasing concentrations of Al_2O_3, CaO, Na_2O, MgO, FeO and TiO_2 against increasing of K_2O and SiO_2. On the other hand, fine-grained gneiss shows deceasing Al_2O_3, K_2O, Na_2O, MgO, FeO and TiO_2 against increasing SiO_2. All concentrations of very fine-grained gneiss are decreasing against increasing SiO_2. For granitic gneiss, only one analysis available reveals the same composition of gneissic group. In general, calc-sillicate rocks have higher content of CaO and Al_2O_3. However, impure marble have even higher CaO contents and lower SiO_2 content than those of the calc-silicate (see Figure 15). These can assume that impure marble may have carbonate composition from limestone while calc-sllicate may occur nearby the contact between limestone and high alumina pelitic rocks.

จุฬาลงกรณ์มหาวิทยาลัย
CHULALONGKORN UNIVERSITY

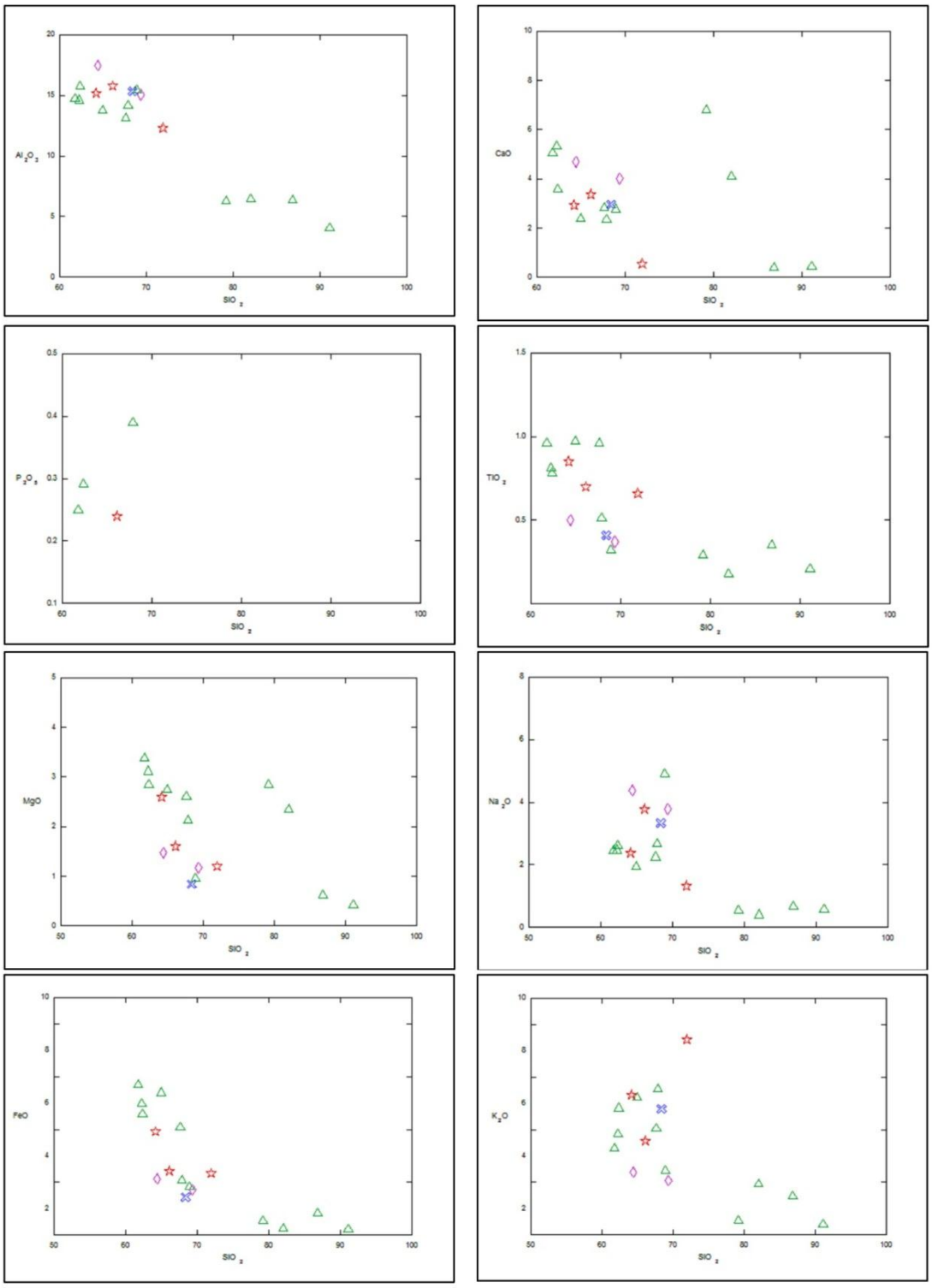

Figure 14. Harker-type variation diagrams of wt% SiO_2 versus selective major and minor oxides of gneissic and granitic gneiss rocks.

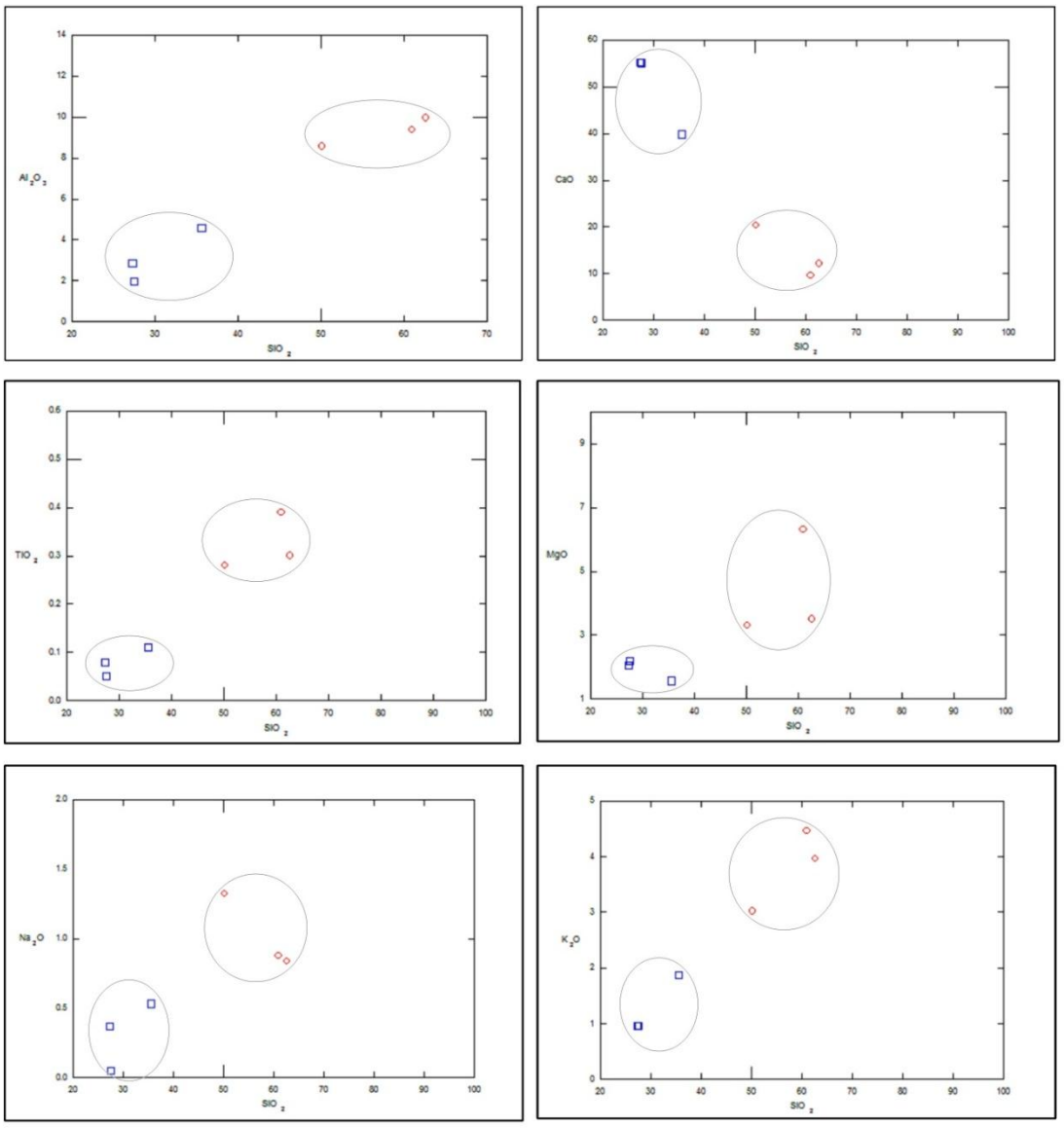

Figure 15. Harker-type variation diagrams of wt% SiO_2 versus selective major and minor oxides of calc-silicate rocks.

4.1.2 Trace Elements

Trace elements were analyzed using Inductively Coupled Plasma-Mass Spectrometer (ICP-MS). Trace elements are allocated in either crystalline or liquid phase. If trace elements are compatible to a mineral, they prefer to crystallize into solid

phase. On the other hand, incompatible elements are preferred to maintain in liquid phase rather than solid phase (Rollinson, 1993). In general, enriched incompatible elements can be mostly found in the partial melting processes of continental crusts, oceanic crusts and also mantle. Incompatible elements can be subdivided into two groups with different charge or size ratio. First group, elements with large ionic radius (e.g., potassium (K), rubidium (Rb), cesium (Cs), strontium (Sr) and barium (Ba)), can be called large-ion lithophile elements (LIL). The second group, high field strength elements (HFS), includes large ionic valences (e.g., zirconium (Zr), niobium (Nb), hafnium (Hf), thorium (Th), uranium (U) and tantalum (Ta)).

Coarse-grained gneisses consist of 700-1150 ppm (av. 987 ppm) barium (Ba), 35-43 ppm (av. 39 ppm) cobalt (Co), 40-70 ppm (av. 55 ppm) chromium (Cr), about 6.00 ppm hafnium (Hf), 8.00-11.00 ppm (av. 9 ppm) niobium (Nb), 13-28 ppm (av. 19 ppm) nickel (Ni), 132 -204 ppm (av. 177 ppm) rubidium (Rb), 6-9 ppm (av. 8 ppm) scandium (Sc), 160-730 ppm (av. 353 ppm) strontium (Sr), 21-27 ppm (av. 25 ppm) thorium (Th), 12-65 ppm (av. 42 ppm) vanadium (V), 3-24 ppm (av. 13 ppm) yttrium (Y), 22-48 ppm (av. 38.33 ppm) zinc (Zn) and 5-227 ppm (av. 147 ppm) zirconium (Zr).

Fine-grained gneisses consist of 350-1260 ppm (av. 849 ppm) barium (Ba), 33-151 ppm (av. 65 ppm) cobalt (Co), 30-90 ppm (av. 62 ppm) chromium (Cr), 10-80 ppm (av. 28 ppm) copper (Cu), 3-11 ppm (av. 7 ppm) hafnium (Hf), 4-22 ppm (av. 11 ppm) niobium (Nb), 14-34 ppm (av. 24 ppm) nickel (Ni), 55-292 ppm (av. 151 ppm) rubidium (Rb), 7-20 ppm (av. 12 ppm) scandium (Sc), 30-210 ppm (av. 123 ppm) strontium (Sr), 7-40 ppm (av. 17 ppm) thorium (Th), 10-89 ppm (av. 45 ppm) vanadium (V), 10-94 ppm (av. 26 ppm) yttrium (Y), 7-63 ppm (av. 34 ppm) zinc (Zn) and 114-368 ppm (av. 222 ppm) zirconium (Zr).

Very fine-grained gneisses consist of 610-740 ppm (av. 675 ppm) barium (Ba), 26-49 ppm (av. 38 ppm) cobalt (Co), about 20 ppm chromium (Cr), 3-4 ppm (av. 4 ppm) hafnium (Hf), 4-6 ppm (av. 5 ppm) niobium (Nb), 12-13 ppm (av. 13 ppm) nickel (Ni), 110-173 ppm (av. 142 ppm) rubidium (Rb), 590-810 ppm (av. 700 ppm) strontium (Sr), 7-9 ppm (av. 8 ppm) thorium (Th), 33-44 ppm (av. 39 ppm) vanadium (V), 6-9 ppm (av. 8 ppm) yttrium (Y), 46-48 ppm (av. 47 ppm) zinc (Zn) and 127-138 ppm (av. 133 ppm) zirconium (Zr).

Granitic gneiss consists of about 1040 ppm barium (Ba), 52 ppm cobalt (Co), 20 ppm chromium (Cr), 5 ppm hafnium (Hf), 6 ppm niobium (Nb), 12 ppm nickel (Ni), 153 ppm rubidium (Rb), 420 ppm strontium (Sr), 17 ppm thorium (Th), 33 ppm vanadium (V), 10 ppm yttrium (Y), 34 ppm zinc (Zn) and 152 ppm zirconium (Zr).

Primitive mantle-normalized spider diagrams normalizing chondrite after Sun and McDonough (1989) are compared with patterns of Average Upper Crust (Avr. Upper Crust) (after Taylor et al. (1981)) and North American Shale Composite or NASC (5) (Gromet et al., 1984). They usually show zigzag patterns of all rock types. Patterns of coarse-grained gneiss, fine-grained gneiss, very fine-grained gneiss and granitic gneiss show closely similar to the Avr. Upper Crust as shown in Figures 16 to 19.

Chulalongkorn University

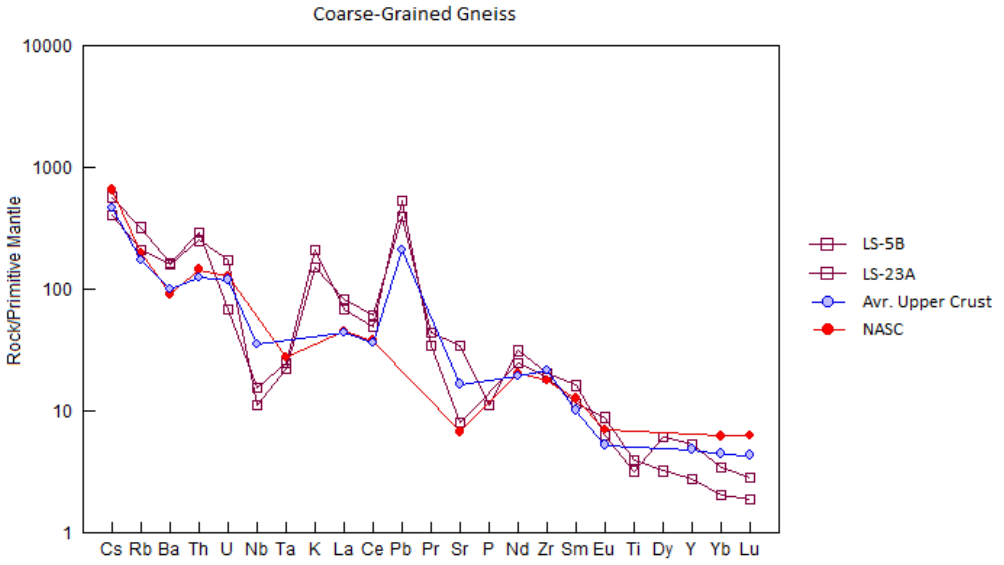

Figure 16. Primitive mantle-normalized spider diagrams (after Sun and McDonough (1989)) of coarse-grained gneiss from Lansang National Park (chondrite's composition and pattern of Avr. Upper Crust of Taylor et al. (1981) and NASC of Gromet et al. (1984)).

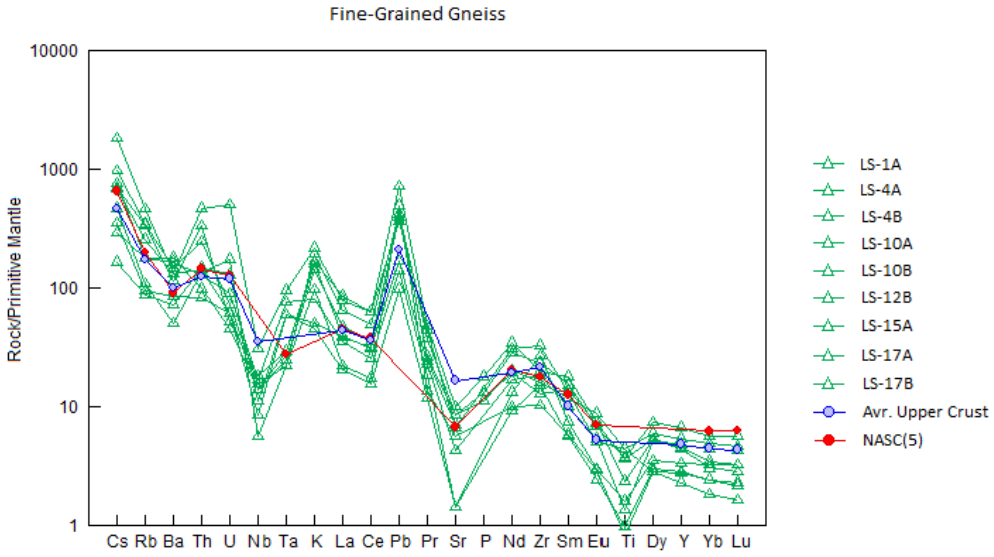

Figure 17. Primitive mantle-normalized spider diagrams (after Sun and McDonough (1989)) of fine-grained gneiss from the Lansang National Park (chondrite's composition and pattern of Avr. Upper Crust of Taylor et al. (1981) and NASC of Gromet et al. (1984)).

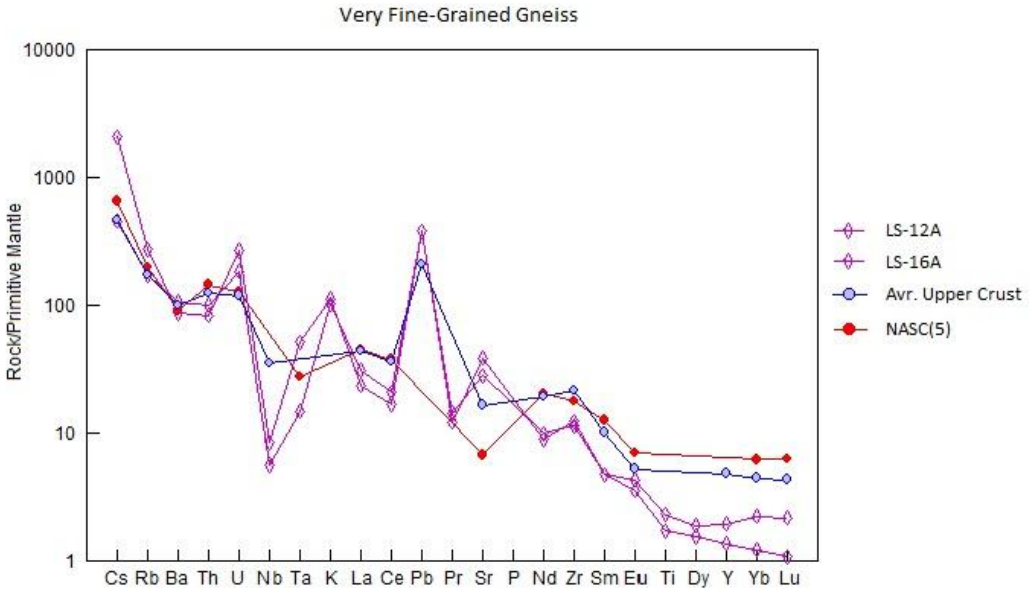

Figure 18. Primitive mantle-normalized spider diagrams (after Sun and McDonough (1989)) of very fine-grained gneiss from the Lansang National Park (chondrite's composition and pattern of Avr. Upper Crust of Taylor et al. (1981) and NASC of Gromet et al. (1984)).

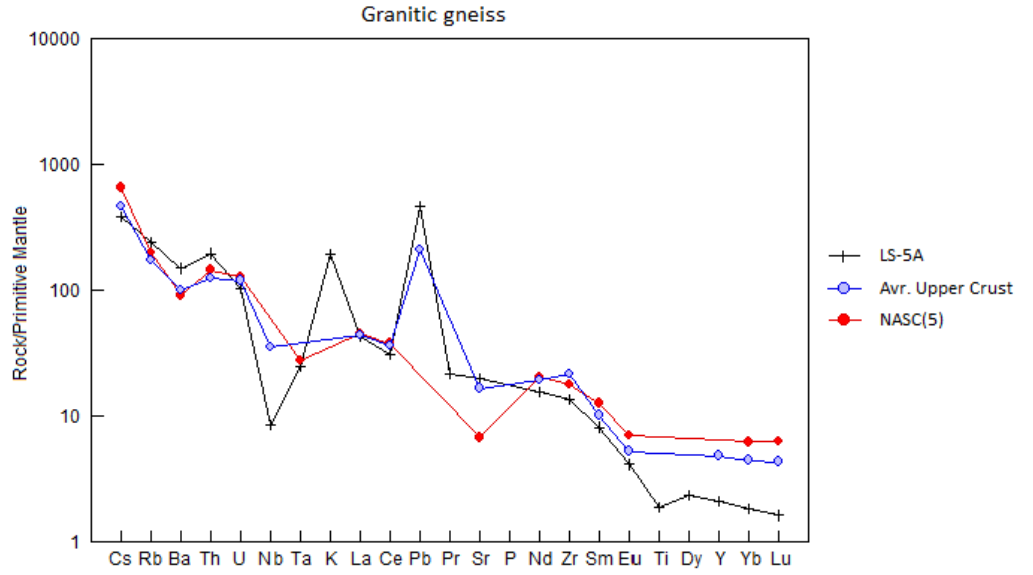

Figure 19. Primitive mantle-normalized spider diagrams (after Sun and McDonough (1989)) of granitic gneiss from Lansang the National Park (chondrite's composition and pattern of Avr. Upper Crust of Taylor et al. (1981) and NASC of Gromet et al. (1984)).

4.1.3 Rare Earth Elements

Rare earth elements are the series of 15 lanthanide elements with yttrium and scandium. There are all metals that can be called rare earth metals or REM. These metals have atomic numbers ranging from 57 to 71 which have similar chemical properties. REE can be subdivided into two groups, light rare earth elements or LREE (e.g., scandium (Sc), lanthanum (La), cerium (Ce), praseodymium (Pr), neodymium (Nd), promethium (Pm), samarium (Sm), europium (Eu), and gadolinium (Gd)) and heavy rare earth elements or HREE (e.g., yttrium (Y), terbium (Tb), dysprosium (Dy), holmium (Ho), erbium (Er), thumium (Tm), ytterbium (Yb), and lutetium (Lu)). Chondrite normalization is usually applied for comparison and interpretation.

Coarse-grained gneisses consist of 68-109 ppm (av. 88 ppm) cerium (Ce), 1-5 ppm (av. 3 ppm) dysprosium (Dy), 0-2 ppm (av. 1 ppm) erbium (Er), about 1 ppm europium (Eu), 14-20 ppm (av. 17 ppm) gallium (Ga), 2-5 ppm (av. 4 ppm) gadolinium (Gd), 0-1 ppm (av. 0 ppm) holmium (Ho), 33-57 ppm (av. 46 ppm) lanthanum (La), 25-42 ppm (av. 34 ppm) neodymium (Nd), 8-12 ppm (av. 10 ppm) praseodymium (Pr), 4-7 ppm (av. 5 ppm) samarium (Sm), 0-1 ppm (av. 0 ppm) terbium (Tb) and 0-2 ppm (av. 1 ppm) ytterbium (Yb).

Fine-grained gneisses consist of 27-112 ppm (av. 65 ppm) cerium (Ce), 2-11 ppm (av. 7 ppm), 1-12 ppm (av. 3 ppm) erbium (Er), 0-1 ppm (av. 1 ppm) europium (Eu), 4-19 ppm (av. 13 ppm) gallium (Ga), 2-6 ppm (av. 4 ppm) gadolinium (Gd), 0-3 ppm (av. 1 ppm) holmium (Ho), 14-59 ppm (av. 33 ppm) lanthanum (La), 12-47 ppm (av. 27 ppm) neodymium (Nd), 3-13 ppm (av. 7 ppm) praseodymium (Pr), 3-8 ppm (av. 5 ppm) samarium (Sm), 0-1 ppm (av. 1 ppm) terbium (Tb), 0-2 ppm (av. 1 ppm) thumium (Tm) and about 13.40 ppm ytterbium (Yb).

Very fine-grained gneisses consist of 30-37 ppm (av. 33 ppm) cerium (Ce), 1-2 ppm (av. 1 ppm) dysprosium (Dy), about 1 ppm erbium (Er), about 1 ppm europium (Eu), 20-24 ppm (av. 23 ppm) gallium (Ga), about 2 ppm gadolinium (Gd), 16-21 ppm (av. 19 ppm) lanthanum (La), 12-14 ppm (av. 13 ppm) neodymium (Nd), 3-4 ppm (av. 4 ppm) praseodymium (Pr), about 2 ppm samarium (Sm) and about 1 ppm ytterbium (Yb).

Granitic gneiss consist of about 55 ppm cerium (Ce), 2 ppm dysprosium (Dy), 1 ppm erbium (Er), 1 ppm europium (Eu), 18 ppm gallium (Ga), 2 ppm gadolinium (Gd), 29 ppm lanthanum (La), 21 ppm neodymium (Nd), 6 ppm praseodymium (Pr), 4 ppm samarium (Sm) and about 1 ppm ytterbium (Yb).

Chondrite-normalized rare earth element patterns show closely similar between coarse-grained gneiss, fine-grained gneiss, very fine-grained gneiss and granitic gneiss which are decreasing patterns from La to Lu (see Figures 20 to 23). These patterns are similar to the pattern of average upper crust (Taylor et al., 1981) with decreasing from LREE to HREE with a negative Eu anomaly.

จุฬาลงกรณ์มหาวิทยาลัย
Chulalongkorn University

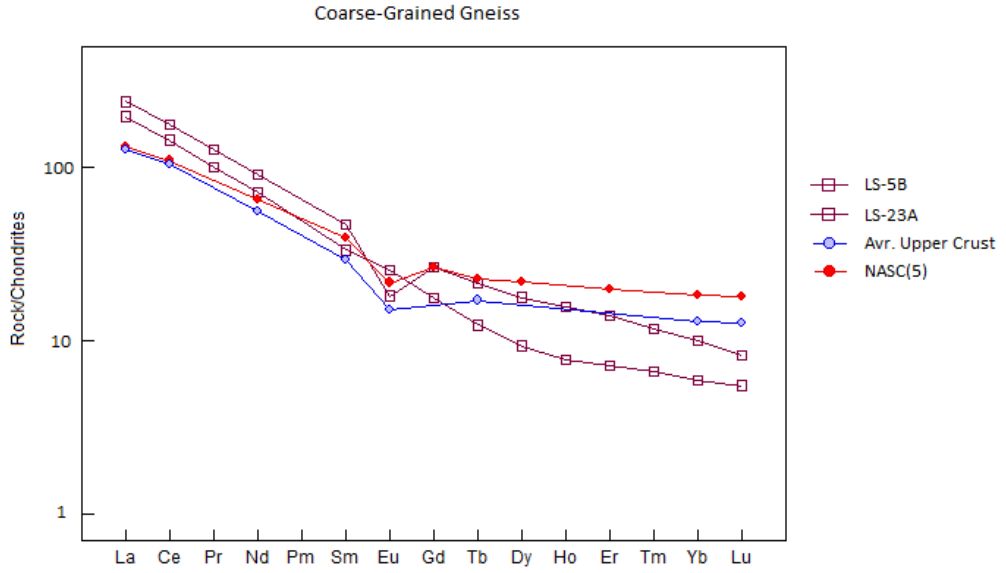

Figure 20. Chondrite-normalized REE (after Sun and McDonough (1989)) plots of coarse-grained gneiss from the Lansang National Park (chondrite's composition and pattern of Avr. Upper Crust of Taylor et al. (1981) and NASC of Gromet et al. (1984)).

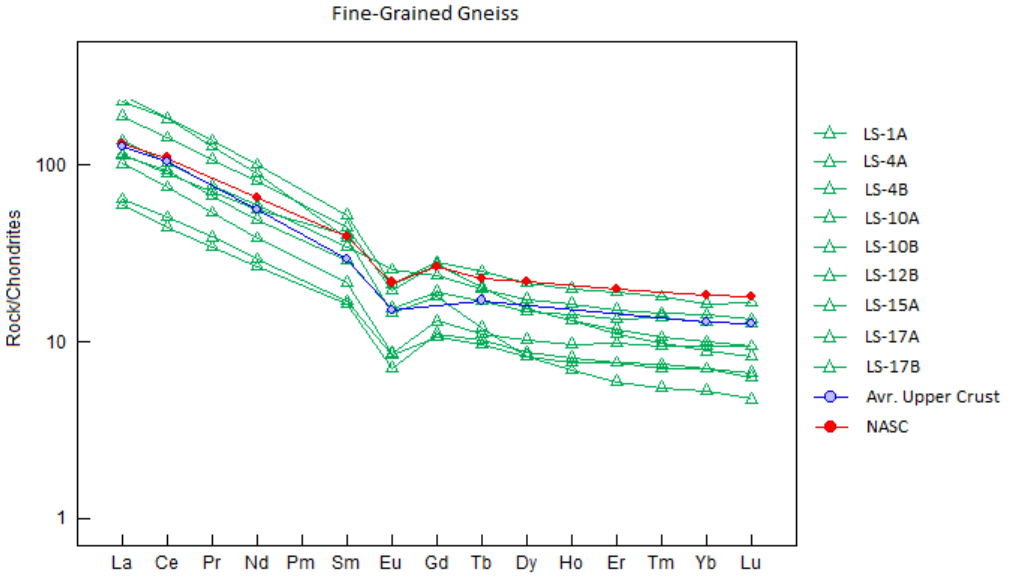

Figure 21. Chondrite-normalized REE (after Sun and McDonough (1989)) plots of fine-grained gneiss from the Lansang National Park (chondrite's composition and pattern of Avr. Upper Crust of Taylor et al. (1981) and NASC of Gromet et al. (1984)).

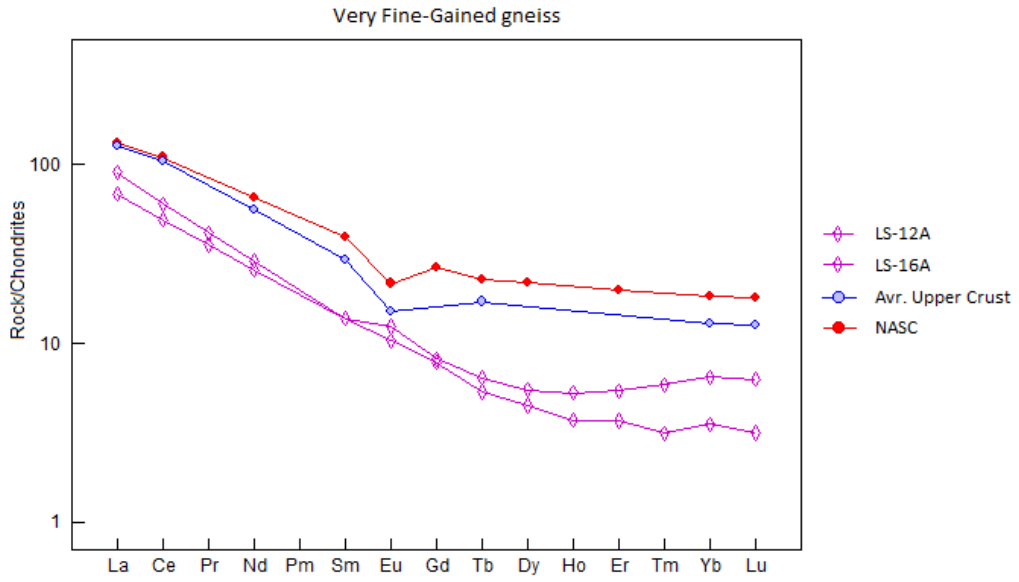

Figure 22. Chondrite-normalized REE (after Sun and McDonough (1989)) plots of very fi ne-grained gneiss from the Lansang National Park (chondrite's composition and pattern of Avr. Upper Crust of Taylor et al. (1981) and NASC of Gromet et al. (1984)).

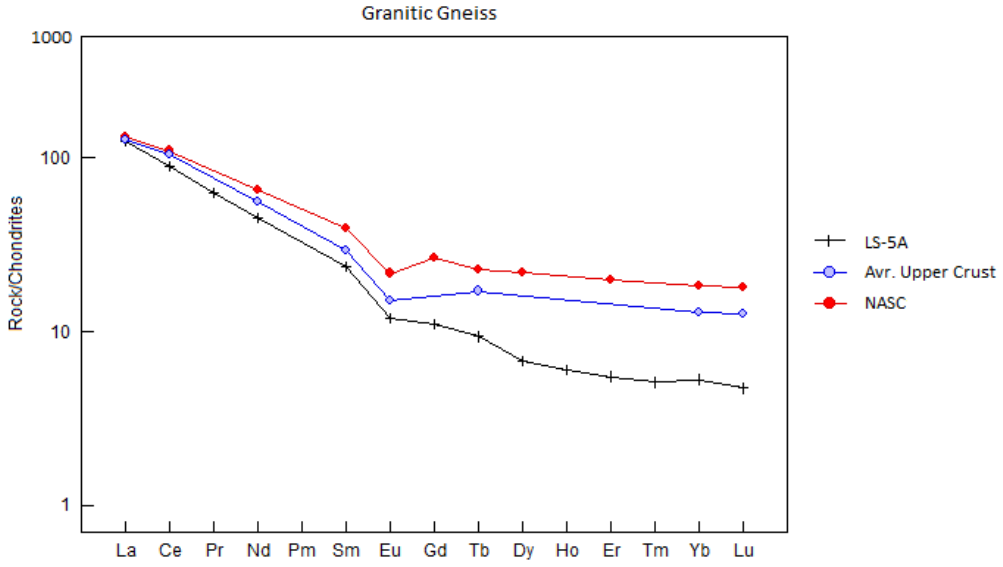

Figure 23. Chondrite-normalized REE (after Sun and McDonough (1989)) plots of granitic gneiss from the Lansang National Park (chondrite's composition and pattern of Avr. Upper Crust of Taylor et al. (1981) and NASC of Gromet et al. (1984)).

4.2 Mineral Chemistry

Electron Probe Micro-Analyzer (EPMA) was engaged to analyze chemical composition of the main mineral assemblages from polished-thin sections in each rock sample. Main mineral components, e.g., amphibole, feldspar, biotite and chlorite, are summarized in Tables 3 to Table 7.

4.2.1 Amphiboles

Amphiboles are mostly found in calc-silicate band and in some fine-grained gneiss sample. The compositions of amphibole were recalculated based on 23 oxygen atoms (O) and then selected to present in Table 3.

Amphiboles in fine-grained gneiss consist of 53.89-57.35 %SiO_2, 0.59-4.41 %Al_2O_3, 6.48-8.03 %FeO_{Total}, 0.15-0.23 %MnO, 12.87-19.55 %MgO, 12.91-24.41 %CaO, 0.00-0.35 % K_2O, 0.12-0.47 %Na_2O and 0.03-0.27 %TiO_2.

Amphiboles in calc-silicate rocks are composed of 55.14-56.70 %SiO_2, 2.02-2.44 %Al_2O_3, 10.36-14.32 %FeO_{Total}, 0.07-0.16 %MnO, 14.33-17.17 %MgO, 12.65-13.53 %CaO, 0.08-0.16 % K_2O, 0.24-0.32 %Na_2O and 0.05-0.18 %TiO_2.

Amphiboles in impure marble consist of 54.96-57.08 %SiO_2, 1.84-3.68 %Al_2O_3, 5.05-9.58 %FeO_{Total}, 0.02-0.07 %MnO, 17.68-20.69 %MgO, 13.18-13.67 % CaO, 0.13-0.18 % K_2O, 0.22-0.39 %Na_2O and 0.03-0.06 % TiO_2.

Atomic Mg-Fe-Ca proportions of amphiboles are plotted in a diagram after Eyuboglu et al. (2011) (see Figure 24). These cations in fine-grained gneiss and calc-silicate rocks yielded similar proportions. Their compositions are close tremolite-actinolite range.

Table3. Representative EPMA analyses of amphiboles in rock samples collected from the Lansang National Park.

Name	Gneissic Rocks					Calc-Silicate Rocks						
	Fine-grained gneiss					Calc-Silicate				Impure marble		
	LS1A-amp1	LS1A-amp3	LS1A-amp4	LS1A-amp8	LS1A-amp11	LS14A-Amp1	LS14A-Amp2	LS14A-Amp4	LS14A-Amp7	LS12C-amp1	LS12C-amp3	LS12C-amp6
SiO_2	56.79	54.54	53.89	57.35	55.04	55.14	56.56	55.85	56.70	57.08	54.96	55.78
TiO_2	0.04	0.27	0.03	0.09	0.22	0.18	0.09	0.07	0.05	0.03	0.06	0.03
Al_2O_3	1.43	4.41	0.59	1.81	3.62	2.40	2.09	2.44	2.02	1.84	3.68	2.28
FeO	7.35	6.83	8.03	7.21	6.48	14.32	10.78	11.94	10.36	5.05	8.83	9.58
MnO	0.15	0.17	0.23	0.16	0.18	0.16	0.07	0.11	0.08	0.02	0.07	0.04
MgO	19.48	18.95	12.87	19.55	19.21	14.33	17.17	15.46	16.92	20.69	17.68	17.88
CaO	13.16	12.95	24.41	13.29	12.91	12.65	12.82	13.53	13.07	13.58	13.67	13.18
Na_2O	0.14	0.47	0.14	0.12	0.33	0.31	0.32	0.24	0.25	0.22	0.39	0.25
K_2O	0.07	0.35	0.00	0.08	0.28	0.15	0.16	0.08	0.11	0.13	0.18	0.17
Total	98.60	98.93	100.19	99.67	98.27	99.63	100.05	99.71	99.55	98.62	99.51	99.20
Si	7.888	7.568	7.703	7.871	7.665	7.827	7.857	7.840	7.897	7.853	7.649	7.793
Ti	0.004	0.028	0.004	0.010	0.023	0.019	0.010	0.007	0.005	0.003	0.006	0.003
Al	0.234	0.721	0.099	0.293	0.593	0.401	0.342	0.404	0.332	0.298	0.603	0.376
Fe^{3+}	0.000	0.000	0.000	0.000	0.000	0.000	0.000	0.000	0.000	0.000	0.000	0.000
Fe^{2+}	0.854	0.793	0.960	0.828	0.755	1.699	1.252	1.402	1.206	0.580	1.027	1.120
Mn	0.018	0.020	0.028	0.018	0.022	0.019	0.008	0.013	0.009	0.002	0.008	0.005
Mg	4.035	3.919	2.742	4.000	3.987	3.032	3.555	3.236	3.514	4.243	3.669	3.724
Ca	1.933	1.901	3.690	1.930	1.901	1.899	1.883	2.009	1.925	1.977	2.012	1.948
Na	0.037	0.125	0.038	0.032	0.090	0.086	0.085	0.064	0.068	0.059	0.105	0.067
K	0.012	0.061	0.000	0.015	0.050	0.027	0.029	0.013	0.020	0.022	0.031	0.030
Total	15.015	15.137	15.263	14.996	15.085	15.010	15.020	14.989	14.976	15.037	15.111	15.064
Atomic %												
Fe	9.9	4.6	3.4	5.5	10.3	22.5	15.4	18.7	16.2	4.6	8.5	11.8
Mg	53.7	58.4	57.4	57.9	53.4	41.1	48.5	43.4	47.3	57.6	51.6	50.8
Ca	36.3	36.9	39.2	36.6	36.3	36.3	36.2	38.0	36.5	37.8	39.9	37.4

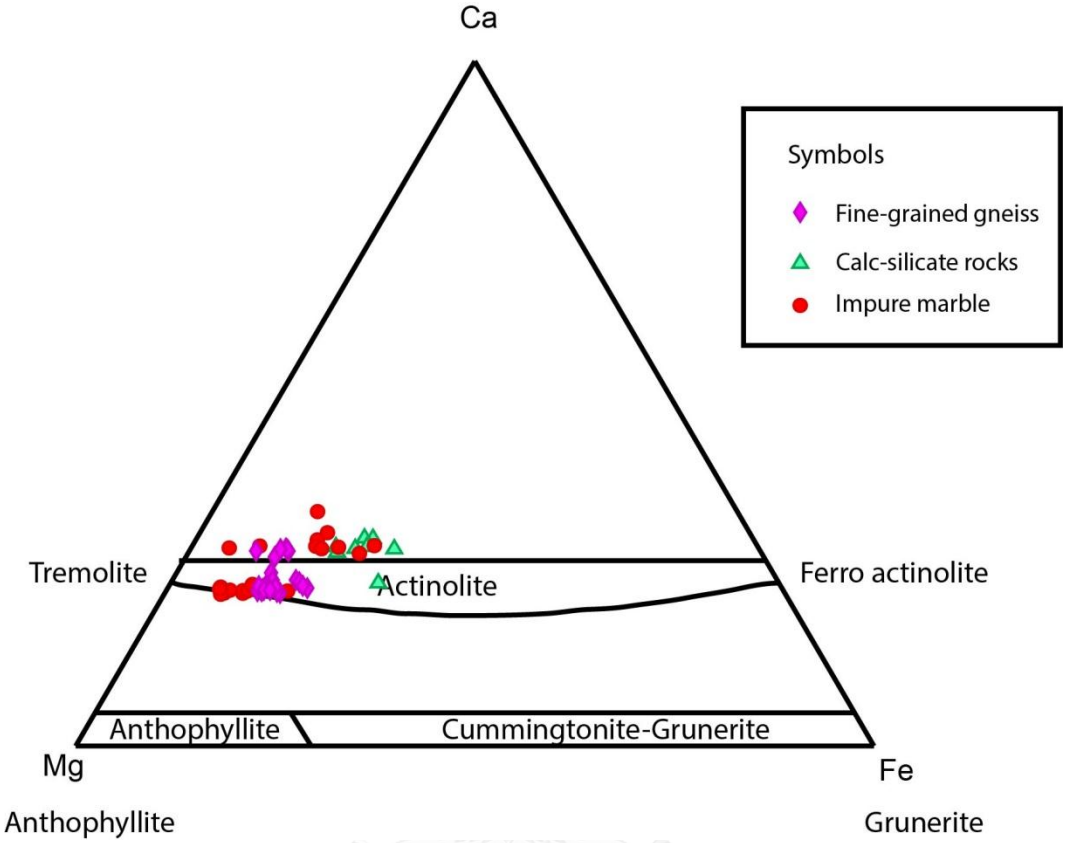

Figure 24. Atomic Mg-Fe-Ca plots showing compositions of amphiboles in rock samples collected from the Lansang National Park (diagram after Eyuboglu et al. (2011)); composition of amphibole are close to tremolite-actinolite composition.

4.2.2 Feldspar

Feldspars are the main component of most rock samples. They can be classified into plagioclase and K-feldspar. Plagioclase grains are mainly found in most rock types, i.e., coarse-grained gneiss, fine-grained gneiss, very fine-grained gneiss and granitic gneiss. The selective analytical data and their recalculated cations based on 8 oxygen atoms are present in Table 4.

Plagioclases are found in most types of sample, i.e., fine-grained gneiss, coarse-grained gneiss, very fine-grained gneiss, granitic gneiss and calc-silicate rocks.

Plagioclases in coarse-grained gneiss consist of 60.16-61.78 %SiO_2, 22.83-22.93 %Al_2O_3, 0.13-0.31 %FeO_{Total}, 8.21-8.77 %CaO, 0.13-0.16 % K_2O, 3.46-4.05 %Na_2O and 0.01-0.03 %TiO_2. Plots of atomic Ca-Na-K proportions are present in Figure 25. They are close composition of oligoclase to labradorite ranging from 52-6 %An, 42-47%Ab and 1 %Or, respectively.

In fine-grained gneiss, plagioclases are mainly composed of 60.22-60.47 %SiO_2, 24.08-25.32 %Al_2O_3, 0.03-0.08 %FeO_{Total}, 6.97-6.99 %CaO, 0.07-0.08 % K_2O and 7.49-7.76 %Na_2O. Plots of atomic Ca-Na-K are present in Figure 25. They are close composition of oligoclase to andesine ranging from 33-34 %An, 66-67 %Ab and about 1 %Or, respectively.

Plagioclases in very fine-grained gneiss consist of 60.60-61.01 %SiO_2, 25.27-25.43 %Al_2O_3, 0.06 %FeO_{Total}, 7.98-8.06 %CaO, about 0.13 % K_2O and 4.10-4.13 %Na_2O. Atomic plots of Ca-Na-K proportions are present in Figure 25. They are close to albite-andesine compositions of about 51 %An, 48 %Ab and 1 %Or respectively.

Plagioclases in only one sample of granitic gneiss are available. They are composed of 60.29-60.56 %SiO_2, 22.57-23.47 %Al_2O_3, 0.05-0.06 %FeO_{Total}, 0.04 %MgO, 8.02-8.11 %CaO, 0.23-0.26 % K_2O, 4.07-4.17 %Na_2O and 0.01-0.02 %TiO_2. Atomic plots of Ca-Na-K proportions are present in Figure 25. They are close to albite-oligoclase composition ranging between 50-51 %An, 47-48 %Ab and 2 %Or, respectively.

For calc-silicate rocks, plagioclases in calc-silicate bands are composed of 55.03-58.54 %SiO_2, 21.95-23.58 %Al_2O_3, 0.03-0.22 %FeO_{Total}, 7.61-8.77 %CaO, 0.13-

0.20 % K_2O, 3.45-5.32 %Na_2O and about 0.02 %TiO_2. Atomic plots of Ca-Na-K proportions are present in Figure 25. They are close andesine-bytownite composition ranging between 43-57 %An, 41-56 %Ab and 1-2 %Or, respectively. On the other hand, plagioclases in impure marble bands consist of 57.24-59.38 %SiO_2, 24.70-25.80 %Al_2O_3, 0.07-0.15 %FeO_{Total}, 7.37-8.19 %CaO, 0.14-0.15 % K_2O and 3.84-4.95 %Na_2O. Atomic plots of Ca-Na-K proportions are present in Figure 25. They are close to labradorite compositiin ranging from 44-53 %An, 46-55 %Ab and 1 %Or, respectively.

All samples containing K-feldspar show significantly weathering; then only some K-feldspar crystals were available for analysis. The selective data and their recalculated cations based on 8 oxygen atoms are summarized in Table 5.

Fine-grained gneiss, K-feldspar are mainly composed of 64.28-64.99 %SiO_2, 17.97-18.24 %Al_2O_3, about 0.10 %FeO_{Total}, about 0.02 %CaO, 15.51-15.68 %K_2O and 0.51-0.66 %Na_2O. Atomic plots of Ca-Na-K proportions are present in Figure 25. They are close to orthoclase composition ranging from 1 %An, 5-6 %Ab and 94-95 %Or respectively.

จุฬาลงกรณ์มหาวิทยาลัย
Chulalongkorn University

K-feldspars in coarse-grained gneiss are mainly composed of 64.70-64.72 %SiO2, 18.01-18.17 %Al2O3, 0.03-0.04 %FeO_{Total}, about 0.05 %CaO, 15.09-15.40 %K_2O and 0.75-1.14 %Na_2O. Plots of atomic Ca-Na-K proportions (represent to anorthite (An), albite (Ab) and orthoclase (Or) end member of feldspar) are present in Figure 25. They are closely orthoclase ranging of 0 %An, 7-10 %Ab and 90-93 %Or respectively.

K-feldspar in very fine-grained gneiss are mainly composed of 63.47-68.67 %SiO_2, 17.80-18.91 %Al_2O_3, 0.11-0.15 %FeO_{Total}, 0.02-0.45 %CaO, 12.34-15.87 %K_2O and 0.49-1.45 %Na_2O. Plots of atomic Ca-Na-K proportions (represent to anorthite (An),

albite (Ab) and orthoclase (Or) end member of feldspar) are present in Figure 25. They are closely orthoclase ranging of 0-3 %An, 4-15 %Ab and 83-95 %Or respectively.

K-feldspar in granitic gneiss consists of 63.59-63.73 %SiO_2, 17.04-18.17 %Al_2O_3, 0.08-0.16 %FeO_{Total}, 15.57-16.06 %K_2O and 0.46-0.63 %Na_2O. Plots of atomic Ca-Na-K proportions (represent to anorthite (An), albite (Ab) and orthoclase (Or) end member of feldspar) are present in Figure 25. They are closely orthoclase ranging of 4-6 %Ab and 94-96 %Or respectively and absent %An.

Impure marble bands have some porphyroblastic K-feldspars; thier are composed of 62.67-63.23 %SiO_2, 18.67-18.70 %Al_2O_3, about 0.04 %FeO_{Total}, about 0.03 %CaO, 15.56-15.81 % K_2O and 0.81-0.72 %Na_2O. Plots of atomic Ca-Na-K proportions (represent to anorthite (An), albite (Ab) and orthoclase (Or) end member of feldspar) are present in Figure 25. They are closely orthoclase ranging of 0 %An, 6-7 %Ab and 93-94 %Or respectively.

จุฬาลงกรณ์มหาวิทยาลัย
Chulalongkorn University

Table 4. Representative EPMA analyses of plagioclase found in rock samples from the Lansang National Park.

Name	Gneissic Rocks						Granitic gneiss		Calc-Silicate Rocks			
	Coarse-grained gneiss		Fine-grained gneiss		Very fine-grained gneiss				Calc-Silicate		Impure marble	
	Ls23C-plg1	Ls23C-plg2	LS1A-plg1	LS1A-plg2	LS12A-plg2c	LS12A-plg3r	LS5A-plg3	LS5A-plg4	LS14A-plg2	LS14A-plg6	LS12C-plg1	LS12C-plg7
SiO_2	61.78	60.16	60.47	60.22	60.60	61.01	60.56	60.29	58.54	55.03	59.38	57.24
TiO_2	0.01	0.03	0.00	0.00	0.00	0.00	0.01	0.02	0.02	0.00	0.00	0.00
Al_2O_3	22.83	22.93	24.08	25.32	25.27	25.43	22.57	23.47	21.95	23.58	24.70	25.80
FeO	0.31	0.13	0.03	0.08	0.06	0.04	0.06	0.05	0.22	0.03	0.07	0.15
MnO	0.01	0.00	0.00	0.00	0.00	0.02	0.00	0.04	0.00	0.00	0.03	0.02
MgO	0.00	0.00	0.00	0.00	0.01	0.00	0.00	0.00	0.13	0.01	0.00	0.00
CaO	8.77	8.21	6.97	6.99	7.98	8.06	8.02	8.11	8.77	7.61	8.19	7.37
Na_2O	3.46	4.05	7.76	7.49	4.10	4.13	4.17	4.07	3.45	5.32	3.84	4.95
K_2O	0.13	0.16	0.07	0.08	0.13	0.13	0.26	0.23	0.20	0.13	0.14	0.15
Total	97.30	95.67	99.39	100.19	98.14	98.83	95.65	96.27	93.27	91.71	96.34	95.68
Si	2.794	2.770	2.710	2.677	2.717	2.717	2.788	2.759	2.771	2.667	2.715	2.648
Ti	0.000	0.001	0.000	0.000	0.000	0.000	0.000	0.001	0.001	0.000	0.000	0.000
Al	1.217	1.245	1.272	1.326	1.335	1.335	1.225	1.265	1.224	1.347	1.331	1.407
Fe	0.012	0.005	0.001	0.003	0.002	0.002	0.002	0.002	0.009	0.001	0.002	0.006
Mn	0.000	0.000	0.000	0.000	0.000	0.001	0.000	0.001	0.000	0.000	0.001	0.001
Mg	0.000	0.000	0.000	0.000	0.001	0.000	0.000	0.000	0.009	0.001	0.000	0.000
Ca	0.420	0.400	0.331	0.329	0.378	0.380	0.391	0.392	0.439	0.390	0.396	0.360
Na	0.303	0.361	0.674	0.646	0.356	0.357	0.372	0.361	0.317	0.500	0.340	0.444
K	0.008	0.009	0.004	0.004	0.008	0.007	0.015	0.013	0.012	0.008	0.008	0.009
Total	4.753	4.792	4.993	4.985	4.797	4.798	4.793	4.795	4.781	4.914	4.794	4.875
Atomic (%)												
An	57.4	51.9	32.8	33.6	51.0	51.0	50.2	51.2	57.2	43.4	53.2	44.3
Ab	41.5	46.9	66.8	66.0	48.0	48.0	47.9	47.1	41.2	55.7	45.7	54.6
Or	1.0	1.2	0.4	0.5	1.0	1.0	1.9	1.7	1.6	0.9	1.1	1.1

Table 5 Representative EPMA analyses of K-feldspar found in rock samples from the Lansang National Park.

Name	Gneissic Rocks						Granitic gneiss		Calc-Silicate Rocks	
	Coarse-grained gneiss		Fine-grained gneiss		Very fine-grained gneiss				Impure marble	
	LS23C-kfs1	LS23C-kfs2	LS1A-kfs1	LS1A-kfs2	LS12A-kfs2	LS12A-kfs3	LS5A-kfs3	LS5A-kfs4	LS12C-kfs1	LS12C-kfs
SiO_2	64.72	64.70	64.28	64.99	68.67	63.47	63.73	63.59	63.23	62.67
TiO_2	0.00	0.04	0.03	0.01	0.00	0.01	0.00	0.01	0.01	0.00
Al_2O_3	18.17	18.01	17.97	18.24	17.80	18.91	17.04	17.17	18.67	18.70
FeO	0.04	0.03	0.00	0.10	0.11	0.14	0.08	0.16	0.04	0.00
MnO	0.00	0.00	0.00	0.00	0.00	0.00	0.00	0.01	0.00	0.01
MgO	0.02	0.01	0.00	0.00	0.00	0.03	0.00	0.00	0.01	0.00
CaO	0.05	0.05	0.02	0.02	0.45	0.02	0.00	0.00	0.00	0.03
Na_2O	0.75	1.14	0.51	0.66	1.45	0.49	0.63	0.46	0.81	0.72
K_2O	15.40	15.09	15.68	15.51	12.34	15.87	15.57	16.06	15.56	15.81
Total	99.14	99.07	98.49	99.54	100.82	98.93	97.05	97.45	98.33	97.94
Si	3.006	3.007	3.009	3.007	3.075	2.967	3.031	3.021	2.971	2.963
Ti	0.000	0.001	0.001	0.000	0.000	0.000	0.000	0.000	0.000	0.000
Al	0.995	0.987	0.991	0.995	0.939	1.042	0.955	0.961	1.034	1.042
Fe	0.002	0.001	0.000	0.004	0.004	0.006	0.003	0.006	0.002	0.000
Mn	0.000	0.000	0.000	0.000	0.000	0.000	0.000	0.000	0.000	0.000
Mg	0.002	0.000	0.000	0.000	0.000	0.002	0.000	0.000	0.000	0.000
Ca	0.002	0.003	0.001	0.001	0.021	0.001	0.000	0.000	0.000	0.002
Na	0.068	0.102	0.047	0.059	0.126	0.044	0.058	0.042	0.074	0.066
K	0.912	0.895	0.936	0.915	0.705	0.946	0.944	0.973	0.933	0.953
Total	4.986	4.996	4.985	4.982	4.870	5.007	4.992	5.005	5.014	5.026
Atomic (%)										
An	0.2	0.3	0.1	0.1	2.5	0.1	0.0	0.0	0.0	0.2
Ab	6.9	10.2	4.7	6.1	14.7	4.4	5.8	4.2	7.3	6.5
Or	92.9	89.5	95.2	93.8	82.7	95.5	94.2	95.8	92.7	93.4

Figure 25 shows widely end member plots of feldspars observed in all rock types. Plagioclases are chemically characterized by wide compositional range crucially from albite to bytownite. Plagioclase in gneissic rocks and granitic gneiss are albite to labradorite. Some andesine to bytownite plagiocalses may have occurred in calc-silicate rocks. Because calc-silicate rocks contain higher calcium in the initial rocks

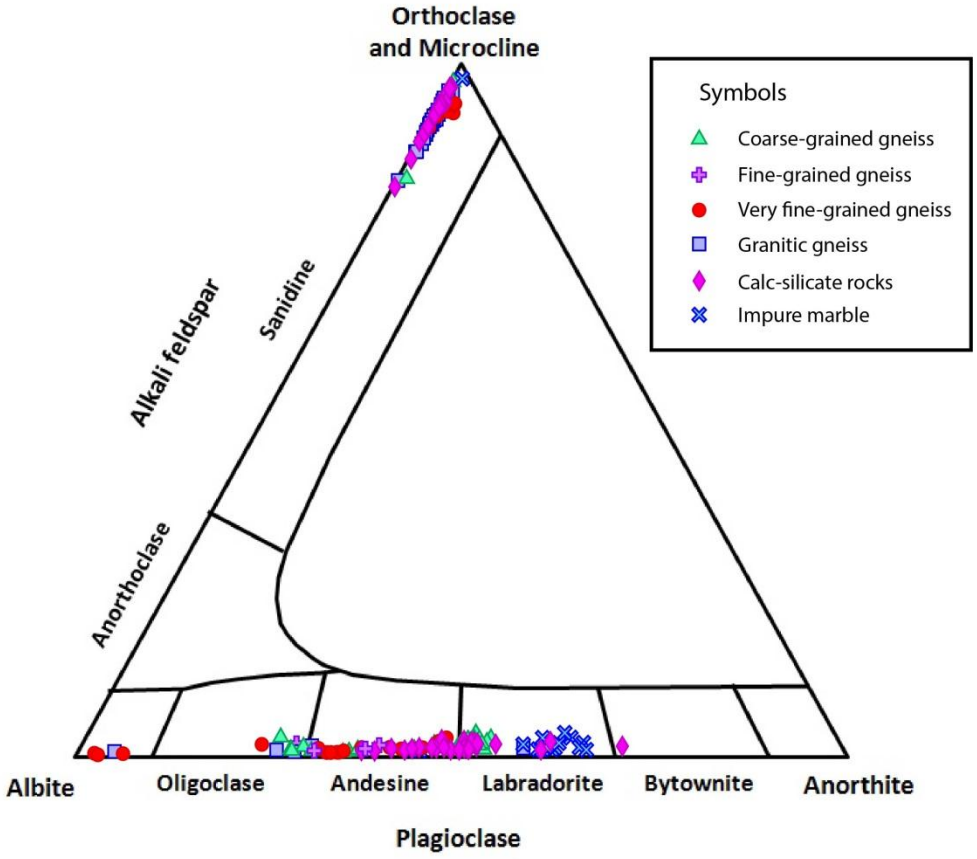

Figure 25. Tertiary feldspar plots between Or-Ab-An (modified from Deer et al. (1992)) showing wide compositional range of plagioclase (albite-bytownite) and narrower range of K-feldspar in orthoclase.

4.2.3 Biotite

Biotite grains are mostly found in coarse-grained gneiss, very fine-grained gneiss and granitic gneiss. The selective analytical data and their recalculated cations based on 11 oxygen atoms are presented in Table 4.6.

In coarse-grained gneiss, biotites are mainly composed of 32.27-38.30 %SiO2, 1.40-3.51 %TiO_2, 17.68-19.54 %Al_2O_3, 21.13-27.35 %FeO_{Total}, 0.00-0.07 % MnO, 7.37-8.73 %MgO, 0.01-0.17 %CaO, 3.17-9.74 % K_2O and 0.01-0.09 %Na_2O.

Biotites in very fine-grained gneiss are mainly composed of 37.78-41.01 %SiO2, 1.11-1.87 %TiO_2, 16.64-17.46 %Al_2O_3, 26.47-20.49 %FeO_{Total}, 0.01-0.16 % MnO, 8.75-9.46 %MgO, 0.04-0.21 %CaO, 8.38-9.73 % K_2O and 0.07-0.27 %Na_2O.

In granitic gneiss, biotites consist of 37.35-37.91 %SiO2, 2.90-4.09 %TiO_2, 15.93-16.00 %Al_2O_3, 20.94-22.12 %FeO_{Total}, 0.20-0.27 % MnO, 8.17-8.83 %MgO, 0.04-0.06 %CaO, 9.62-9.67 % K_2O and about 0.07 %Na_2O.

จุฬาลงกรณ์มหาวิทยาลัย
Chulalongkorn University

Table 6 Representative EPMA analyses of biotite found in rock samples from the Lansang National Park.

Name	Gneissic Rocks							Granitic gneiss		
	Coarse-grained gneiss					Very fine-grained gneiss				
	LS23C-Bi1r	LS23C-Bi1c	LS23C-Bi2	LS23C-Bi3r	LS23C-bi7c	LS16-Bi3	LS16-Bi4	LS5A-bi3	LS5A-bi4	LS5A-bi2
SiO_2	37.18	32.27	37.12	38.30	37.22	41.01	37.78	37.73	37.91	37.35
TiO_2	3.40	1.40	1.40	1.44	3.51	1.11	1.87	3.61	2.90	4.09
Al_2O_3	17.68	19.54	19.13	19.40	18.19	17.46	16.64	16.00	15.93	15.97
FeO	21.72	27.35	22.22	21.13	22.07	16.47	20.49	21.60	20.94	22.12
MnO	0.03	0.07	0.01	0.00	0.02	0.01	0.16	0.27	0.25	0.20
MgO	7.71	8.56	7.93	8.73	7.37	8.75	9.46	8.45	8.83	8.17
CaO	0.01	0.09	0.17	0.06	0.04	0.21	0.04	0.06	0.05	0.04
Na_2O	0.09	0.01	0.02	0.06	0.09	0.27	0.07	0.07	0.07	0.07
K_2O	9.74	3.17	7.18	9.15	9.73	8.38	9.73	9.62	9.67	9.66
Total	97.56	92.45	95.17	98.27	98.24	93.66	96.22	97.42	96.55	97.67
Si	2.787	2.554	2.810	2.814	2.773	3.065	2.857	2.836	2.866	2.810
Ti	0.192	0.083	0.079	0.080	0.197	0.062	0.106	0.204	0.165	0.231
Al	1.562	1.823	1.706	1.680	1.597	1.538	1.483	1.418	1.419	1.416
Fe^{3+}	0.000	0.000	0.000	0.000	0.000	0.000	0.000	0.000	0.000	0.000
Fe^{2+}	1.362	1.810	1.406	1.298	1.375	1.029	1.296	1.358	1.324	1.392
Mn	0.002	0.005	0.000	0.000	0.001	0.001	0.010	0.017	0.016	0.013
Mg	0.862	1.009	0.895	0.956	0.819	0.975	1.067	0.947	0.995	0.916
Ca	0.001	0.007	0.013	0.005	0.003	0.017	0.003	0.005	0.004	0.003
Na	0.013	0.002	0.004	0.009	0.012	0.039	0.010	0.011	0.010	0.011
K	0.932	0.320	0.693	0.857	0.925	0.798	0.938	0.922	0.933	0.927
Total	7.712	7.612	7.606	7.699	7.701	7.523	7.769	7.717	7.731	7.719

4.2.4 Chlorite

Chlorite grains show lepidobalstic texture occurred around biotite grains. They are mostly found in coarse-grained gneiss, very fine-grained gneiss, granitic gneiss and calc-silicate. The selective analytical data and their recalculated cations based on 14 oxygen atoms are present in Table 4.7.

In coarse-grained gneiss, chlorites are mainly composed of 25.91-27.03 %SiO2, 0.16-0.46 %TiO_2, 20.44-21.36 %Al_2O_3, 28.63-31.29 %FeO_{Total}, 0.09-0.13 % MnO, 9.99-11.51 %MgO, 0.03-0.08 %CaO, 0.00-0.03 %Na_2O and 0.02-0.66 %K_2O.

Very fine-grained gneiss, chlorites consist of 28.30-28.44 %SiO2, 0.01-0.04 %TiO_2, 20.12-20.23 %Al_2O_3, 27.18-27.22 %FeO_{Total}, 0.13-0.18 % MnO, 13.48-13.89 %MgO, 0.05-0.08 %CaO, about 0.02 %Na_2O and 0.01-0.02 %K_2O.

Chlorites in granitic gneiss are composed of 27.64-36.74 %SiO2, 0.27-0.71 %TiO_2, 16.64-18.24 %Al_2O_3, 18.35-25.70 %FeO_{Total}, 0.04-0.07 % MnO, 8.94-11.38 %MgO, 0.10-0.58 %CaO, 0.05-0.73 %Na_2O and 1.73-5.90 %K_2O.

In addiotion, chlorites in calc-silicate rocks are composed of 46.30-46.35 %SiO2, 0.30-0.33 %TiO_2, 16.58-16.71 %Al_2O_3, 9.20-9.33 %FeO_{Total}, 0.02-0.05 % MnO, 8.71-8.79 %MgO, about 0.11 %CaO, about 0.33 %Na_2O and 11.29-11.34 %K_2O.

Table 7 Representative EPMA analyses of chlorite found in rock samples from the Lansang National Park.

Name	Gneissic Rocks						Granitic gneiss			Calc-Silicate Rocks	
	Coarse-grained gneiss				Very fine-grained gneiss					Calc-Silicate	
	LS23C-chl1	LS23C-chl2	LS23C-chl3	LS23C-chl4	LS12A-chl1	LS12A-chl2	LS5A-Chl3	LS5A-Chl4	LS5A-Chl5	LS14A-plg2	LS14A-plg6
SiO_2	25.91	26.01	27.03	26.76	28.30	28.44	36.74	30.72	27.64	46.35	46.30
TiO_2	0.24	0.30	0.46	0.16	0.04	0.01	0.71	0.35	0.27	0.30	0.33
Al_2O_3	21.36	21.12	20.44	21.30	20.12	20.23	16.64	18.24	18.24	16.58	16.71
FeO	31.29	30.16	28.63	30.80	27.18	27.22	18.35	22.26	25.70	9.20	9.33
MnO	0.13	0.09	0.11	0.12	0.13	0.18	0.04	0.06	0.07	0.02	0.05
MgO	9.99	10.71	11.17	11.51	13.48	13.89	8.94	10.70	11.38	8.71	8.79
CaO	0.03	0.08	0.05	0.06	0.05	0.08	0.58	0.13	0.10	0.11	0.11
Na_2O	0.00	0.03	0.01	0.02	0.02	0.02	0.73	0.06	0.05	0.33	0.33
K_2O	0.02	0.27	0.66	0.12	0.02	0.01	5.90	3.75	1.73	11.29	11.34
Total	88.97	88.77	88.57	90.85	89.34	90.09	88.62	86.25	85.18	92.88	93.26
Si	2.765	2.773	2.866	2.784	2.929	2.919	3.734	3.273	3.030	4.304	4.286
Ti	0.019	0.024	0.037	0.012	0.003	0.001	0.054	0.028	0.022	0.021	0.023
Al	2.687	2.652	2.553	2.611	2.454	2.447	1.993	2.290	2.357	1.814	1.823
Fe^{3+}	0.000	0.000	0.000	0.000	0.000	0.000	0.000	0.000	0.000	0.000	0.000
Fe^{2+}	2.793	2.688	2.538	2.679	2.353	2.336	1.559	1.983	2.356	0.714	0.722
Mn	0.012	0.008	0.010	0.011	0.011	0.016	0.003	0.006	0.007	0.002	0.004
Mg	1.590	1.702	1.765	1.785	2.081	2.125	1.355	1.699	1.861	1.205	1.213
Ca	0.004	0.008	0.005	0.007	0.005	0.009	0.062	0.015	0.011	0.010	0.010
Na	0.000	0.006	0.003	0.005	0.004	0.004	0.144	0.011	0.010	0.059	0.058
K	0.002	0.037	0.089	0.016	0.003	0.001	0.765	0.510	0.242	1.337	1.339
Total	9.873	9.899	9.866	9.909	9.844	9.859	9.670	9.815	9.896	9.466	9.478

CHAPTER V
DISCUSSIONS AND CONCLUSIONS

5.1 Petrochemistry Genesis

ACF diagram of Eskola (1915) (Figure 26) was applied for plotting mole proportions between A (Al_2O_3 + Fe_2O_3 - (Na_2O + K_2O)), C (CaO - 3.33P_2O_5) and F (FeO + MgO + MnO). As the results, coarse-grained gneiss, fine-grained gneiss, very fine-grained gneiss and granitic gneiss were plotted mainly within quartzo-feldspartic rock field that may indicate protoliths' composition of greywacke sandstone, siltstone and granitiod. On the other hand, calc-silicate rock and impure marble are plotted within calcareous region. Regarding to FeO +MgO versus K_2O/(K_2O+Na_2O) diagram (Pettijohn et al., 1987; Taylor and McLennan, 1985), fine-grained gneiss and very fine-grained gneiss would have initial composition related to sedimentary rocks of arkose and shale (see in Figure 27). In the discrimination diagram of Hayashi et al. (1997) plotting between weight% Ti_2O and Zr (ppm), coarse-grained gneiss and granitic gneiss may have felsic composition (see Figure 28). According to Zr versus 10^4 Ga/Al diagram after Whalen et al. (1987), the composition of coarse-grained gneiss and granitic gneiss may relate to I- and S-type granitiod composition (see in Figure 29).

According to the depositional tectonic discrimination diagram using K_2O/Na_2O against SiO_2 with fields from Roser and Korsch (1986), all initial rocks would have occurred within an active continental margin (see in Figure 30).

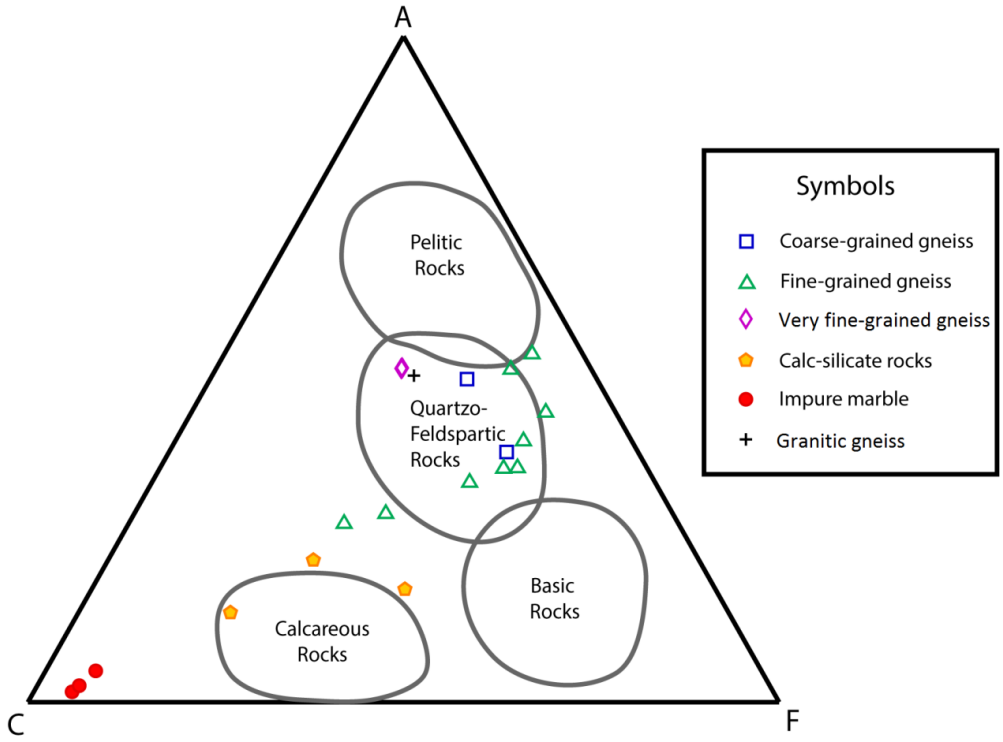

Figure 26. ACF diagram (Eskola, 1915) showing whole-rock compositions of each rock type inform the Lansang National Park area and their related initial rocks (protoliths).

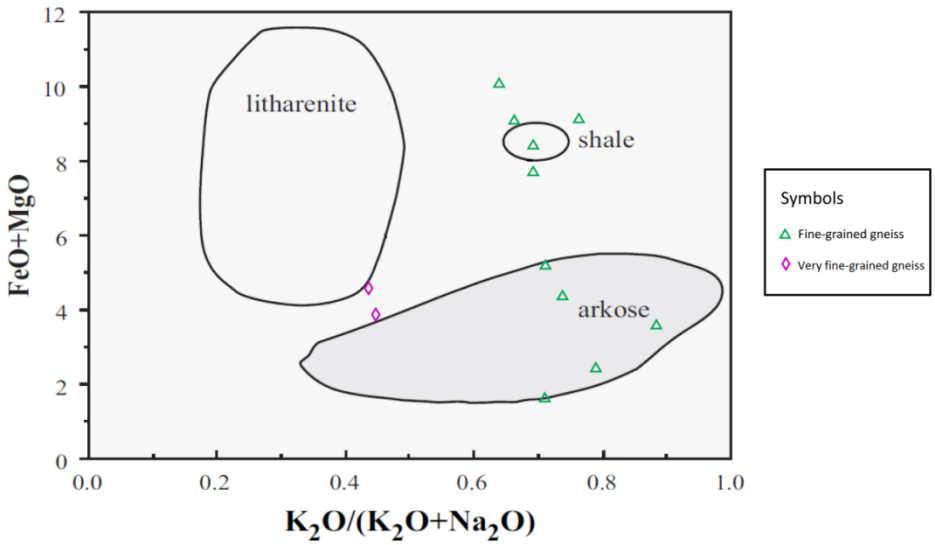

Figure 27. Diagram of FeO +MgO versus $K_2O/(K_2O+Na_2O)$ (Pettijohn et al., 1987; Taylor and McLennan, 1985) showing fine-grained gneisses and very fine-grained gneiss may relate to arkosic and shale compositions.

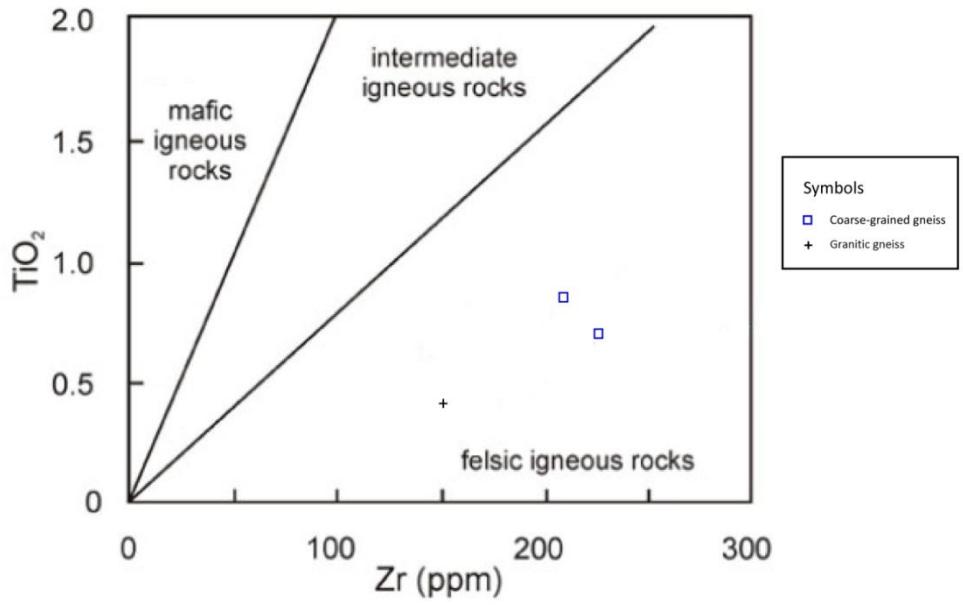

Figure 28. Discrimination diagram of Hayashi et al. (1997) showing compositional plots Ti_2O versus Zr (ppm) of coarse-grained gneiss and granitic gneiss fall within felsic composition.

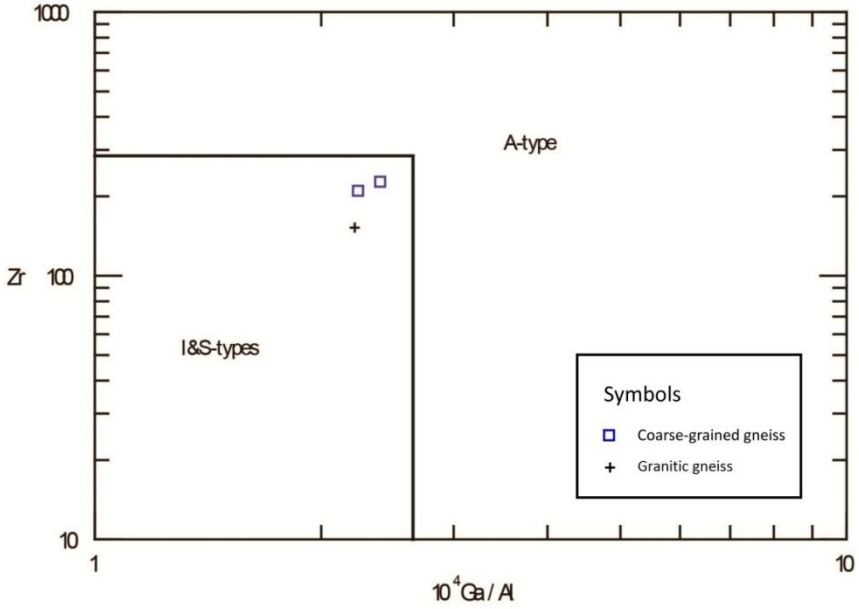

Figure 29. Zr versus 10^4 Ga/Al diagram (Whalen et al., 1987) showing the compositional plots of coarse-grained gneiss and granitic gneiss related to I- and S-types.

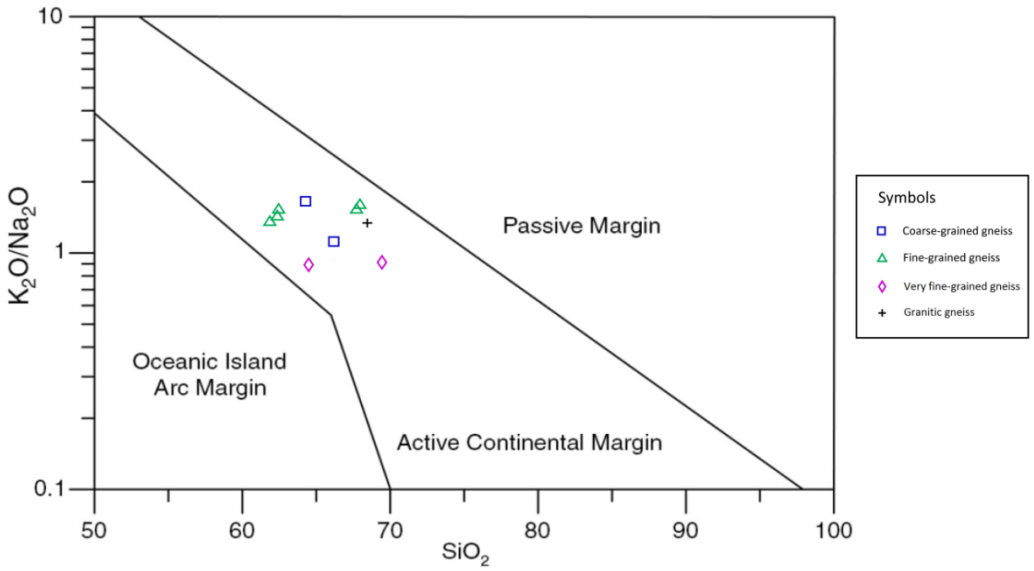

Figure 30. Tectono diagram of Roser and Korsch (1986) showing compositional plots of K_2O/Na_2O versus SiO_2 of gneissic rocks and granitic gneiss related to active continental margin.

Chondrite-normalized REE patterns (chondrite composition after Sun and McDonough, 1989) (see in Figures 31 to 34) of all gneisss are comparable to the pattern of paragneiss from the Çine submassif of the Menderes massif, Western Anatolia (Sengun et al., 2006) and pattern of orthogneiss from Wenquan metamorphic core complex in NW Chinese Tianshan (Wang et al., 2014). REE elements may indicate sedimentary provenance. Most of coarse-grained gneiss (Figure 31) and fine-grained gneiss (Figure 32) have similar patterns with elevated LREE and relatively flat HREE with strong negative EU anomaly. Eu anomalies should be effected by feldspar content in the rocks. Eu is compatible to plagioclase and potassium feldspar. Moreover, two samples of very fine-grained gneiss (Figure 33) are slightly decreasing from LREE to HREE. However, only one sample of granitic gneiss do not show negative Eu anomaly (Figure 34).

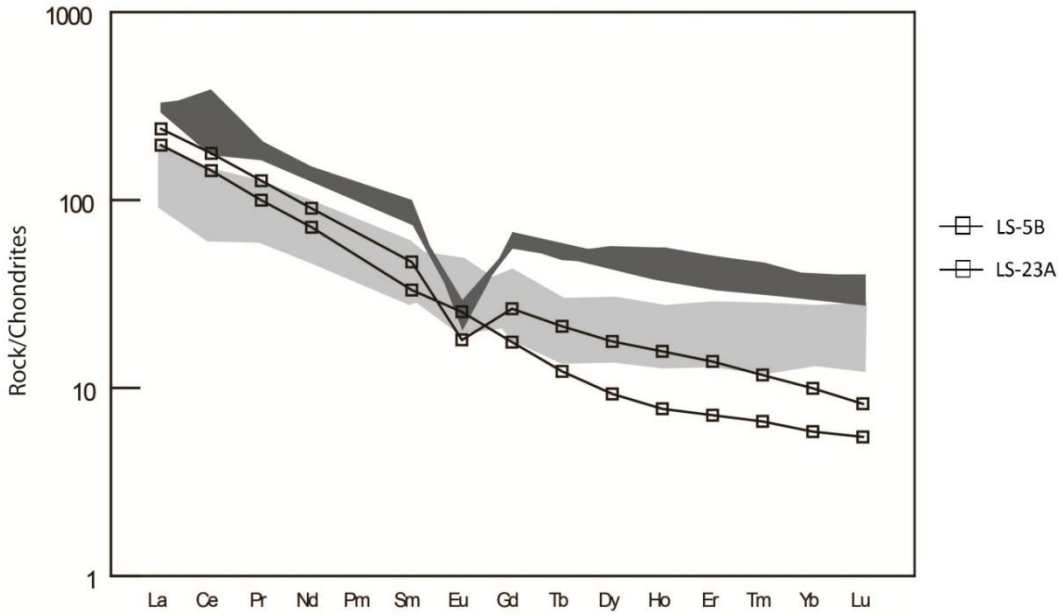

Figure 31. Chondrite-normalized REE pattern (chondrite composition after Sun and McDonough (1989)) of coarse-grained gneiss samples compared to light grey shade pattern of paragneiss from the Çine submassif of the Menderes massif, Western Anatolia (Sengun et al., 2006) and dark grey shade pattern of orthogneiss from Wenquan metamorphic core complex in NW Chinese Tianshan (Wang et al., 2014).

จุฬาลงกรณ์มหาวิทยาลัย
Chulalongkorn University

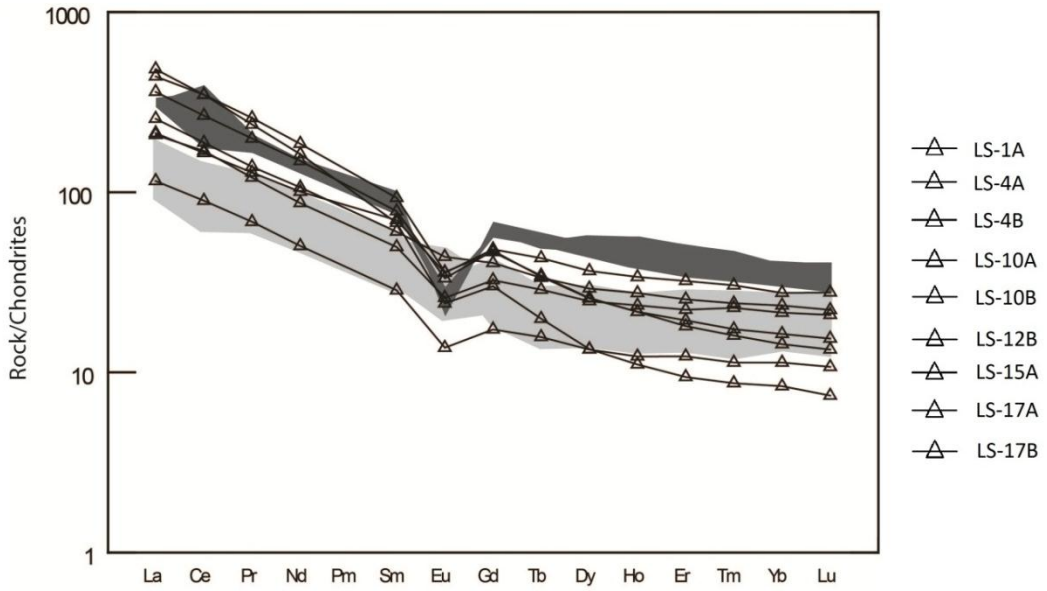

Figure 32. Chondrite-normalized REE diagrams (chondrite composition after Sun and McDonough (1989)) of fine-grained gneiss samples compared to light grey shade pattern of paragneiss from the Çine submassif of the Menderes massif, Western Anatolia (Sengun et al., 2006) and dark grey shade pattern of orthogneiss from Wenquan metamorphic core complex in NW Chinese Tianshan (Wang et al., 2014).

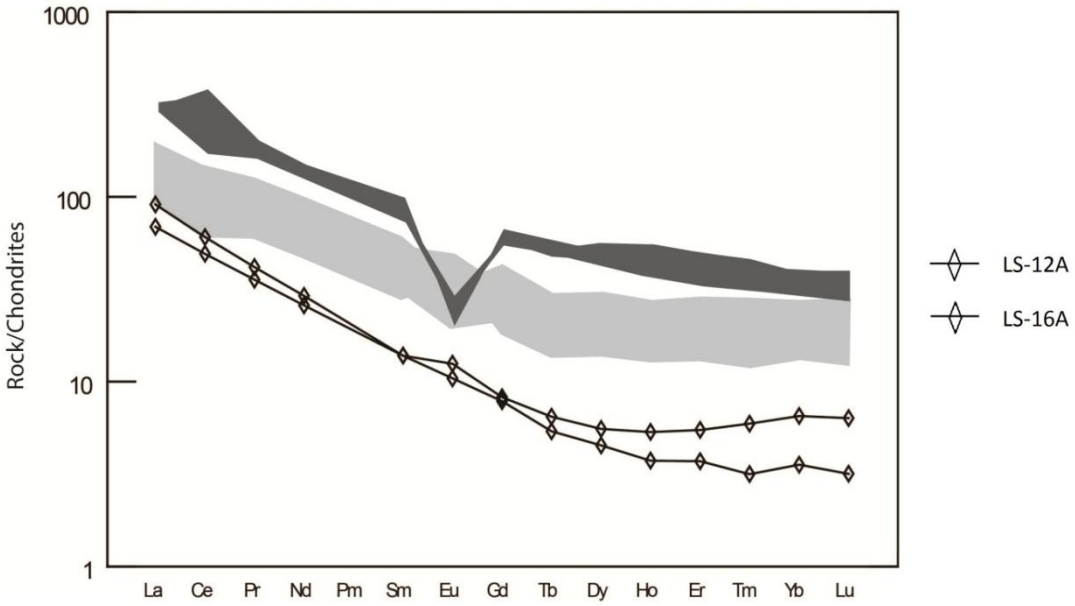

Figure 33. Chondrite-normalized REE diagrams (chondrite composition after Sun and McDonough (1989)) of very fine-grained gneiss samples compared to light grey shade pattern of paragneiss from the Çine submassif of the Menderes massif, Western Anatolia (Sengun et al., 2006) and dark grey shade pattern of orthogneiss from Wenquan metamorphic core complex in NW Chinese Tianshan (Wang et al., 2014).

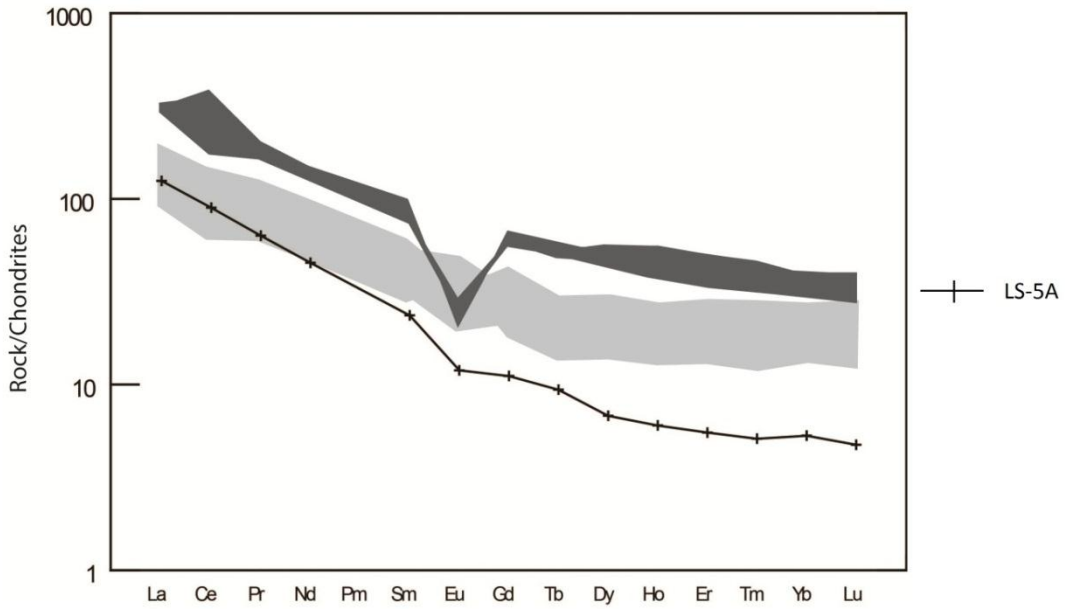

Figure 34. Chondrite-normalized REE diagrams (chondrite composition after Sun and McDonough (1989)) of granitic gneiss sample compared to light grey shade pattern of paragneiss from the Çine submassif of the Menderes massif, Western Anatolia (Sengun et al., 2006) and dark grey shade pattern of orthogneiss from Wenquan metamorphic core complex in NW Chinese Tianshan (Wang et al., 2014).

5.2 Metamorphism

Lansang metamorphic suites located in the western Thailand is a part of Chiang Mai-Lincang Belt (CM-LB) and it is associated with plutonic intrusion (Lacassin et al., 1993; Palin et al., 2013) Based on field investigation and petrographic study, these metamorphic suites are mostly represented by gneissic rock, calc-silicate rocks and granitic gneiss under high-grade metamorphism condition. Gneissic rocks are composed of quartz, plagioclase, K-feldspar, biotite, chlorite and perhaps amphibole in some samples. Calc-silicate rocks consist of calcite matrix, porphyroblasts of quartz, plagioclase, K-feldspar with minor amounts of amphibole, diopside, biotite, chlorite and fine-grained garnet. Two stages of metamorphism are observed. The first stage has

been metamorphosed under the high-grade equilibrium condition represented by granoblastic texture with nematoblastic texture of amphibole, biotite and plagioclase. Metamorphic reactions may be involved by amphibole, plagioclase, biotite, K-feldspar and quartz. In calc-silicate rocks, metamorphic reactions may be essentially involved by calcite, dolomite, quartz, diopside, amphibole and fine-grained garnet.

The other stages are observed in fine-grained gneiss which may have been metamorphosed under the low-grade equilibrium condition represented by lepioblastic texture and reaction rim between biotite and chlorite. In gneissic rocks, metamorphic reactions may be essentially involved by biotite, chlorite, plagioclase, K-feldspar and quartz. In calc-silicate rocks, metamorphic reactions may be essentially involved by calcite, dolomite, quartz, plagioclase, K-feldspar and chlorite.

ACF tertiary diagram are applied to plot mole proportions between A = (Al_2O_3 + Fe_2O_3) - (Na_2O + K_2O), C = (CaO - 3.33P_2O_5) and F = (FeO + MgO + MnO). All samples were selected for presentation of metamorphic facies, particularly for gneissic rocks in this study. Consequently, these rocks are significantly corresponding to amphibolite and greenschist facies, based on their mineral assemblages after Eskola (1915) and Woudloper (2009). Gneissic rocks and granitic gneiss are plotted in the field of quartzo-feldspartic composition whereas calc-silicae rocks fall within calcareous field (Figure 35), which may indicate protoliths prior to metamorphism.

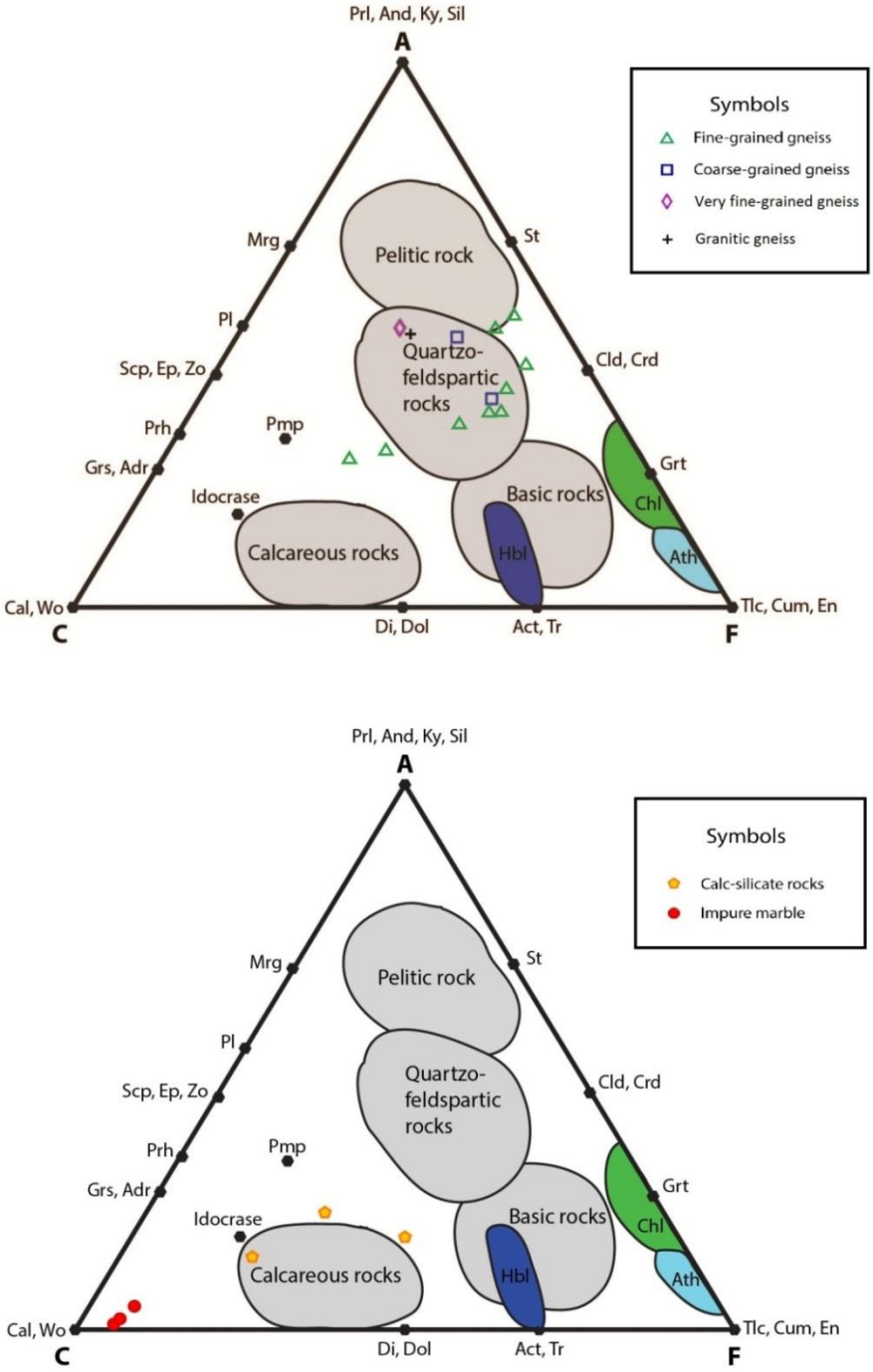

Figure 35. ACF diagrams (Eskola, 1915; Woudloper, 2009) showing the whole-rock chemical plots and main mineral assemblages of metamorphic rocks. (a) gneissic rocks and granitic gneiss. (b) calc-slicate rocks and impure marble.

Pressure and temperature (P-T) condition can be obtained in several methods using analytical data, e.g., mineral assemblages, whole-rock geochemistry and mineral chemistry.

1. P-T conditions calculated from Geothermobarometer using evaluated data from mineral assemblages of rock samples. To select Geothermometer (GT) and Geobarometer (GB) from Mineral Chemistry for using Petrological Elementary Tools (PET) for Mathematica 5.2.msi (Dachs, 1998, 2004).
2. P-T Conditions calculated using data from psudosection and mineral isopleths. All analytical data such as petrography including mineral assemblages and whole-rock geochemistry to calculate psudosection using PerPlex (vertex.exe, psvdraw.exe and pssect.exe) (Connolly, 1995, 2005). And using the data from mineral isopleth from mineral assemblages and mineral chemistry with werami.exe and pscontor.exe programs. After that use program MathLab to read the Mineral Isopleths.

Petrological Elementary Tools or PET is an easy tool using Mathematica to calculate mineral equilibria from consistent thermodynamic stability and standard data sets in the program (Berman, 1991; Holland and Powell, 1990), which contains more than 25 common thermometers and 10 barometers. Thermodynamic function calculated from several solid solutions, projection of the composition of a phase to analysis of mineral assemblages.

Estimation of these geothermobarometries has been using PET for Mathematica calculation (Dachs, 1998, 2004). The amphibole-plagioclase equilibrium may provide P-T of metamorphism peak. Various compositions of mineral assemblages have been obtained from Electron Probe Micro-Analyzer (EPMA). In addition, mineral isopleths of

plagioclase mostly observed in all type of samples were used to estimate in conjunction with geothermobarometric model and psuedosection. All symbols for rock-forming minerals used for estimate P-T condition in this study have been given by Bucher and Grapes (2011).

Four samples were selected including LS-23A of coarse-grained gneiss, LS-1A of fine-grained gneiss, LS-12A of very fine-grained gneiss and LS-12C of impure marble.

For coarse-grained gneiss, geothermometry based on biotite-chlorite (GT4) and mineral isopleths of plagioclase (Xan) were used to find the pressure and temperature. In fine-grained gneiss, Al in amphibole barometry (GB13) (Hollister et al., 1987; Schmidt, 1992) and mineral isopleths of plagioclase (Xan) were selected to calculate pressure and temperature of peak metamorphism, that are suitable for fine-grained gneiss. The lepidoblastic amphiboles observed in many samples are mostly actinolite-tremolite situated within plagioclase groundmass. Very fine-grained gneiss and calc-silicate rocks were used mineral isopleths of plagioclase (Xan) to estimate P-T of metamorphism.

Results of P-T estimation from combination of psuedosection and geoberometric model are described below.

Chulalongkorn University

According to coarse-grained gneiss (LS-23A), psuedosection shows a group of mineral assemblages (Figure 36). The representative filed which contains mineral assemblages of Chl-Pl-Phl-Ann-Kfs-Qtz-H_2O is stable in P-T field. Mineral isopleths of plagioclase (Xan) and biotite-chlorite geothermometry were taken into psuedosection. Consequently, range of P-T condition of coarse-grained gneiss fall within 560-580°C and 5.7-7.5 Kbar.

Fine-gained gneiss (LS-1A) comprises major of quartz, plagioclase, K-feldspar, amphibole and chlorite. This sample shows group mineral assemblages of Pl-Cpx-Tr-Kfs-Qtz- H_2O (Cpx is absent phase) (see Figure 37). Mineral isopleths of plagioclase (Xan) and Al in amphibole barometry show P-T range of 545-560°C and low pressure between 0.5-0.8 Kbar.

Very fine-grained gneiss (LS-12A) shows mineral assemblage of Pl-Cpx-Opx-Phl-Kfs-Qtz-H_2O (Cpx-Opx are absent phases) (Figure 38). P-T estimation were calculated from mineral isopleths of plagioclase (Xan) that indicate P-T range is closely 440-500°C and 3.0-5.0 Kbar.

Impure marble (LS-12C) shows the stability of mineral assemblages of Chl-Pl-Opx-Cpx-Phl-Kfs-Qtz-H_2O (Cpx-Opx are absent phases) (Figure 39). P-T psuedosection and mineral isopleths of plagioclase (Xan) indicate P-T range of about 480-510°C and 6.0-6.8 Kbar.

จุฬาลงกรณ์มหาวิทยาลัย
Chulalongkorn University

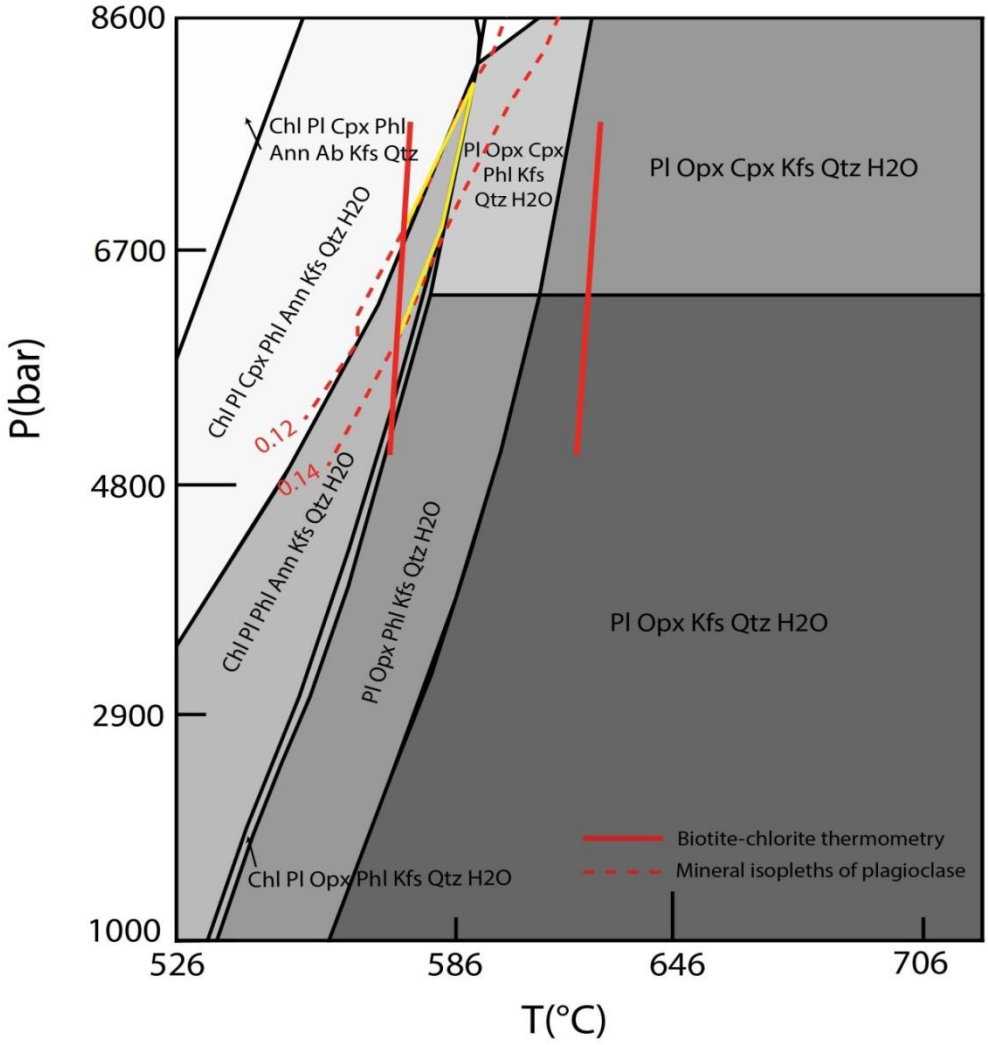

Figure 36. Plots of pressure and temperature (P-T) of biotite-chlorite thermometry and mineral isopleths of plagioclase. Psuedosection showing range of peak metamorphism of coarse-grained gneiss.

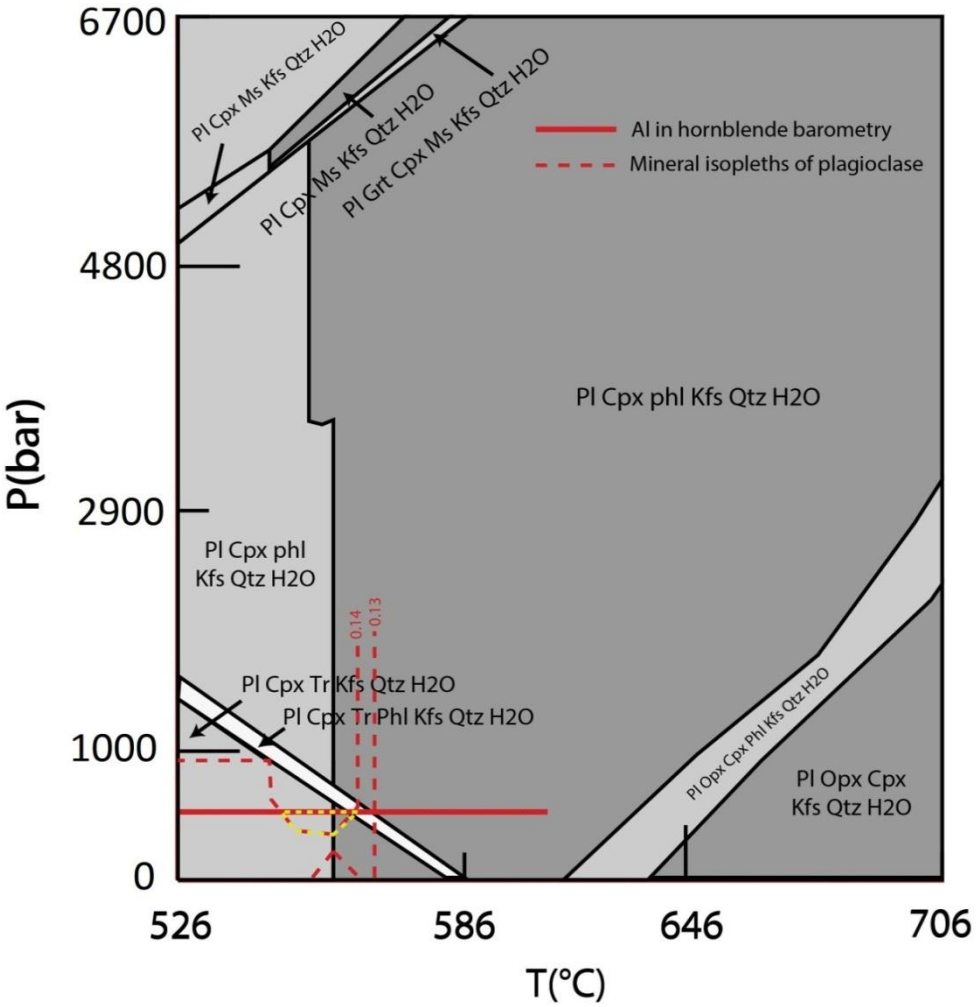

Figure 37. Plots of pressure and temperature (P-T) of Al in hornblende barometry and mineral isopleths of plagioclase. Psuedosection showing range of peak metamorphism of fine-grained gneiss.

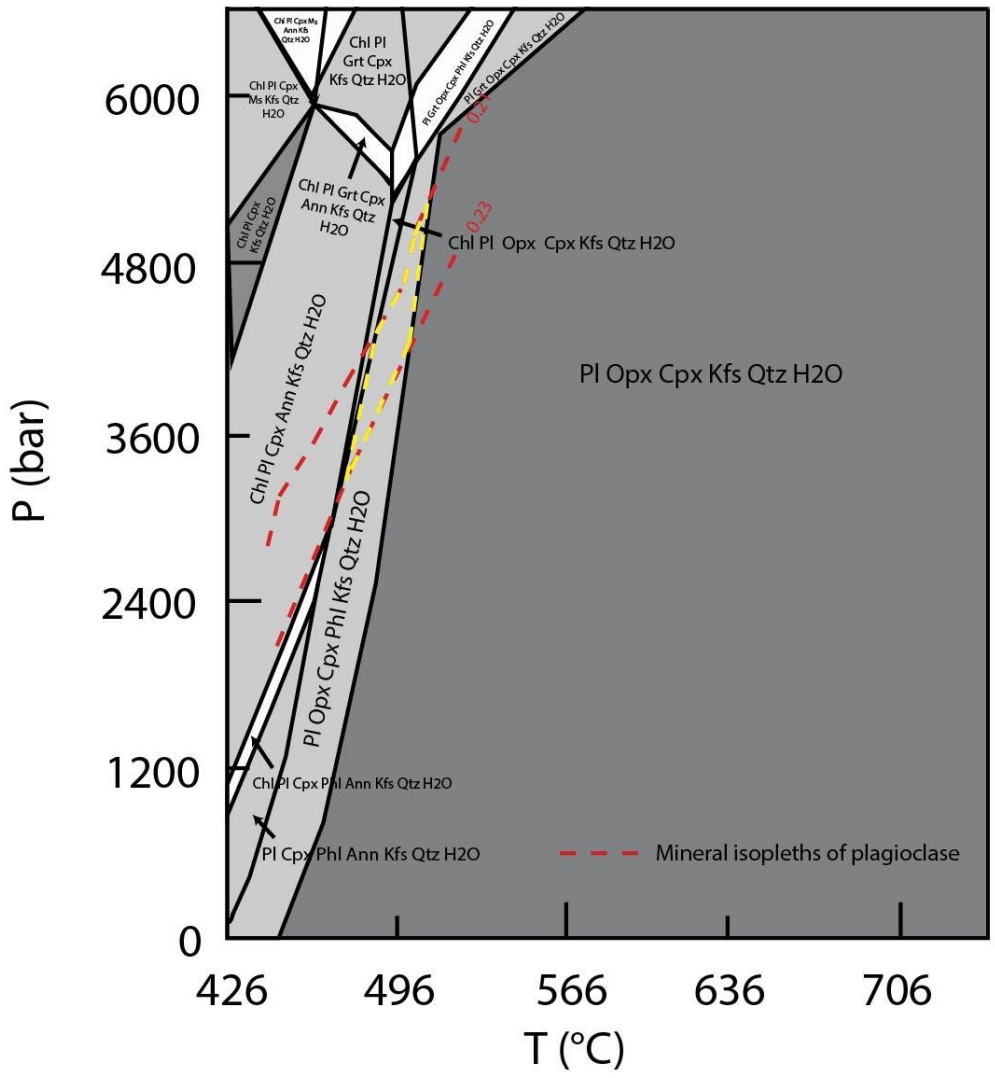

Figure 38. Plots of pressure and temperature (P-T) used mineral isopleths of plagioclase. Psuedosection showing range of peak metamorphism of very fine-grained gneiss.

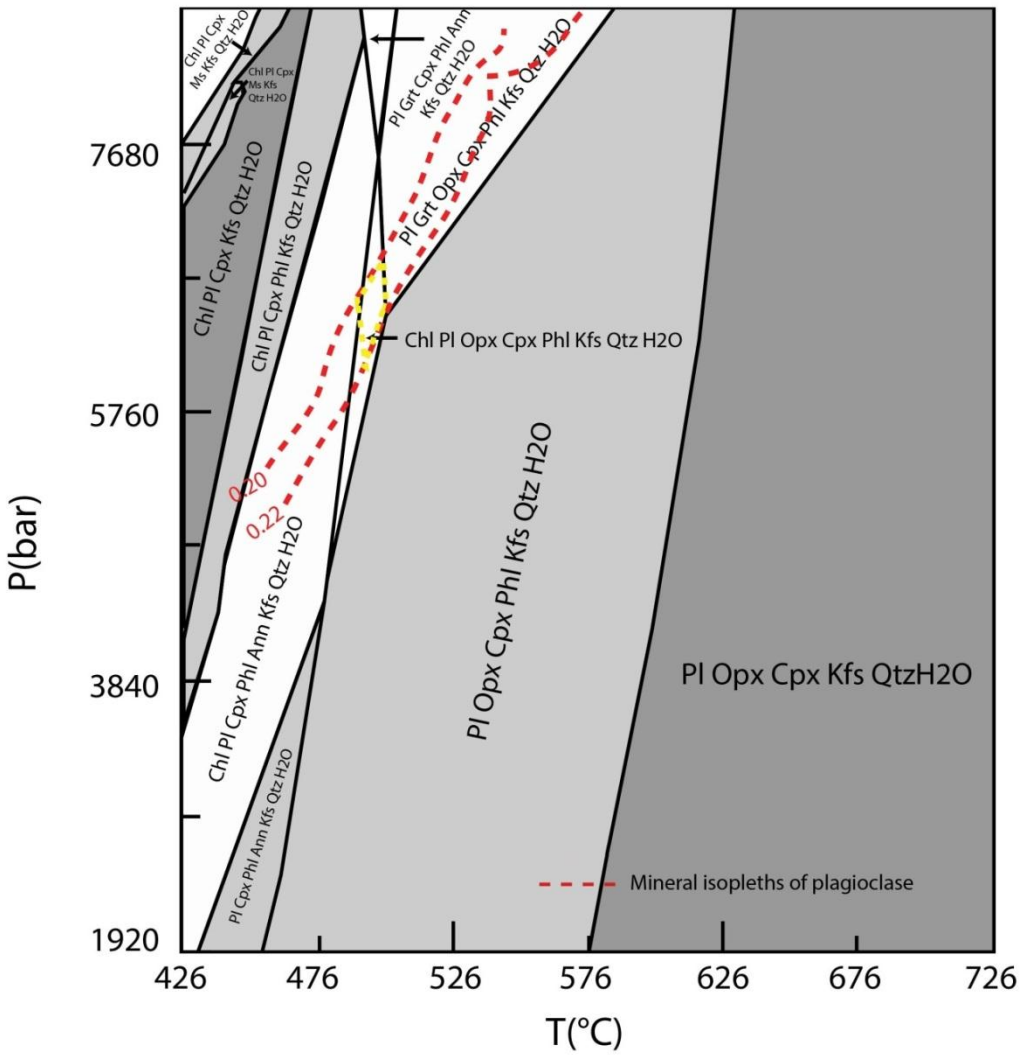

Figure 39. Plots of pressure and temperature (P-T) used mineral isopleths of plagioclase. Psuedosection showing range of peak metamorphism of impure marble.

All temperature and pressure ranges which were estimated from psuedosections, geothermobarometry and mineral isopleths are also plotted in Figure 40. This is belonging to lower amphibolite facies to upper greenschist facies under P-T ranges of 440-580°C and 0.5.7-7.5 Kbar. These results are close to previous researches of orthogneiss and paragneiss from Doi Intanon Core Complex (MacDonald et al., 1993; Macdonald et al., 2010). This suggests that range of temperature should be between ca.725°C down to 535°C and pressure range from 7 kbar down to 3 kbar. Previous research from Nantasin et al. (2012) indicate that rocks of Thabsila metamorphic complex undertaken medium amphibolite facies about 640-710°C and 5.5-8 kbar. Regional geology of Lansang Natioanl Park suggested that mylonitied gneiss mainly belonges to greenschist facies (Kanjanapayont et al., 2011).

Figure 40 shows pressure and temperature (P-T) plots of gneissic rocks and impure marble from the Lansang National Park, Changwat Tak indicating P-T ranges of representative rock within lower amphibolite facies to upper greenschist facies.

จุฬาลงกรณ์มหาวิทยาลัย
Chulalongkorn University

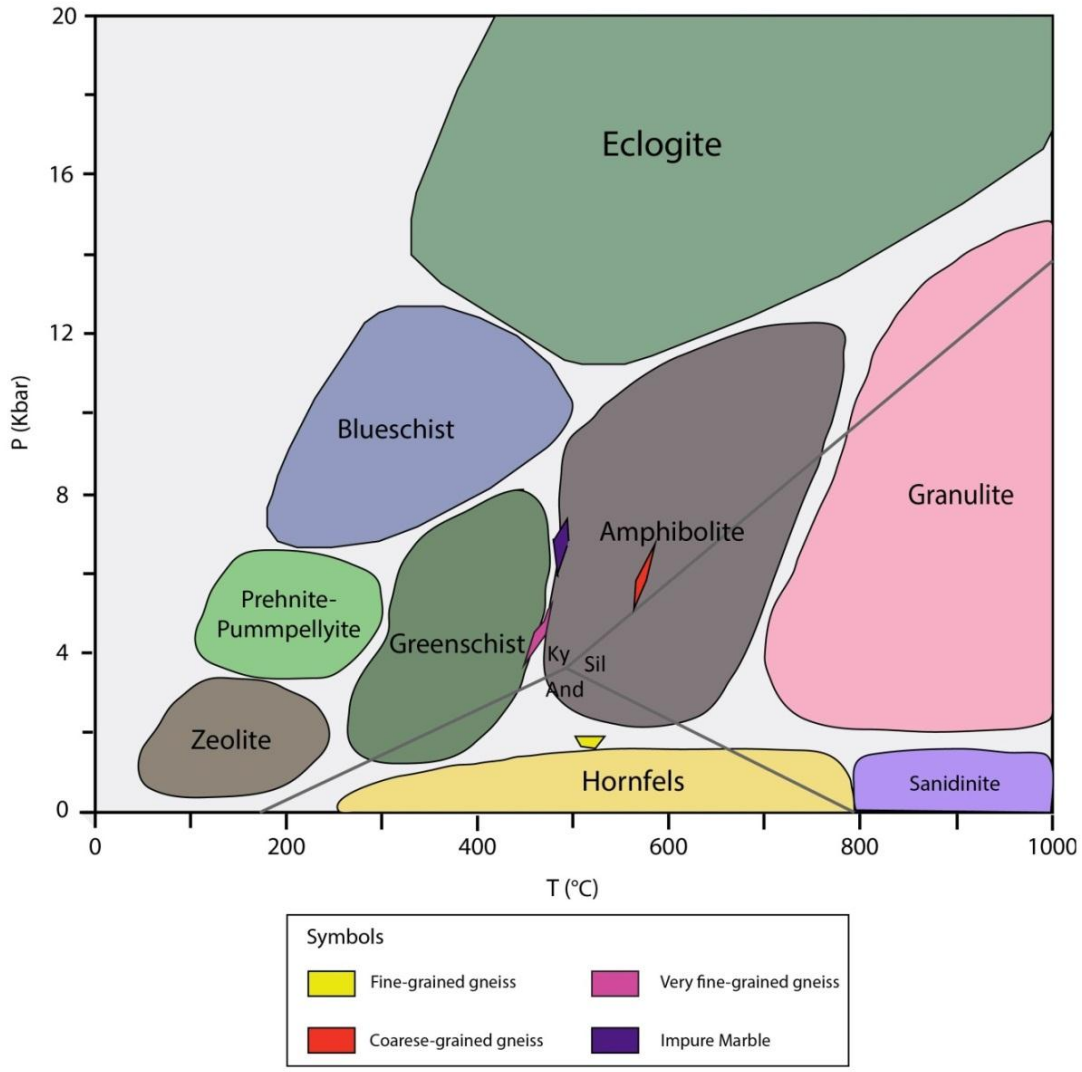

Figure 40. Plots of pressure and temperature (P-T) ranges of coarse-grained gneiss, fine-grained gneiss, very fine-grained gneiss and impure marble from the Lansang Natioanl Park, Changwat Tak under this study in correlation with metamorphic facies after Woudloper (2008).

5.3 Ancient Tectonic Setting

Petrochemical and Whole-rock geochemical data of gneissic rocks and related rocks represent initial sources of granitic rocks and sedimentary rocks prior to metamorphism at different metamorphic grades. Trace elements and REE elements of coarse-grained gneiss and granitic gneiss also show the composition similar to fine-

grained gneiss signature of Average Upper Crust as well as spider diagram patterns are close to orthogneiss from Wenquan metamorphic core complex in NW Chinese Tianshan (Wang et al., 2014). They reported orthogneiss derived from S-type granite. Trace elements and REE elements of fine-grained gneiss show the compositional signature of Average Upper Crust (Avr. Upper crust) and North American Shale Composite (NASC) composition as well as their spider diagram patterns are similar to paragneiss from the Çine submassif of the Menderes massif, Western Anatolia (Sengun et al., 2006) in which they have been reported as paragneiss metamorphosed from mudstone and subarkosic composition.

The main tectonic event in the study area, Lansang National Park, may have sarted from collision between Western Burma block and Shan-Thai. Western Burma block was rifted from Gonwanaland in the Late Triassic (Metcalfe, 1996). During Cretaceous, of Western Burma had accreted and collided to the Shan Thai (Metcalfe, 1996). Geochemical and geochronological studies of the adjacent area such as Mogok Belt and Slate belt in eastern Myanmar (Barley et al., 2003; Searle et al., 2007) may be supported evidences, these studies indicate age of magmatic arc active in Late Jurassic-Early Cretaceous (between 170-120 Ma; U-Pb zircon). More evidences are clearly that regional magmatism was occurred in Cretaceous.

MacDonald et al. (1993) and Dunning et al. (1995), studied metamorphic event of Doi Inthanon metamorphic core complex in northern Thailand. U-Pb zircon dating of megacrystic orthogneiss indicates that initial age of granitic source would have formed during Late Triassic-Early Jurassic (203±4 Ma and between 203-211 Ma) which appear to have under taken high grade metamorphism in Late Cretaceous (72±1 Ma, 84±2 Ma and 72±1 Ma, based on U-Pb monazite from orthogneiss). In addition, zircon dating using U-Pb indicated crystallization age of Mea Cham granitic pluton that shows the

จุฬาลงกรณ์มหาวิทยาลัย
Chulalongkorn University

evidence of orthogneiss may be crystallized from this granitic pluton (MacDonald et al., 1993)

In addition, geochonological data suggested metamorphism age of Thabsila metamorphic complex between 51–57 Ma prior to India-Eurasia collision before basement cooling at about 32–36 Ma (Nantasin et al., 2012).

Consequently, the initial granite of coarse-grained gneiss from Lansang may intrude in Late Triassic-Early Jurassic (203±4 Ma and between 203-211 Ma) (Dunning et al., 1995; MacDonald et al., 1993), which probably occurred from partial melting after collisions between Shan Thai, Nakhon-Thai, Lampang- Chiang Rai and Indochina during Late Jurassic-Early Cretaceous (see in Figure 41).

In Late Cretaceous to Paleocene, thermal overprinting event from regional metamorphism has been identified in granite-migmatite gneiss complex in Thailand along Northward to Southward core complex. Radiometric dating studies (ages between 80 and 60 Ma) was investigated and interpreted as partial melting of granitic dyke cross cutting into host rock that are observed in this area (Ahrendt et al., 1997; Palin et al., 2013). Data of U-Pb dating of Monazite can confirm and indicate upper amphibolite facies metamorphism of granite-migmatite gneiss while partial melting may take place at the same time during Late Cretaceous (Dunning et al., 1995; MacDonald et al., 1993).

Subsequently, ductile stage evidences from Mae Ping strike-slip fault (MPF fault) during the period of 45-37 Ma (Palin et al., 2013) after India and Eurasia collision during Early Eocene between 50-55 Ma (Hutchison, 2007) which indicate the lower limit of maximum age of left-lateral shear fabrics and initiation of MPF prior to transpressional uplifting of mylonite zone at about 23.5 Ma. These observations have been corroborated by ^{40}Ar-^{39}Ar biotite cooling age (Lacassin et al., 1997).

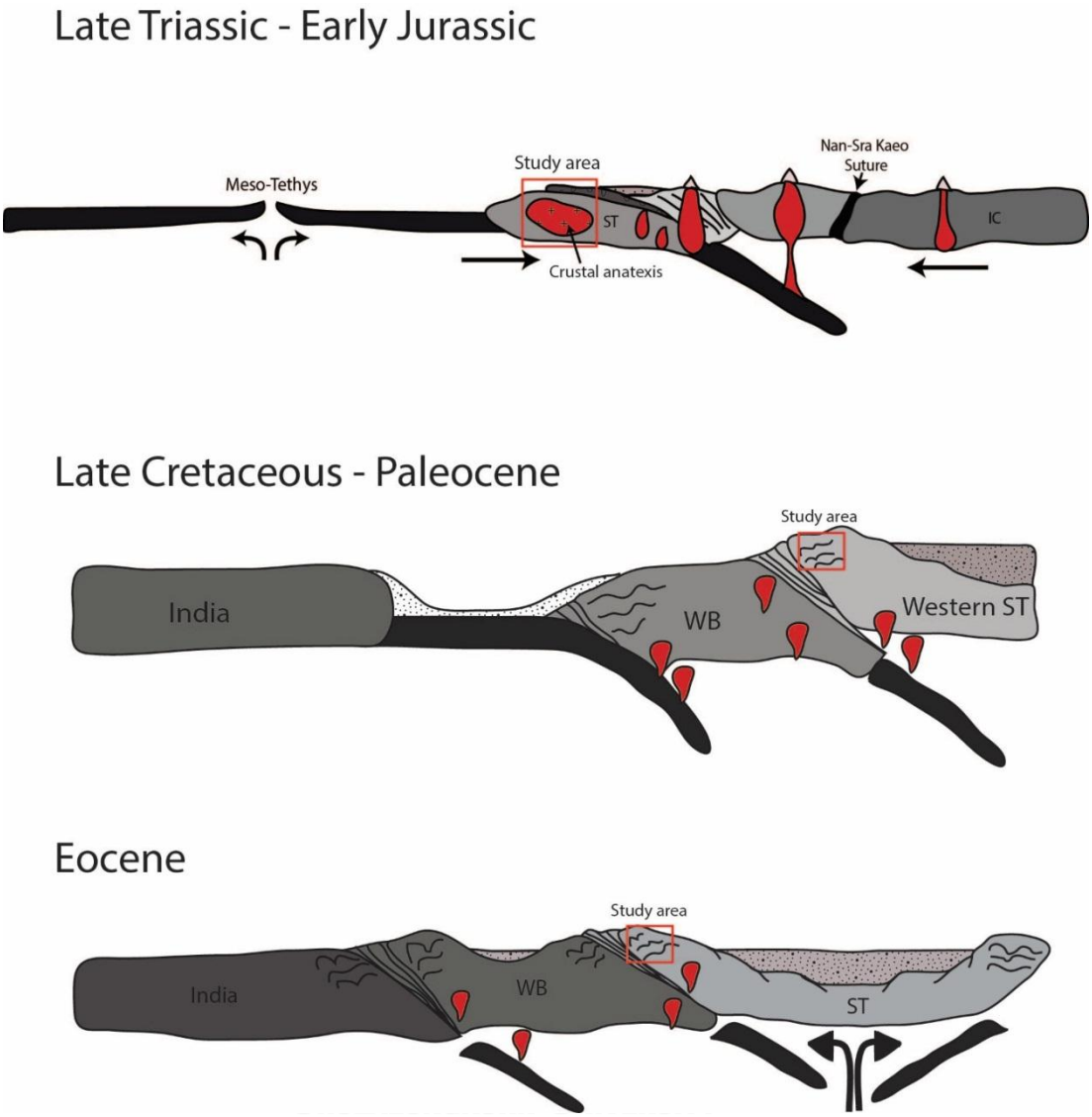

Figure 41. Tectonic evolution model of the study area in the Lansang Natioanl Park, Changwat Tak (revise after Charusiri et al. (2002); (Sone and Metcalfe (2008))). Starting from initial rock of granitic pluton and sedimentary rocks after collisions of Shan Thai (ST), Nakhon-Thai, Lampang- Chiang Rai and Indochina (IC) in Late Trissic-Early Jurassic. Subsequently, metamorphism has occurred prior to collision between Indian plate and Western Burma plate. Subsequently, Indian-Eurasian collision may have reached to next stage of metamorphism and ductile-brittle stage along the sinistral strike-slip Mae Ping Fault during Eocene period.

5.4 Conclusions

The metamophic basement of the Lansang metamorphic suites can be described as followed:

1. Lansang Metamorphic Suites located in the Lansang National Park, Changwat Tak. These metamorphic suites can be divided into three main groups, based on petrographic studies, whole-rock geochemistry and mineral chemistry. They are composed of gneissic rock (i.e., coarse-grained gneiss, fine-grained gneiss and very fine-grained gneiss), calc-silicte rock (i.e., calc-silicate and impure marble) and granitic gneiss.
2. Coarse-grained gneisses are composed of quartz, plagioclase, K-feldspar, biotite and chlorite. Analytical data indicate initial rock of quartzo-feldsparthic rocks which are close to S-type granite. It may be partially melted from crustal antexis, undertaken lower amphibolite to upper greenschist facies with P-T range between 565-590°C and 5.7-7.8 Kbar.
3. Fine-grained gneisses mainly consist of quartz, plagioclase, K-feldspar, biotite and minor of amphibole. Their geochemistry falls within the same ranges assuming that they probably have quartzo-feldsparthic protolith close to shale and arkosic composition before undertaking regional metamorphism of lower amphibolite to upper greenschist facies with P-T range of about 545-560°C and 0.5-0.7 Kbar
4. Very fine-grained gneisses mainly consist of quartz, plagioclase, K-feldspar, biotite and minor of chlorite. Geochemical data show quartzo-feldsparthic protolith which may be related to arkosic composition before undertaking metamorphism of lower amphibolite to upper greenschist facies within P-T rang of about 440-480°C and 1.1-5.7 Kbar.

จุฬาลงกรณ์มหาวิทยาลัย
Chulalongkorn University

5. Granitic gneiss is composed of quartz, plagioclase, K-feldspar, biotite and chlorite. Analytical data indicate quartzo-feldsparthic composition of protolith before undertaking metamorphism of lower amphibolite to upper greenschist facies.
6. Calc-silicate rock and impure marble are found interbeded with gneissic rock with strongly deformation that show foliation parallel to the host rocks. Their mineral assemblages are composed of quartz, feldspar, calcite, garnet and minor amounts of pyroxene, amphiole. In addition, whole-rock geochemistry is different from gneissic rock and granitic gneiss. They may occur from initial rock of impure limestone composition. They may have metamorphed under 460-480°C and 5.9-6.8 Kbar in lower amphibolite to upper greenschist metamorphism facies.
7. Tectonic evolution of the study area (revised after Charusiri et al., 2002) started from initial rock of granitic anatexis and sedimentary rocks after collision between Shan Thai and Indochina in Early Triassic-Early Jurassic. Subsequently, metamorphism may have occurred prior to collision between Indian plate and Western Burma plate. Subsequently, collision between Indian plate and Eurasian plate may be reached to metamorphism and ductile-brittle stage of these rocks along the sinistral strike-slip Mae Ping Fault during Eocene period before transpressional uplifting of mylonite zone.

REFERENCES

Ahrendt, H., Hansen, B.T., Lumjuan, A., Mickein, A., Wemmer, K., 1997. Tectonometamorphic evolution of NW-Thailand deduced from U/Pb-, Rb/Sr-, Sm/Nd- and K/Ar-isotope investigations. The International Conference on Stratigraphy and Tectonic Evolution of Southeast Asia and the South Pacific, 314-319.

Barley, M.E., Pickard, A.L., Zaw, K., Rak, P., Doyle, M.G., 2003. Jurassic to Miocene magmatism and metamorphism in the Mogok metamorphic belt and the India-Eurasia collision in Myanmar. Tectonics 22.

Baum, F., Braun, E.v., Hahn, L., Hess, A., Koch, K.E., Krause, G., Quarsh, H., Siebenhuner, M., 1970. On the geology of northern Thailand. Beih. Geol. Jb., Hannover 102, 1-24.

Beckinsale, R.D., Suensilpong, S., Nakapadungrat, S., Walsh, J.N., 1979. Geochronology and geochemistry of granite magmatism in Thailand in relation to a plate tectonic model. Journal of the Geological Society 136, 529-537.

Berman, R.G., 1991. Thermobarometry using multi-equilibrium calculations: a new technique, with petrological applications. Canadian Mineralogist 29 (1991), 833–855.

Bucher, K., Grapes, R., 2011. Petrogenesis of Metamorphic Rocks, 8 ed. Springer-Verlag Berlin Heidelberg.

Bunopas, S., 1981. Paleogeographic History of Western Thailand and Adjacent Parts of Southeast Asia: A Plate Tectonic Interpretation. Victoria University of Wellington, New Zealand, p. 810.

Bunopas, S., Vella, P., 1992. Geotectonics and geologic evolution of Thailand, National Conference on Geologic Resources of Thailand: Potential for Future Development, Bangkok, Thailand.

จุฬาลงกรณ์มหาวิทยาลัย
Chulalongkorn University

Campbell, K.V., 1975. Basement complexes, In: Stokes, R.B., Tantisukrit, C., Campbell, K.V. (Eds.), in: Proceedings of the conference on the geology of Thailand, Dept. Geol. Sciences, Chaing Mai Univ., Thailand, Spec. Publ, pp. 3-12.

Charusiri, P., Clark, A.H., Farrar, E., Archibald, D., Charusiri, B., 1993. Granite belts in Thailand: evidence from the 40Ar/39Ar geochronological and geological syntheses. Journal of Southeast Asian Earth Sciences 8, 127-136.

Charusiri, P., Daorerk, V., Archibald, D., Hisada, K., Ampaiwan, T., 2002. Geotectonic evolution of Thailand, A New Synthesis. Journal of the Geological Society of Thailand, 1-20.

Connolly, J.A.D., 1995. Phase diagram methods for graphitic rocks and application to the system C−O−H−FeO−TiO2−SiO2. Contr. Mineral. and Petrol. 119, 94-116.

Connolly, J.A.D., 2005. Computation of phase equilibria by linear programming: A tool for geodynamic modeling and its application to subduction zone decarbonation. Earth and Planetary Science Letters 236, 524-541.

Dachs, E., 1998. PET: petrological elementary tools for mathematica. Computers & Geosciences 24, 219-235.

Dachs, E., 2004. PET: Petrological Elementary Tools for Mathematica®: an update. Computers & Geosciences 30, 173-182.

Deer, W.A., Howie, R.A., Zussman, J., 1992. An Introduction to the Rock-forming Minerals, 2nd ed. ed. Essex: Longman Scientific and Technical; New York: Wiley.

Department of Mineral Resources, D., 1999. Geological map of Thailand, scale 1:1,000,000. Geological Survey Division, Department of Mineral Resources, Bangkok, Thailand.

Department of Mineral Resources, D., 2007. Geology of Thailand, 2nd edition ed. Department of Mineral Resources, Bangkok, Thailand.

Dheeradilok, P., Lumjuan, A., 1983. On the metamorphic and Precambrian rock of Thailand. Conferences on Geology and Mineral Resources of Thailand, Bangkok, Thailand, 113-119.

Dunning, G.R., Macdonald, A.S., Barr, S.M., 1995. Zircon and monazite U□Pb dating of the Doi Inthanon core complex, northern Thailand: implications for extension within the Indosinian Orogen. Tectonophysics 251, 197-213.

Eskola, P., 1915. On the relation between chemical and mineralogical composition in the metamorphic rocks of the Orijarvi region. Comm. Geol. Finlande Bull. 44, 114-117.

Eyuboglu, Y., Santosh, M., Bektas, O., Chung, S.-L., 2011. Late Triassic subduction-related ultramafic–mafic magmatism in the Amasya region (eastern Pontides, N. Turkey): Implications for the ophiolite conundrum in Eastern Mediterranean. Journal of Asian Earth Sciences 42, 234-257.

Gromet, L.P., Haskin, L.A., Korotev, R.L., Dymek, R.F., 1984. The “North American shale composite”: Its compilation, major and trace element characteristics. Geochimica et Cosmochimica Acta 48, 2469-2482.

Hahn, L., Koch, K.E., Witte Kindt, H., 1986. Outline of the geology and mineral potential of Thailand. Geologische Jahrbuch, Reihe B.49, 3-49.

Hayashi, K.-I., Fujisawa, H., Holland, H.D., Ohmoto, H., 1997. Geochemistry of ～1.9 Ga sedimentary rocks from northeastern Labrador, Canada. Geochimica et Cosmochimica Acta 61, 4115-4137.

Holland, T.J.B., Powell, R., 1990. An enlarged and updated internally consistent thermodynamic dataset with uncertainties and correlations: the system K2O-Na2O-CaOMgO-MnO-FeO-Fe2O3-Al2O3-TiO2-SiO2-C-H2-O2. Journal of metamorphic Geology 8, 89-124.

Hollister, L.S., Grissom, G.C., Peters, E.K., Stowell, H.H., Sisson, V.B., 1987. Confrrmation of the empirical correlation of Al in hornblende with pressure of solidification of calc-alkaline plutons. American Mineralogis 72, 231-239.

Hutchison, C.S., 2007. Geological Evolution of Southeast Asia, 2nd Ed. ed. Geological Society of Malaysia, Kuala Lumpur.

Kanjanapayont, P., Grasemann, B., Edwards, M.A., Fritz, H., 2012. Quantitative kinematic analysis within the Khlong Marui shear zone, southern Thailand. Journal of Structural Geology 35, 17-27.

Kanjanapayont, P., Kieduppatum, P., Klötzli, U., Klötzli, E., Charusiri, P., 2013. Deformation history and U–Pb zircon geochronology of the high grade metamorphic rocks within the Klaeng fault zone, eastern Thailand. Journal of Asian Earth Sciences 77, 224-233.

Kanjanapayont, P., KlÖtzli, U., Charusiri, P., KlÖtzli, E., 2011. LA-MC-ICP-MS U-Pb zircon geochronology of the Lan Sang and Nong Yai gneisses, Thailand, In: Satarugsa, P., Lertsirivorakul, R., Kromkhun, K., Promkotra, S. (Eds.), In Proceedings of International Conference on Geology, Geotechnology and Mineral Resources of Indochina (GEOINDO 2011), Khon Kaen, Thailand, pp. 62-64.

Lacassin, R., Leloup, P.H., Tapponnier, P., 1993. Bounds on strain in large Tertiary shear zones of SE Asia from boudinage restoration. Journal of Structural Geology 15, 677-692.

Lacassin, R., Maluski, H., Leloup, P.H., Tapponnier, P., Hintong, C., Siribhakdi, K., Chuaviroj, S., Charoenpravat, A., 1997. Tertiary diachronic and deformation of western Indochina: structural and 40Ar/39Ar evidence from NW Thailand. Journal of Geophysical Research 102 (1997), 10013–10037.

MacDonald, A.S., Barr, S.M., Dunning, G.R., Yaowanoiyothin, W., 1993. The Doi Inthanon metamorphic core complex in NW Thailand: age and tectonic significance. Journal of Southeast Asian Earth Sciences 8, 117-125.

Macdonald, A.S., Barr, S.M., Miller, B.V., Reynolds, P.H., Rhodes, B.P., Yokart, B., 2010. P–T–t constraints on the development of the Doi Inthanon metamorphic core complex domain and implications for the evolution of the western gneiss belt, northern Thailand. Journal of Asian Earth Sciences 37, 82-104.

Metcalfe, I., 1996. Gondwanaland dispersion, Asian accretion and evolution of eastern Tethys. Australian Journal of Earth Sciences 43, 605-623.

Mickein, A., 1996. U/Pb-, Rb/Sr- und K/Ar-Untersuchungen zur metamorphen Entwicklung und Altersstellung des "Prakambriums" in NW-Thailand.

Mitchell, A., Chung, S.-L., Oo, T., Lin, T.-H., Hung, C.-H., 2012. Zircon U–Pb ages in Myanmar: Magmatic–metamorphic events and the closure of a neo-Tethys ocean? Journal of Asian Earth Sciences 56, 1-23.

Mitchell, A.H.G., 1977. Tectonic setting for emplacement of SE Asia tin granitoids. Bulletin of Geological Society of Malaysia 9 (1977), 123-140.

Morley, C.K., 2002. A tectonic model for the Tertiary evolution of strike–slip faults and rift basins in SE Asia. Tectonophysics 347, 189-215.

Morley, C.K., 2004. Nested strike-slip duplexes, and other evidence for Late Cretaceous–Palaeogene transpressional tectonics before and during India–Eurasia collision, in Thailand, Myanmar and Malaysia. Journal of the Geological Society 161, 799-812.

Morley, C.K., 2012. Late Cretaceous–Early Palaeogene tectonic development of SE Asia. Earth-Science Reviews 115, 37-75.

Morley, C.K., Racey, A., 2011. Chapter 9 Tertiary, In: In: M.F. Ridd, A.J.B.a.M.A.C. (Ed.), Geology of Thailand Geological Society of London Special Publication, pp. 224-271.

Morley, C.K., Smith, M., Carter, A., Charusiri, P., Chantraprasert, S., 2007. Evolution of deformation styles at a major restraining bend, constraints from cooling histories, Mae Ping fault zone, western Thailand. Geological Society, London, Special Publications 290, 325-349.

Nantasin, P., Hauzenberger, C., Liu, X., Krenn, K., Dong, Y., Thöni, M., Wathanakul, P., 2012. Occurrence of the high grade Thabsila metamorphic complex within the low grade Three Pagodas shear zone, Kanchanaburi Province, western Thailand: Petrology and geochronology. Journal of Asian Earth Sciences 60, 68-87.

Osanai, Y., Nakano, N., Owada, M., Nam, T.N., Miyamoto, T., Minh, N.T., Nam, N.V., Tri, T.V., 2008. Collision zone metamorphism in Vietnam and adjacent South-eastern Asia: Proposition for Trans Vietnam Orogenic Belt. Journal of Mineralogical and Petrological Sciences 103, 226-241.

Palin, R.M., Searle, M.P., Morley, C.K., Charusiri, P., Horstwood, M.S.A., Roberts, N.M.W., 2013. Timing of metamorphism of the Lansang gneiss and implications for left-lateral motion along the Mae Ping (Wang Chao) strike-slip fault, Thailand. Journal of Asian Earth Sciences 76, 120-136.

Pettijohn, F.J., Potter, P.E., Siever, R., 1987. Sand and Sandstone, 2nd ed. ed. Springer, New York (1987)

Polachan, S., Pradidtan, S., Tongtaow, C., Janmaha, S., Intarawijitr, K., Sangsuwan, C., 1991. Development of Cenozoic basins in Thailand. Marine and Petroleum Geology 8, 84-97.

Powell, R., Holland, T.J.B., 1988. An internally consistent dataset with uncertainties and correlations: 3. Applications to geobarometry, worked examples and a computer program. Journal of Metamorphic Geology 6, 173-204.

Rhodes, B.P., Blum, J., Devine, T., 1997. Geology of the Doi Suthep metamorphic complex and adjacent Chiang Mai Basin., In: In: Dheeradilok, P.E. (Ed.), Proceedings of the International Conference on Stratigraphy and Tectonic Evolution of Southeast Asia and the South Pacific, Department of Mineral Resources, Bangkok, Thailand, pp. 305–313.

Rhodes, B.P., Blum, J., Devine, T., 2000. Structural development of the Mid-Tertiary Doi Suthep Metamorphic Complex and Western Chiang Mai Basin, Northern Thailand. Journal of Asian Earth Sciences 18, 97-108.

Rollinson, H.R., 1993. Using geochemical data: evaluation, presentation and interpretation. Harlow: Longman Scientific and Tecnical Ltd.

Roser, B.P., Korsch, R.J., 1986. Determination of tectonic setting of sandstone - mudstone suits using SiO2 content and K2O/Na2O ratio. Journal of Geology 94, 635-650.

Salayapongse, S., 2002. Metamorphic rocks of Thailand. The Symposium on Geology of Thailand, In: N. Mantajit, S.P. (Ed.), Proceedings of the Symposium on Geology of Thailand 2002, Department of Mineral Resources, Bangkok (2002), pp. 253-260.

Schmidt, M., 1992. Amphibole composition in tonalite as a function of pressure: an experimental calibration of the Al-in-hornblende barometer. Contr. Mineral. and Petrol. 110, 304-310.

Searle, M.P., Noble, S.R., Cottle, J.M., Waters, D.J., Mitchell, A.H.G., Hlaing, T., Horstwood, M.S.A., 2007. Tectonic evolution of the Mogok metamorphic belt, Burma (Myanmar) constrained by U-Th-Pb dating of metamorphic and magmatic rocks. Tectonics 26, n/a-n/a.

Searle, M.P., Yeh, M.-W., Lin, T.-H., Chung, S.-L., 2010. Structural constraints on the timing of left-lateral shear along the Red River shear zone in the Ailao Shan and Diancang Shan Ranges, Yunnan, SW China. Geosphere 6, 316-338.

Sengun, F., Candan, O., Özcan, D.O., Ersin, K.O., 2006. Petrography and Geochemistry of Paragneisses in the Çine Submassif of the Menderes Massif, Western Anatolia. Turkish Journal of Earth Sciences (Turkish J. Earth Sci.) 15, 321-342.

Singharajwarapan, S., Saengsrichan, W., 1999. Mineralogy and Petrology of the Chiang Mai Gneiss. in: Khantaprab, C., ed., Proceedings of the Symposium on Mineral, Energy and Water Resources of Thailand: Towards the Year 2000, Chulalongkorn University, 115-127.

Sone, M., Metcalfe, I., 2008. Parallel Tethyan sutures in mainland Southeast Asia: New insights for Palaeo-Tethys closure and implications for the Indosinian orogeny. Comptes Rendus Geoscience 340, 166-179.

Streckeisen, A.L., 1976. To each plutonic rock its proper nam. Earth Sci. Rev. 12 (1976), 1–32.

Sun, S.S., McDonough, W.F., 1989. Chemical and isotopic systematics of oceanic basalts: implications for mantle composition and processes. Geological Society, London, Special Publications 42, 313-345.

Tapponnier, P., Lacassin, R., Leloup, P.H., Scharer, U., Dalai, Z., Haiwei, W., Xiaohan, L., Shaocheng, J., Lianshang, Z., Jiayou, Z., 1990. The Ailao Shan/Red River metamorphic belt: Tertiary left-lateral shear between Indochina and South China. Nature 343, 431-437.

Tapponnier, P., Peltzer, G., Armijo, R., 1986. On the mechanics of the collision between India and Asia. Geological Society, London, Special Publications 19, 113-157.

Taylor, S.R., McLennan, S.M., 1985. The continental crust, its composition and evolution : an examination of the geochemical record preserved in sedimentary rocks. Blackwell Scientific, Oxford; Boston.

Taylor, S.R., McLennan, S.M., Armstrong, R.L., Tarney, J., 1981. The Composition and Evolution of the Continental Crust: Rare Earth Element Evidence from Sedimentary Rocks [and Discussion]. Philosophical Transactions of the Royal Society of London A: Mathematical, Physical and Engineering Sciences 301, 381-399.

Teggin, D.E., 1975. The Granites of Northern Thailand. University of Manchester, U.K.

Upton, D.R., 1999. A regional fission track study of Thailand: implication for thermal history and denudation. University of London.

Wang, B., Liu, H., Shu, L., Jahn, B.-m., Chung, S.-l., Zhai, Y., Liu, D., 2014. Early Neoproterozoic crustal evolution in northern Yili Block: Insights from migmatite, orthogneiss and leucogranite of the Wenquan metamorphic complex in the NW Chinese Tianshan. Precambrian Research 242, 58-81.

Whalen, J.B., Currie, K.L., Chappell, B.W., 1987. S-type granites: geochemical characteristics, discrimination and petrogenesis. Contr. Mineral. and Petrol. 95,, 407-419.

Woudloper, 2008. Diagram for metamorphic facies in the Earth's interior., https://en.wikipedia.org/wiki/Metamorphic_facies#/media/File:Metamorphic_facies_blanc.svg.

Woudloper, 2009. Triangular diagrams showing the aluminium (A), calcium (C) and iron (F) content of the main phases in metamorphic rocks in various facies,

https://en.wikipedia.org/wiki/Metamorphic_facies#/media/File:ACF_triangles_EN.svg.

จุฬาลงกรณ์มหาวิทยาลัย
Chulalongkorn University

APPENDICES

APPENDICES

APPENDIX A

Geochronological Data

จุฬาลงกรณ์มหาวิทยาลัย
Chulalongkorn University

Geochronological data in the Lansang National Park and adjacent areas.

AGE (Ma)	Rock/Mineral	Method	Remark	Location	Ref.
203 ± 4	Megacrystic orthogneiss/Zircon	U/Pb	Late Triassic-Early Jurassic granitic protolith	Doi Inthanon core complex	Macdonald et al.,1993
72 ± 1	Megacrystic orthogneiss/Monazite	U/Pb	High-grade metamorphism which created the gneiss dome in Late Cretaceous	Doi Inthanon core complex	Macdonald et al.,1993
209 ± 4	Porphyritic phase of granitic pluton /Zircon	U/Pb	Triassic-Jurassic crystallization age (Megacrystic orthogneiss came from this granitic pluton)	Mae Chaem pluton (west of Doi Inthanon)	Macdonald et al.,1993
25 ± 4	Biotite microgranite/Monazite	U/Pb	Late Oligocene crystallization age (pluton intrude after post metamorphism, which founded in orthogneiss and	Mae Klang pluton (east of Doi Inthanon)	Macdonald et al.,1993
208 ± 16	Tak granite	Rb/Sr WR Isochron		Tak granite/Tak	Miekein, 1997
210 I.R. = 0.7122	Tak granite	U/Pb			
208 ± 4 I.R. = 0.7162 ± 66	White granite	Rb/Sr WR Isochron (using decay constant = 1.29 X 10^{-11}Yr)		Tak	Teggin, 1975
212 ± 4 I.R. = 0.7110 ± 77	Pink granite				

Geochronological data in the Lansang National Park and adjacent areas.

AGE (Ma)	Rock/Mineral	Method	Remark	Location	Ref.
213 ± 10 I.R. =0.7158 ±18	White granite	Rb/Sr WR Isochron (using decay constant = 1.42×10^{-11} Yr)		Tak	Beckinsale et al.,1979
219 ± 13 I.R. = 0.7104 ± 19	Pink granite				
~200	Lansang gneiss/Zircon	U/Pb		Lansang area (Tak-Mae Sot)	Ahrendt et al., 1993
27 - 29	Gneiss/Biotite and Muscovite	K/Ar	Tertiary cooling	Bhumipol Dam	Ahrendt et al., 1993
18 - 22	Gneiss/Biotite and Muscovite	K/Ar	Tertiary cooling	Chiang Mai	
29.9 ± 0.6, 31.0 ± 0.6, 31.9 ± 1.6	Lansang gneiss/Biotite	K/Ar	Left-lateral shear	Lansang area (Tak-Mae Sot)	Ahrendt et al., 1993
29.6 ± 1.2 30.5 ± 1.0	Lansang gneiss/Illite		Low T° Left-lateral shear		
203 – 211	Orthogneiss/Zircon	U/Pb	Age of granitic intrusion	Doi Inthanon core complex	Dunning et al., 1995
84 ± 2 and 72 ± 1	Orthogneiss/Monazite	U/Pb	Age of high-grade metamorphism	Doi Inthanon core complex	Dunning et al., 1995
26.8 ± 0.5	Granite/Monazite and Zircon	U/Pb	Emplaced during Oligo-Miocene low angle normal faulting concurrent with	Mae Klang pluton (east of Doi Inthanon)	Dunning et al., 1995

AGE (Ma)	Rock/Mineral	Method	Remark	Location	Ref.
33.1 ± 0.4	Lansang gneiss/Biotite	$^{40}Ar/^{39}Ar$	Left-lateral shear	Lansang area	Lacassin et al., 1997
33.0 ± 0.2	Lansang gneiss/Biotite				
31.3 ± 0.7	Lansang gneiss/Biotite				
30.6 ± 0.3	Lansang gneiss/Biotite				
Rapid cool ~30.5,	Lansang gneiss/ K-feldspar	$^{40}Ar/^{39}Ar$	Left-lateral shear		
30 – 24 Ma; Isothermal ~ 185 ˚c					
Rapid cool ~23.5			Cooling/uplift		
123 and 114	Lansang orthogneiss/Monazite	Tb-Pb	Magmatic protolith emplacement (Early Cretaceous)	Lansang area	Palin et al., 2013
66.2±1.6 Ma	Granite dyke/Monazite	Tb-Pb		Bhumipol Lake	Palin et al., 2013
c.45-37	Lansang gneiss/Monazite	Tb-Pb	Eocene metamorphic event/Maximum age of left-lateral shear fabric	Lansang area	Palin et al., 2013
51–57 Ma	Thabsila metamorphic complex/Zircon	LA-ICP-MS U-Pb	Metamorphism age between India and Eurasia collision	Thabsila metamorphic complex/Three Pagodas	Nantasin et al., 2012
32–36 Ma	Thabsila metamorphic complex/Biotite	Rb–Sr isochron	Cooling age with temperature of 350-300°	Thabsila metamorphic complex/Three Pagodas	Nantasin et al., 2012
78.6±0.7 Ma	Nong Yai Gneiss/Zircon	LA-MC-ICP-MS U-Pb	Leucogranite intrusion and magmatic crystallization	Nong Yai Gneiss along Klaeng fault zone	Kanjanapayont et al., 2013
67±1 to 72.1±0.6 Ma	Nong Yai Gneiss/Zircon	LA-MC-ICP-MS U-Pb	Second crystallization (Late Cretaceous during Western Burma and Shan Thai	Nong Yai Gneiss along Klaeng fault zone	Kanjanapayont et al., 2013

Remark : WR = Whole Rock , I.R. = Initial $^{87}Sr/^{86}Sr$ Ratio

APPENDICES

APPENDIX B

List of Sample Location

จุฬาลงกรณ์มหาวิทยาลัย
Chulalongkorn University

Date	Station	Location		Elevation (m)	Sample No.		Structural data	
							Plane	L/F/C/J
23-FEB-2012	LAN-01	N 16.78069˚	E 099.01635˚	255			322˚/52˚	L 152˚/4˚
	LAN-02	N 16.78187˚	E 099.01685˚	258			341˚/49˚, 336˚/46˚	
	LAN-03	47Q 0501686	UTM 1855246	269			324˚/55˚	
	LAN-04	N 16.78006˚	E 099.01555˚	265				
	LAN-05	N 16.77993˚	E 099.01540˚	271				Axial plane (calc-silicate) 330˚/64˚, 336˚/58˚
	LAN-06	N 16.77992˚	E 099.01489˚	273				
	LAN-07	N 16.77991˚	E 099.01469˚	278				
24-FEB-2012	LAN-08	N 16.77985˚	E 099.01426˚	258	LS-1A	343˚/56˚	335˚/66˚	
	LAN-09	N 16.77986˚	E 099.01413˚	277	LS-1B	334˚/42˚		
	LAN-10	N 16.77985˚	E 099.01346˚	286				
	LAN-11	N 16.77852˚	E 099.01235˚	311				F 254˚/82˚
	LAN-12	N 16.77748˚	E 099.01180˚	319	LS-4A	334˚/68˚		
					LS-4B			
	LAN-13	N 16.77676˚	E 099.01162˚	295	LS-5A	356˚/58˚		
					LS-5B	324˚/63˚		
25-FEB-2012	LAN-14	N 17.00195˚	E 098.98526˚	178				
	LAN-15	N 16.99703˚	E 098.97651˚	193				
	LAN-16	N 16.99587˚	E 098.97596˚	197				

Date	Station	Location		Elevation (m)	Sample No.		Structural data	
	LAN-17	N 16.99602˚	E 098.97498˚	257				
	LAN-18	N 16.99594˚	E 098.97341˚	282				
	LAN-19	N 16.99483˚	E 098.97042˚	300	LS-6A	310˚/27˚	304˚/32˚, 309˚/36˚, 308˚/31˚	
	LAN-20	N 16.99465˚	E 098.97031˚	323	LS-7A			
					LS-7B			
					LS-7C			
26-FEB-2012	LAN-21	N 16.82071˚	E 099.00730˚	183	LS-8A	330˚/20˚		
	LAN-22	N 16.85318˚	E 098.97424˚	222				
	LAN-23	N 16.85338˚	E 098.97341˚	182			284˚/73˚(sand), 150˚/52˚(sand), 135˚/61˚(silt)	
	LAN-24	N 16.85467˚	E 098.95156˚	255	LS-9A	323˚/55˚	331˚/77˚, 334˚/48˚, 327˚/68˚, 324˚/56˚	R 271˚/73˚, R 208˚/81˚ ทั้งสองค่าวัดจากแนว fracture ที่เกิดจาก shear หลัก (radial?)

Date	Station	Location		Elevation (m)	Sample No.		Structural data	
					LS-9B			
					LS-9C			
27-FEB-2012	LAN-25	N 16.77659˚	E 099.01141˚	306			0˚/49˚, 320˚/62˚ (Bi-gneiss)	
	LAN-26	N 16.77662˚	E 099.01059˚	306	LS-10A	335˚/66˚	335˚/69˚	
					LS-10B	330˚/64˚		
	LAN-27	N 16.77661˚	E 099.00989˚	301	LS-11A	325˚/60˚	323˚/58˚	
	LAN-28	N 16.77777˚	E 099.00385˚	326				
	LAN-29	N 16.77718˚	E 099.00326˚	327	LS-12A	280˚/56˚	325˚/58˚ (Augen gneiss) ,345˚/55˚	
					LS-12B	355˚/22˚		
					LS-12C	274˚/17˚		
	LAN-30	N 16.77701˚	E 099.00300˚	360				
	LAN-31	N 16.77681˚	E 099.00291˚	346				
	LAN-32	N 16.77590˚	E 099.00285˚	377	LS-13A	334˚/42˚		
					LS-13B	346˚/60˚		
					LS-13C	195˚/80˚		

Date	Station	Location		Elevation (m)	Sample No.		Structural data	
					LS-13D	348˚/50˚		
					LS-13E	342˚/52˚		
	LAN-33	N 16.77537˚	E 099.00281˚	358	LS-14A	175(+180)˚/76˚	355˚/76˚	
					LS-14B	168˚/54˚		
28-FEB-2012	LAN-34	N 16.77520˚	E 099.00281˚	358				
	LAN-35	N 16.77367˚	E 099.00214˚	374	LS-15A	321˚/69˚	316˚/63˚	L 114˚/22˚, J 194˚/46˚, F/S 253˚/84˚
					LS-15B	128˚/82˚		
	LAN-36	N 16.77415˚	E 099.00246˚	375	LS-15C	110˚/80˚		
					LS-15D	190˚/73˚		
					LS-15E	318˚/?˚		
					LS-15F	314˚/82˚		
					LS-15G			
	LAN-37	N 16.77321˚	E 099.00222˚	403	LS-16A	270˚/42˚		
	LAN-38	N 16.77288˚	E 099.00186˚	417				
	LAN-39	N 16.77210˚	E 099.00042˚	446	LS-17A	327˚/44˚		
					LS-17B	312˚/58˚		
	LAN-40	N 16.77067˚	E 098.99451˚	511	LS-18A	304˚/63˚		
	LAN-41	N 16.76977˚	E 098.99438˚	526				
	LAN-42	N 16.76942˚	E 098.99406˚	539			325˚/56˚, 340˚/48˚,	J 8˚/26˚

Date	Station	Location		Elevation (m)	Sample No.		Structural data	
29-FEB-2012	LAN-44	N 16.99640˚	E 098.96893˚	303	LS-19A	50˚/89˚		
					LS-19B	112˚/53˚		
	LAN-45	N 16.99496˚	E 098.96739˚	323				
	LAN-46	N 16.99469˚	E 098.96709˚	321	LS-20A	352˚/64˚	327˚/63˚	
	LAN-47	N 16.99459˚	E 098.96664˚	318				
	LAN-48	N 16.99307˚	E 098.96619˚	330	LS-21A	163˚/34˚		
					LS-21B	134˚/27˚		
					LS-21C	163˚/85˚		
	LAN-49	N 16.99185˚	E 098.96472˚	355				
	LAN-50	N 16.99209˚	E 098.96411˚	371	LS-22A	5˚/29˚		
	LAN-51	N 16.99141˚	E 098.96149˚	396	LS-22B	72˚/39˚		
01-MAR-2012	LAN-52	N 16.99435˚	E 098.97201˚	268	LS-23A	334˚/40˚	323˚/55˚, 329˚/62˚, 333˚/58˚, 326˚/59˚, 331˚/61˚, 336˚/60˚, 330˚/56˚	J 220˚/70˚, J 62˚/70˚, J 218˚/85˚, J 190˚/89˚, J 205˚/88˚
					LS-23B	327˚/64˚		
					LS-23C	192˚/80˚		
					LS-23D	85˚/42˚		

Date	Station	Location		Elevation (m)	Sample No.		Structural data	
					LS-23D	85˚/42˚		
					LS-23E			
					LS-23F			
	LAN-53	N 16.77995˚	E 099.01602˚	275			330˚/62˚	J 198˚/87˚, J 54˚/80˚
	LAN-54	N 16.77988˚	E 099.01453˚	277	LS-24A	276˚/75˚		

จุฬาลงกรณ์มหาวิทยาลัย
Chulalongkorn University

VITA

Ms. Somporn Wonglak was born on March 3, 1989 and raised in Bangkok, Thailand. She graduated in compulsory education from Rittiyawannalai School in 2006. She was studying in BSc. (Geology) at the Department of Geology, Faculty of Science, Chulalongkorn University before achievement of Bachelor's Degree (B.Sc.) in 2010. During her studying in Bachelor program, she had focused on petrography and mineral chemistry of corundum–bearing rock from Winza in Tanzania. After graduation, she continued her studies in MSc. Program at the Department of Geology, Faculty of Science, Chulalongkorn University. She also has focused on petrography and metamorphism of the Lan Sang metamorphic suites in Lan Sang National Park, Changwat Tak, Thailand.

จุฬาลงกรณ์มหาวิทยาลัย
Chulalongkorn University